Photo-Catalytic Degradation of some dyes by nanoparticles : Kinetics and mechanistic study

MINOR RESEARCH PROJECT

FINAL WORK DONE REPORT

(FROM 28 JAN 2015 TO 27 JAN 2017)

SUBMITTED TO

ज्ञान-विज्ञान विमुक्तये

UNIVERSITY GRANTS COMMISSION

WESTERN REGIONAL OFFICE

PUNE – 411007

BY

MR. S. G. JADHAV

DEPARTMENT OF CHEMISTRY,

SHRI SHIVAJI MAHAVIDYALAYA,

BARSHI - 413411

DISTRICT-SOLAPUR.(M.S.)

Scanned by CamScanner

SHRI SHIVAJI SHIKSHAN PRASARAK MANDAL, BARHSI'S

Shri Shivaji Mahavidyalaya, Barshi.

(Arts & Science - Junior & Senior)

Post Box-4,A/P Barsi-413411,Dist.-Solapur,MH–India

NAAC Re-accredited "A "Grade

Prin.Dr. P. R. Thorat, M. Sc., M.Phil., Ph. D.

☎**Off.** : (02184) 222382 •**Fax** : (02184) 222382 •**E-Mail** : ssmb_barshi@rediffmail.com

•Jr.Reg.No.HSC/976/13792 (S.Y.)dt. 7-5-1976•Sr. Affi. Letter No. GEN/Affi/2832 dt. 4-3-1964 Shivaji Uni.

•P.G.Language / BG / BUTR / I / 30471 dt.27-5-1972•Social Sciences / PW / BUTR / 3906 / dt. 30-9-1972

Ref. No.SSMB/Sr./UGC/ 37

Date : 28/05/2020

To,
The Joint Secretary,
Western Regional Office,
University Grants Commission,
Ganesh khind, Pune-411007

Subject: - Final Report Submission of Minor Research Project

Ref: -Approval Letter No F-.47-630/13 dated 28-01-2015

Respected Sir,

I am forwarding herewith, the Final Completion report of minor research project entitled "**Photo-Catalytic Degradation of some dyes by nanoparticles :Kinetics and mechanistic study**" duly completed by **Mr. S. G. Jadhav** from **Chemistry** Department of this college, along with the audited statement of expenditure, utilization certificate, summary report of the project and other related documents.

I request you to accept the same & kindly release the remaining amount of Rs.60, 000/- (In words Rs. Sixty thousand only) towards the project.

Thanking You

Yours faithfully

PRINCIPAL
Shri Shivaji Mahavidyalaya,
Barshi, Dist. Solapur-413411

Encl:-as above
Copy to:- **Director**
INFLIBNET Centre, Gandhinagar,
An Inter University Centre of University Grants Commission,
Infocity Gandhinagar - 382007. Gujarat, INDIA.

Scanned by CamScanner

INDEX

SR. NO.	DETAILS	PAGE NO.
1	Audited Consolidated Statement of Expenditure with item wise details under 'non-recurring & 'recurring' heads for the amount actually incurred duly signed by the Principal & C. A. with stamp & Registration No. **Annexure III (Annual)**	1-2
2	Statement of Expenditure on Field Work, if applicable, in the prescribed formats as per UGC guidelines. **Annexure IV (Annual)**	3
3	Audited Consolidated Utilization Certificate for the amount actually incurred, duly signed by the Principal & C. A. with stamp. **Annexure V (Annual)**	4
4	Audited Consolidated Statement of Expenditure with item wise details under 'non-recurring & 'recurring' heads for the amount actually incurred duly signed by the Principal & C. A. with stamp & Registration No. **Annexure III (Final)**	5-6
5	Statement of Expenditure on Field Work, if applicable, in the prescribed formats as per UGC guidelines. **Annexure IV(Final)**	7
6	Audited Consolidated Utilization Certificate for the amount actually incurred, duly signed by the Principal & C. A. with stamp. **Annexure V (Final)**	8
7	Certificate **(Utilization of grant within tenure)**	9
8	Accession Certificate **(Books and Journal)**	10
9	Assets Certificate.**(Equipments)**	11
10	A copy of the proof about uploading of Executive summary of the report, Research documents, monograph, academic papers published under **Minor Research Project on the website of the College**	12-13
11	Annual Report	14-17
12	Final Report	18-21
13	Final report of the work done in the prescribed formats as per UGC guidelines, chapters I, II, III, IV	22-112
14	Acknowledgements	113
15	MRP sanction letter	114-116
16	MRP acceptance letter	117

Scanned by CamScanner

Annexure-III (Annual)

UNIVERSITY GRANTS COMMISSION

BAHADUR SHAH ZAFAR MARG

NEW DELHI-110002

Statement of Expenditure in Respect of Minor Research Project

1. Name of Principal Investigator : **Mr. S. G. Jadhav**

2. Deptt. of University/College : Department of Chemistry,
Shri Shivaji Mahavidyalaya, Barshi413411

3. UGC approval No. and Date : F-.47-630/13 dated 28-01-2015

4. Title of Research : **"Photo-Catalytic Degradation of some dyes by nanoparticles :Kinetics and mechanistic study"**

5. Effective date of starting the project : 28 JAN 2015

6. (a) Period of Expenditure : From 28 JAN 2015 TO 27 JAN 2016

(b) Details of Expenditure :

Sr. No.	Item	Amount Approved in Rs.	Expenditure Incurred in Rs.
I	Books/Journals	25000/-	25918/-
II	Equipment	160000/-	162550/-
III	Contingency	20000/-	20160/-
IV	Field Work/ Travel	10000/-	10400/-
V	Chemicals and Glassware	30000/-	31126/-
	Total	**245000/-**	**250154/-**

c) Staff : Not Applicable (minor Research)

7. If as a result of check or audit objection some irregularity is noticed at later date, action will be taken to refund, adjust or regularize the objected amounts.

8. It is certified that the grant of Rs.245000/- (Rupees two lakh forty five Thousand only) sanctioned from the University Grants Commission under the scheme of support for

Scanned by CamScanner

Minor Research Project entitled "**Photo-Catalytic Degradation of some dyes by nanoparticles :Kinetics and mechanistic study**" vide UGC letter No. F-.47-630/13 dated 28-01-2015 has been fully utilized for the purpose for which it was sanctioned and in accordance with the terms and conditions laid down by the University Grants Commission.

Principal Investigator

Principal Investigator
(Minor Research Project)

PRINCIPAL

PRINCIPAL
Shri Shivaji Mahavidyalaya,
Barshi, Dist. Solapur-413411

Scanned by CamScanner

Annexure - IV ((Annual))

UNIVERSITY GRANTS COMMISSION

BAHADUR SHAH ZAFAR MARG

NEW DELHI – 110 002

STATEMENT OF EXPENDITURE INCURRED ON FIELD WORK

Name of the Principal Investigator: Mr. S. G. Jadhav

Name of the Place visited	Duration of the Visit	Mode of Journey	Expenditure Incurred (Rs.)
	From - To		
Shivaji University Kolhapur	19 /09/2015	Car	4700/-
Pune University	23/12/2015	Car	4500/-
Solapur university Solapur	08/01/2016	Car	1200/-
		Total	**10400/-**

Certified that the above expenditure is in accordance with the UGC norms for Minor Research Projects.

SIGNATURE OF PRINCIPAL INVESTIGATOR

Principal Investigator
Minor Research Project

PRINCIPAL

Shri Shivaji Mahavidyalaya,
Barshi, Dist. Solapur-413411

3

Scanned by CamScanner

Annexure – V ((Annual))

UNIVERSITY GRANTS COMMISSION

BAHADUR SHAH ZAFAR MARG

NEW DELHI – 110 002

Utilization certificate

It certified that the grant of Rs.245000/- (Rupees two lakh forty five Thousand only) sanctioned from the University Grants Commission under the scheme of support of Minor Research Project entitled "**Photo-Catalytic Degradation of some dyes by nanoparticles :Kinetics and mechanistic study**" vide UGC letter No. **F-.47-630/13 dated 28-01-2015** has been fully utilized for the purpose for which it was sanctioned and in accordance with the terms and conditions laid down by the University Grants Commission.

If as a result of check or audit objection, some irregularity is noticed at a later stage action will be taken to refund or regularize the objected amount. Total actual expenditure incurred for this project is of Rs 2,50154/- **(Rs. Two lakh fifty thousand one hundred fifty four only.)**

Principal Investigator

Principal

PRINCIPAL
Shri Shivaji Mahavidyalaya,
Barshi, Dist. Solapur-413411

Statutory Auditor

GAT AND ASSOCIATES CHARTERED ACCOUNTANTS PUNE-1

4

Scanned by CamScanner

Annexure-III (Final)

UNIVERSITY GRANTS COMMISSION

BAHADUR SHAH ZAFAR MARG

NEW DELHI-110002

Statement of Expenditure in Respect of Minor Research Project

1. Name of Principal Investigator : **Mr. S. G. Jadhav**

2. Deptt. of University/College : Department of Chemistry,
Shri Shivaji Mahavidyalaya, Barshi413411

3. UGC approval No. and Date : F-.47-630/13 dated 28-01-2015

4. Title of Research : **"Photo-Catalytic Degradation of some dyes by nanoparticles :Kinetics and mechanistic study"**

5. Effective date of starting the project : 28 JAN 2015

6. (a) Period of Expenditure : From 28 JAN 2015 TO 27 JAN 2017

(b) Details of Expenditure :

Sr. No.	Item	Amount Approved in Rs.	Expenditure Incurred in Rs.
I	Books/Journals	25000/-	25918/-
II	Equipment	160000/-	162550/-
III	Contingency	40000/-	40460/-
IV	Field Work/ Travel	20000/-	20900/-
V	Chemicals and Glassware	60000/-	61437/-
	Total	**305000**	**311265/-**

c) Staff : Not Applicable (minor Research)

7. If as a result of check or audit objection some irregularity is noticed at later date, action will be taken to refund, adjust or regularize the objected amounts.

8. It is certified that the grant of Rs.305000/- (Rupees three lakh five Thousand only) sanctioned from the University Grants Commission under the scheme of support for

5

Scanned by CamScanner

Minor Research Project entitled "**Photo-Catalytic Degradation of some dyes by nanoparticles :Kinetics and mechanistic study**" vide UGC letter No. F-.47-630/13 dated 28-01-2015 has been fully utilized for the purpose for which it was sanctioned and in accordance with the terms and conditions laid down by the University Grants Commission.

Principal Investigator

Principal Investigator
Minor Research Project

PRINCIPAL

PRINCIPAL

Shri Shivaji Mahavidyalaya,
Barshi, Dist. Solapur-413411

DATAT AND ASSOCIATES
CHARTERED ACCOUNTANTS
FRN 130069W
PUNE-1

6

Scanned by CamScanner

Annexure - IV (Final)

UNIVERSITY GRANTS COMMISSION

BAHADUR SHAH ZAFAR MARG

NEW DELHI – 110 002

STATEMENT OF EXPENDITURE INCURRED ON FIELD WORK

Name of the Principal Investigator: Mr. S. G. Jadhav

Name of the Place visited	Duration of the Visit	Mode of Journey	Expenditure Incurred (Rs.)
	From - To		
Shivaji University Kolhapur	19 /09/2015	Car	4700/-
Pune University	23/12/2015	Car	4500/-
Solapur university Solapur	08/01/2016	Car	1200/-
Rajarshi Chhatrapati Shahu College Kolhapur	10/02/2016	Car	4700/-
Babasaheb Ambedkar Marathwada University Aurangababad	30/11/2016	Car	4900/-
BAMU Subcenter Osmanabad	26/12/2016	Car	900/-
		Total	**20900/-**

Certified that the above expenditure is in accordance with the UGC norms for Minor Research Projects.

SIGNATURE OF PRINCIPAL INVESTIGATOR

Principal Investigator
Minor Research Project

PRINCIPAL

PRINCIPAL
Shri Shivaji Mahavidyalaya,
Barshi, Dist. Solapur-413411

VIJAY GARAT AND ASSOCIATES
CHARTERED ACCOUNTANTS
FRN 135008W
PUNE

7

Scanned by CamScanner

Annexure – V (Final)

UNIVERSITY GRANTS COMMISSION

BAHADUR SHAH ZAFAR MARG

NEW DELHI – 110 002

Utilization certificate

It certified that the grant of **Rs.305000/- (Rupees three lakh five Thousand only)** sanctioned from the University Grants Commission under the scheme of support of Minor Research Project entitled "**Photo-Catalytic Degradation of some dyes by nanoparticles :Kinetics and mechanistic study**" vide UGC letter No. **F-.47-630/13 dated 28-01-2015** has been fully utilized for the purpose for which it was sanctioned and in accordance with the terms and conditions laid down by the University Grants Commission.

If as a result of check or audit objection, some irregularity is noticed at a later stage action will be taken to refund or regularize the objected amount. Total actual expenditure incurred for this project is of Rs **311265/- (Rs. Three lakh eleven thousand two hundred sixty five only.)**

Principal Investigator

Principal Investigator
(Minor Research Project)

Principal

PRINCIPAL
Shri Shivaji Mahavidyalaya,
Barshi, Dist. Solapur-413411

Statutory Auditor

VIJAY GAPAT AND ASSOCIATES
CHARTERED ACCOUNTANTS
FRN 135006W
PUNE-1

8

Scanned by CamScanner

UNIVERSITY GRANTS COMMISSION

BAHADUR SHAH ZAFAR MARG

NEW DELHI-110002

(Utilization of grant within tenure)

CERTIFICATE

It certified that the grant of **Rs.305000/- (Rupees three lakh five Thousand only)** sanctioned from the University Grants Commission under the scheme of support of Minor Research Project entitled "**Photo-Catalytic Degradation of some dyes by nanoparticles :Kinetics and mechanistic study**" vide UGC letter No. **F-.47-630/13 dated 28-01-2015** has been utilized within the period **28-01-2015 to 27-01-2017** of minor research project.

Principal

PRINCIPAL
Shri Shivaji Mahavidyalaya,
Barshi, Dist. Solapur-413411

9

Scanned by CamScanner

UNIVERSITY GRANTS COMMISSION

BAHADUR SHAH ZAFAR MARG

NEW DELHI-110002

ACCESSION CERTIFICATE

(BOOKS AND JOURNALS)

Minor Research Project

It is certified that the grant of **Rs.25918/- (Rupees Twenty five thousand nine hundred eighteen only)** sanctioned to **Mr. S. G. Jadhav** by University Grants Commission vide its sanction letter No. **F-.47-630/13 dated 28-01-2015** has been utilized for the purpose of books and journals and the same have been accessioned and noted in the accession register from **accession No. 9922 to 9957** being maintained by the college. The last accession number prior to the utilization of these grants for books purchased from UGC was **9921.**

Principal Investigator

Principal Investigator
(Minor Research Project)

Librarian

LIBRARIAN
Shri Shivaji Mahavidyalaya
,Barshi.

Principal

PRINCIPAL
Shri Shivaji Mahavidyalaya,
Barshi, Dist. Solapur-413411

10

Scanned by CamScanner

UNIVERSITY GRANTS COMMISSION

BAHADUR SHAH ZAFAR MARG

NEW DELHI-110002

ASSETES CERTIFICATE FOR EQUIPMENT

Minor Research Project

It is certified that following equipments are purchased from MRP grants (**F-.47-630/13 dated 28-01-2015)** have been handed over to the college and have been duly entered in the stock register maintained by the college.

1. Photoreactor
2. Dell Laptop
3. Flame photometer
4. Spectrophotometer
5. Back up/inverter

Principal Investigator

Principal Investigator
Minor Research Project

Head of the Department

Dr. T. N. Lokhande
M. Sc. Ph. D.
Head, Dept. of Chemistry
Shri Shivaji Mahavidyalaya
Barshi - 413411, Dist. Solapur

Principal

PRINCIPAL
Shri Shivaji Mahavidyalaya,
Barshi, Dist. Solapur-413411

11

Scanned by CamScanner

UNIVERSITY GRANTS COMMISSION

BAHADUR SHAH ZAFAR MARG

NEW DELHI-110002

(Project Report, papers etc. uploading on college website)

CERTIFICATE

It certified that the **executive summary of the report, research documents, monograph, academic papers published** under Minor Research Project entitled "**Photo-Catalytic Degradation of some dyes by nanoparticles :Kinetics and mechanistic study**" funded by **University Grants Commission(WRO) Pune** to **Mr. S. G. Jadhav** are **uploaded on the website of the College www.ssmbarshi.org.in**

Principal

PRINCIPAL
Shri Shivaji Mahavidyalaya,
Barshi, Dist. Solapur-413411

12

Scanned by CamScanner

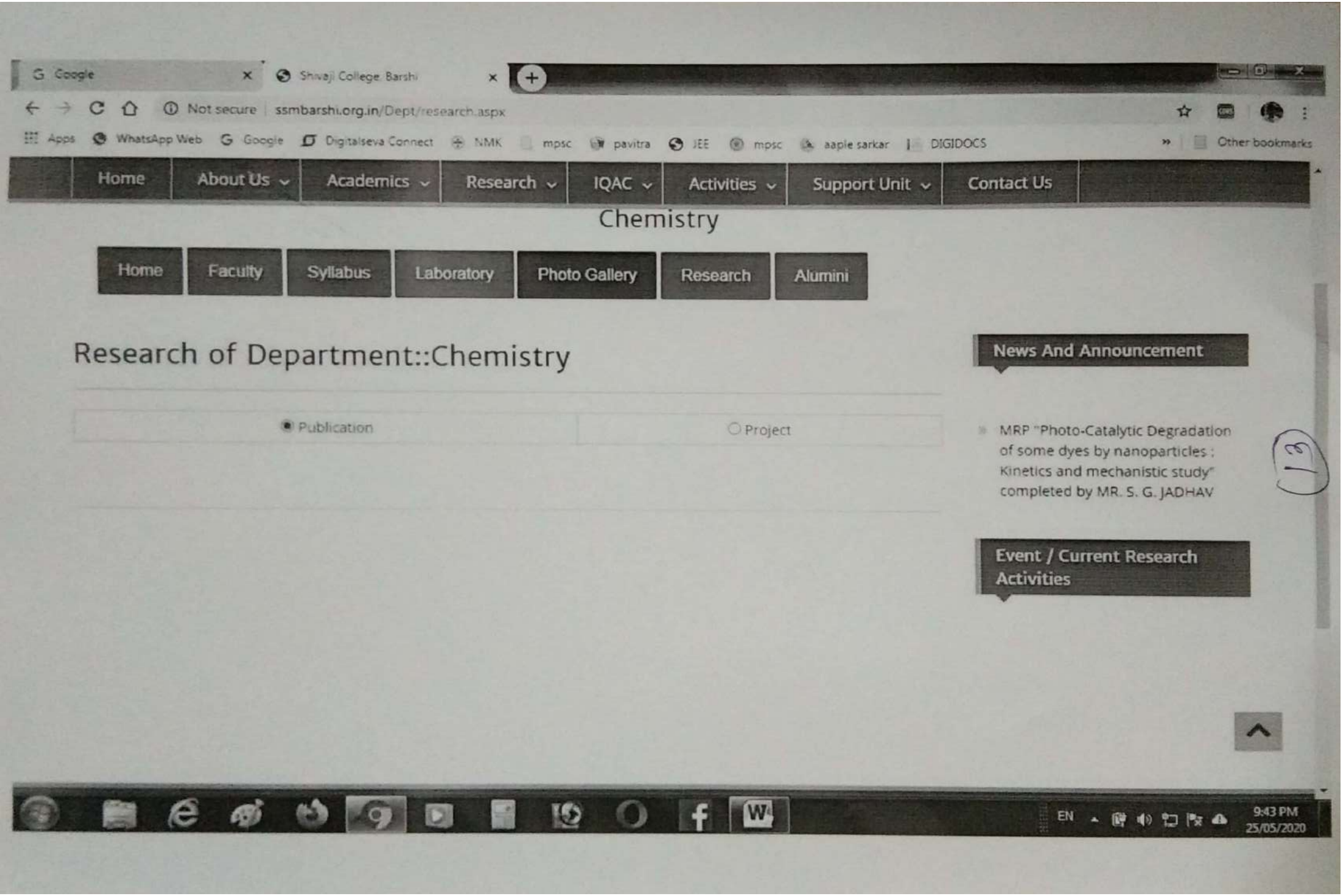

Scanned by CamScanner

Annexure -VI

UNIVERSITY GRANTS COMMISSION

BAHADUR SHAH ZAFAR MARG

NEW DELHI – 110 002.

Annual Report of the work done on the Minor Research Project.

(Report to be submitted within 6 weeks after completion of each year)

1. Project report No. 1st /Final : **1st**

2. UGC Reference No.F. : **47-630/13 dated 28-01-2015**

3. Period of report: **from 28/01/2015 to 27/01/2016**

4. Title of research project : "**Photo-Catalytic Degradation of some dyes by nanoparticles :Kinetics and mechanistic study**"

5. (a) Name of the Principal Investigator: **Mr. S. G. Jadhav**

(b) Department. : **Chemistry**

(c) College where work has progressed : **Shri Shivaji Mahavidyalaya Barshi**

6. Effective date of starting of the project: **28/01/2015**

7. Grant approved and expenditure incurred during the period of the report:

a. Total amount approved Rs. : **245000/-(First year)**

b. Total expenditure Rs. : **250154/-**

c. Report of the work done: **Separate sheet is attached**

i. Brief objective of the project :

- To synthesize TiO_2 , ZnO, AgO etc. catalyst and to characterize the same.

(14)

Scanned by CamScanner

- To study the oxidation of some dyes like malachite green, Indigo dye, methyl orange, methyelene blue, rhodamine B etc. by TiO_2 ZnO, AgO etc. nanoparticles.
- To develop benign process for degradation of dyes.

ii. Work done so far and results achieved and publications, if any, resulting from the work (Give details of the papers and names of the journals in which it has been published or accepted for publication): **nil**

iii. Has the progress been according to original plan of work and towards achieving the objective. if not, state reasons:**Yes**

iv. please enclose a summary of the findings of the study. One bound copy of the

final report of work done may also be sent to the concerned Regional Office of the UGC.: **N/A**

v. Any other information:**N/A**

PRINCIPAL INVESTIGATOR
Principal Investigator
(Minor Research Project)

PRINCIPAL
PRINCIPAL
Shri Shivaji Mahavidyalaya,
Barshi, Dist. Solapur-413411.

Scanned by CamScanner

Report of the work done in First Year

1) Literature survey is done on the dye degradation by different methodss. Purchase of chemicals, glass wares and equipments for project work. Nanoparticles of ZnO and mixed metal oxides were are synthesized by the reported method and characterization of these Nanoparticles is carried out.

2) The nanosized ZnO rods were prepared by microwave-assisted method. Aqueous solution of zinc nitrate (0.01M) and polyvinyl alcohol (1 % w/v) were mixed and the solution thus prepared was set to stir constantly with addition of (0.01M) solution of sodium hydroxide simultaneously for half an hour. After completion of the reaction, white precipitate of zinc hydroxide was obtained. The solution was then centrifuged in presence of water and acetone to remove all the impurities. The process of centrifugation was repeated three times to remove most of the impurities from the solution. The precipitated zinc hydroxide solution was kept for 10 minutes under microwave irradiation with a power output of 695 W by following on-off cycle. The solution was allowed to cool up to room temperature and allowed to dry naturally. Annealing of the product was carried out at various temperatures for three hour in temperature controlled furnace. The physiochemical properties solely depend upon preparation of materials. In our study it is planned to use minimal energy to form complete growth of ZnO nanorods with desired size and shape. and used for the characterization.

The mixed metal oxide system $CuFe_{2-x}Mn_x O_4$ where x = 0.0, 0.5, 1.0, 1.5 and 2.0 were prepared by sol-gel autocombution method. Analytical grade ferric nitrate [Fe $(NO_3)_2.6H_2O$],copper nitrate $[Cu(NO_3)_3.3H_2O]$, manganese nitrate $[Mn(NO_3)_2.4H_2O]$, and citric acid $[C_6H_8O_7.H_2O]$ were used to prepare system compositions.Metal nitrates and citric acid were dissolved in minimum quantity of deionized water with 1:1 molar ratio for all compositions. The pH of the solution was adjusted to about 9.0 to 9.5 using ammonia solution. This solution transforms to dry gel on heating to 353K. On further heating the dried gel undergo a self propagating combustion process and transform to floppy loose powder. The obtained powder was

PG

Scanned by CamScanner

then calcined at 1173 K for 8 h in air atmosphere. The calcined powders were mixed with 2 % polyvinyl alcohol and pressed to pellets by applying uniaxial pressure of 8 ton /cm^2. These pellets were gradually heated to about 773K to remove out the volatile organic binder materials

3) Prepared nanoparticles were characterized by using IR spectra, SEM, TGA, XRD, EDAX spectra etc.

4) Prepared nanoparticles were tested for degradation of some dyes

Principal Investigator
Principal Investigator
(Minor Research Project)

PRINCIPAL
Shri Shivaji Mahavidyalaya,
Barshi, Dist. Solapur-413411

~~20~~
17

Scanned by CamScanner

BAHADUR SHAH ZAFAR MARG

NEW DELHI – 110 002.

Final Report of the work done on the Minor Research Project.

(Report to be submitted within 6 weeks after completion of each year)

1. Project report No. 1st /Final : **Final**

2. UGC Reference No.F. : **47-630/13 dated 28-01-2015**

3. Period of report: **from 28/01/2015 to 27/01/2017**

4. Title of research project : "**Photo-Catalytic Degradation of some dyes by nanoparticles :Kinetics and mechanistic study**"

5. (a) Name of the Principal Investigator: **Mr. S. G. Jadhav**

(b) Department. : **Chemistry**

(c) College where work has progressed : **Shri Shivaji Mahavidyalaya Barshi**

6. Effective date of starting of the project: **28/01/2015**

7. Grant approved and expenditure incurred during the period of the report:

a. Total amount approved Rs. : 305000/-(two years)

b. Total expenditure Rs. : 311265/-

c. Report of the work done: **Separate sheet is attached**

i. Brief objective of the project :

- To synthesize TiO_2 , ZnO, AgO etc. catalyst and to characterize the same.
- To study the oxidation of some dyes like malachite green, Indigo dye, methyl orange, methyelene blue, rhodamine B etc. by TiO_2 ZnO, AgO etc. nanoparticles.
- To develop benign process for degradation of dyes.

(18)

Scanned by CamScanner

ii. Work done so far and results achieved and publications, if any, resulting from the work (Give details of the papers and names of the journals in which it has been published or accepted for publication): **Nil**

iii. Has the progress been according to original plan of work and towards achieving the objective. if not, state reasons:**Yes**

iv. please enclose a summary of the findings of the study. One bound copy of the

final report of work done may also be sent to the concerned Regional Office of the UGC.: **Enclosed bound copy of final report**

v. Any other information:**N/A**

PRINCIPAL INVESTIGATOR
Principal Invesugator
Minor Research Project

PRINCIPAL
Shri Shivaji Mahavidyalaya,
Barshi, Dist. Solapur-413411

19

Scanned by CamScanner

Final Report of the work done

(First Year and second year)

First year:

1) Literature survey is done on the dye degradation by different methodss. Purchase of chemicals, glass wares and equipments for project work. Nanoparticles of ZnO and mixed metal oxides were are synthesized by the reported method and characterization of these Nanoparticles is carried out.

2) The nanosized ZnO rods were prepared by microwave-assisted method. Aqueous solution of zinc nitrate (0.01M) and polyvinyl alcohol (1 % w/v) were mixed and the solution thus prepared was set to stir constantly with addition of (0.01M) solution of sodium hydroxide simultaneously for half an hour. After completion of the reaction, white precipitate of zinc hydroxide was obtained. The solution was then centrifuged in presence of water and acetone to remove all the impurities. The process of centrifugation was repeated three times to remove most of the impurities from the solution. The precipitated zinc hydroxide solution was kept for 10 minutes under microwave irradiation with a power output of 695 W by following on-off cycle. The solution was allowed to cool up to room temperature and allowed to dry naturally. Annealing of the product was carried out at various temperatures for three hour in temperature controlled furnace. The physiochemical properties solely depend upon preparation of materials. In our study it is planned to use minimal energy to form complete growth of ZnO nanorods with desired size and shape. and used for the characterization.

The mixed metal oxide system $CuFe_{2-x}Mn_x O_4$ where x = 0.0, 0.5, 1.0, 1.5 and 2.0 were prepared by sol-gel autocombution method. Analytical grade ferric nitrate [$Fe(NO_3)_2.6H_2O$],copper nitrate [$Cu(NO_3)_3.3H_2O$], manganese nitrate [$Mn(NO_3)_2.4H_2O$], and citric acid [$C_6H_8O_7.H_2O$] were used to prepare system compositions.Metal nitrates and citric acid were dissolved in minimum quantity of deionized water with 1:1 molar ratio for all compositions. The pH of the solution was adjusted to about 9.0 to 9.5 using ammonia solution. This solution transforms to dry gel on heating to 353K. On further heating the dried gel undergo a self propagating combustion process and transform to floppy loose powder. The obtained powder was then calcined at 1173 K for 8 h in air atmosphere. The calcined powders were mixed with 2 % polyvinyl alcohol and pressed to pellets by applying uniaxial pressure of 8 ton /cm^2. These pellets were gradually heated to about 773K to remove out the volatile organic binder materials

20

Scanned by CamScanner

3) Prepared nanoparticles were characterized by using IR spectra, SEM, TGA, XRD, EDAX spectra etc.

4) Prepared nanoparticles were tested for degradation of some dyes

Second year:

The photocatalytic activities of samples were evaluated for degradation of methyl orange (MO) after irradiating the samples with 125 W high-pressure lamp with maximum emission at 365 nm. The average light intensity was 0.9mW/cm2. MO solution (100 mL, 1.0×10−5 mol/dm3) containing 20 mg of as photocatalyst sample, ZnO was placed in a glass beaker. Irradiation of the solution was carried out with constant stirring for 30 min to ensure adsorption equilibrium between the catalyst and dye. 3 mL of above solution was taken out at different time intervals and separated through centrifugation and the absorbance of reaction solution was measured by a UV-3600 (Shimadzu) spectrophotometer in the range wavelength range from 350 to 550 nm.

Reaction suspensions were prepared by adding photocatalyst, ZnO (20 mg) powder into 100 ml Rhodamine (Rh.B) solutions. The suspensions were ultrasonically sonicated for 30 minutes and then magnetically stirred in dark for about 30 minutes to ensure adsorption equilibrium prior to the UV-irradiation.The suspensions containing RhB and photocatalyst were irradiated by the UV light. In this manner, the photodegradation of RhB in aqueous solution by using powder of ZnO nanorods as a photocatalyst was studied spectrophotometrically. The maximum absorption peak of RhB was obtained at 557 nm.

The catalytic activity of the photocatalyst, substituted MnCopper Ferrite nanoparticles was studied by following the rate of photodegradation of Methyl Red. The experiment of photocatalytic reaction was conducted in a 100-ml Pyrex glass vessel with magnetic stirring and a UV lamp (8W, with the main wavelength of 253.7nm) positioned over the glass beaker. The as-prepared substituted MnCopper Ferrite nanoparticles were used as photocatalyst during the activity. It can be, concluded that enhanced photodegradation is directly related to the reduced particle size of the ferrite, which implies that photosensitization is the process primarily involved. The photocatalytic activity goes on decreasing with substitution of Mn content. Therefore, this study reveals that Copper Ferrite shows better photocatalytic activity towards Methyl red as compared to other Copper Magnite.

Principal Investigator
Principal Investigator
(Minor Research Project)

PRINCIPAL
Shri Shivaji Mahavidyalaya,
Barshi, Dist. Solapur-413411

21

Scanned by CamScanner

Annexure – VII

UNIVERSITY GRANTS COMMISSION

BAHADUR SHAH ZAFAR MARG

NEW DELHI – 110 002

PROFORMA FOR SUBMISSION OF INFORMATION AT THE TIME OF SENDING THE FINAL REPORT OF THE WORK DONE ON THE PROJECT

1. Title of the Project: "**Photo-Catalytic Degradation of some dyes by nanoparticles :Kinetics and mechanistic study**"

2. NAME AND ADDRESS OF THE PRINCIPAL INVESTIGATOR: **Mr. S. G. Jadhav, Department of Chemistry, Shri Shivaji Mahavidyalaya Barshi**

3. NAME AND ADDRESS OF THE INSTITUTION :**Shri Shivaji Mahavidyalaya Barshi, Dist: Solapur 413411.**

4. UGC APPROVAL LETTER NO. AND DATE: **47-630/13 dated 28-01-2015**

5. DATE OF IMPLEMENTATION: **28-01-2015**

6. TENURE OF THE PROJECT: **Two years (28-01-2015 to 27-01-2017)**

7. TOTAL GRANT ALLOCATED : **305000/-**

8. TOTAL GRANT RECEIVED: **245000/-**

9. FINAL EXPENDITURE : 311265/-

22

Scanned by CamScanner

10. TITLE OF THE PROJECT : "**Photo-Catalytic Degradation of some dyes by nanoparticles :Kinetics and mechanistic study**"

11. OBJECTIVES OF THE PROJECT :

- **To synthesize TiO2 , ZnO, AgO etc. catalyst and to characterize the same.**
- **To study the oxidation of some dyes like malachite green, Indigo dye, methyl orange, methyelene blue, rhodamine B etc. by TiO2 ZnO, AgO etc. nanoparticles.**
- **To develop benign process for degradation of dyes.**

12. WHETHER OBJECTIVES WERE ACHIEVED (GIVE DETAILS):

a) Nanoparticles of ZnO and mixed metal oxides were synthesized and characterized by IR, XRD, TGA, SEM, EDAX etc.

b) The degradation of methyl orange, rhodamine-B etc. by nanoparticles were studied

c) On the basis of experimental results, the mechanism for these reactions were proposed.

13. ACHIEVEMENTS FROM THE PROJECT

i) **Preparation of the ZnO and mixed metal oxide nanoparticles.**
ii) **The characterizations of these nanoparticles.**
iii) **The study of photocatalytic applications of these nanoparticles for dye degradations and the mechanism for these reactions were proposed.**

14. SUMMARY OF THE FINDINGS (IN 500 WORDS):

Scanned by CamScanner

We have employed ZnO nanorods for its photocatalytic activity in the degradation of methyl orange and rhodamine-B. The microwave assisted method is very simple to implement, which can be easily extended to the preparation of other oxide nanoparticles also. It was found that the ZnO nanorods prepared by microwave assisted method played the key role in the photocatalytic performance through studying the degradation efficiency of ZnO photocatalyst. The shape of ZnO is nanorods with wurtzite structure. As the annealing temperature increases the particle size and crystallinity increases. Annealing temperature for the ZnO was reduced as low as 200°C. Also the SEM images of the samples with and without microwave irradiation show the possible role of microwave irradiation in controlling shape and size of nanorods. The photocatalytic results indicated that the catalyst loading and pH values affected the degradation efficiency of ZnO nanorods. Obviously, we learned that the photodegradation efficiency might be increased with the increase of catalyst loading. The 95% photocatalytic decomposition of methyl orange is most efficient at pH 7 and 0.2g/ dm3 loading of catalyst.

The catalytic activity of the photocatalyst, MnCopper Ferrite nanoparticles was studied by following the rate of photodegradation of Methyl Red. The experiment of photocatalytic reaction was conducted in a 100-ml Pyrex glass vessel with magnetic stirring and a UV lamp (8W, with the main wavelength of 253.7nm) positioned over the glass beaker. The as-prepared substituted MnCopper Ferrite nanoparticles were used as photocatalyst during the activity. It can be, concluded that enhanced photodegradation is directly related to the reduced particle size of the ferrite, which implies that photosensitization is the process primarily involved. The photocatalytic activity goes on decreasing with substitution of Mn content. Therefore, this study reveals that Copper Ferrite shows better photocatalytic activity towards Methyl red as compared to other Copper Magnite.

15. CONTRIBUTION TO THE SOCIETY (GIVE DETAILS)

Wastewaters containing dyes and organic pollutants from dyeing and finishing industry represent an increasing and worldwide environmental hazard. It has been estimated that over 15% of the total world production of dyes is lost in their synthesis and dyeing process. Azo dyes are synthetic organic dyes used in large quantities in several industries such as textile, cosmetic, paper, drug and food processing. They are the largest group of synthetic colorants known and difficult to degrade by biological

Scanned by CamScanner

treatments due to their complex structure and their stability. Most of these dyes are carcinogenic, harmful and reduce the light penetration in aqueous systems; thus causing a negative effect on photosynthesis and are harmful to human health. The complete removal of the pollutant from wastewater is therefore necessary and subject of widespread research. Photocatalytic degradation of dyes using nanoparticles will contribute to solve these issues.

16. WHETHER ANY PH.D. ENROLLED/PRODUCED OUT OF THE PROJECT: **N/A**

17. NO. OF PUBLICATIONS OUT OF THE PROJECT : **No**

PRINCIPAL INVESTIGATOR
Principal Investigator
Minor Research Project)

PRINCIPAL
Shri Shivaji Mahavidyalaya,
Barshi, Dist. Solapur-413411

25

Scanned by CamScanner

Introduction

Scanned by CamScanner

Introduction:

Advanced materials are the key in the development of civilization. Ferrites are the most widely used advanced materials in the magnets and it comprises 52% of the world market. Since the discovery of multiferroics, these materials have generated a great deal of interest both because of their magnetic and electric properties and application in electronic devices [1, 2]. Recently, there has been growing interest in the fabrication of synthetic multiferroics. Artificial synthesis of magneto electric devices promises to solve the problem of weak magneto electric coupling that exists in naturally occurring multiferroics, since the intrinsic electric and magnetic properties of the ferroelectric and ferromagnetic components allow for a measurable shift in the internal magnetization of the material when an external electric field is applied. Several groups have already attempted to fabricate composite ferroelectric/ ferromagnetic nanostructures [3].The advancement in ferrites is initiated by the work of Snock [4] who found that manganese zinc ferrite, copper zinc ferrite and nickel zinc ferrite provide a family of magnetic materials useful for radio and TV sets as well as carrier telephony as inductors, transformers and so forth.

Naturally occurring multiferroics such as Cr_2O_3, Ti_2O_3, $GaFeO_3$, $PbFe_{0.50}Nb_{0.50}O_3$, and numerous others have been widely investigated [5-8]. Although these materials exhibit the magneto electric effect, the changes are not significant enough to allow for large scale applications [9]. Mixed metal oxides possessing spinel structure have been investigated by a number of workers [10-13] as they exhibit interesting structural, electrical and magnetic properties. These properties are dependent on the nature of ions, their charges and their distribution among tetrahedral and octahedral sites. Ternary oxides crystallizing with spinel structures were found to exhibit interesting solid state and catalytic properties.

Spinel Structures:

Unit cell of spinel ferrite AB_2O_4 consists of 32 oxygen,16 trivalent iron and 8 divalent metal ions. The unit cell has two types of interstices in between close packed anions

a) Tetrahedrally co-ordinated interstices (A site) which are surrounded by 4

Scanned by CamScanner

nearest oxygen ions

b) Octahedral co-ordinated interstices (B site) which are co-ordinated by 6 nearest oxygen ions

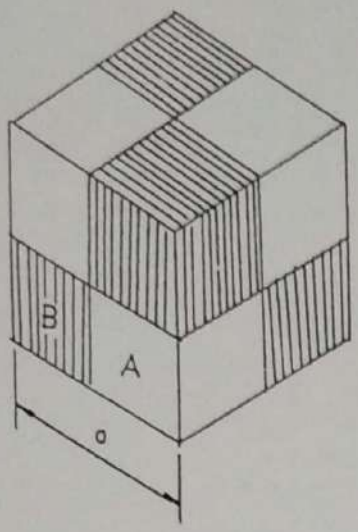

The shaded and non-shaded octants are occupied by octahedral & tetrahedral metal ions respectively.

1(a)

O oxygen
o A site ions
• B site ions

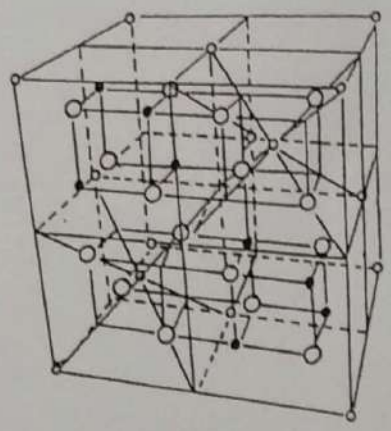

1(b)

Figure 1(a) eight octants in the unit cell
1(b) Unit cell of spinel lattice

Depending upon cation distribution in interstices the spinel is broadly divided into two groups,

A) Normal Spinel:

In this spinel structure all the 8 divalent metal ions occupy A sites and all the 16 trivalent ions occupy B sites [14]. In this metal oxide the divalent metal ions occupy

Scanned by CamScanner

site A and consequently there is no AB interaction. The negative BB interaction now makes itself felt and trivalent iron ions aligns themselves in anti parallel fashion, producing net magnetization zero [15] e.g.$ZnFe_2O_4$.

B) Inverse Spinel:

In inverse spinel structure, all the 8 divalent metal ions occupy B sites and 8 trivalent ions occupy A sites while remaining 8 trivalent ions occupy B sites [14]. In this structure the divalent ions occupy site B and trivalent ion is evenly divided between A and B sites.e.g.$CuFe_2O_4$ and $MnFe_2O_4$.

Substitution in Spinels:

In this some of the trivalent ions in spinel are replaced by trivalent ion of another metal. The effect of substitution on the magnetization of spinel depends on the site preferred by the substituent eg.Aluminium prefers the octahedral coordination and therefore reduces the magnetization of substituted ferrite and Gallium prefers tetrahedral site and increases the magnetization of substituted ferrite [15]. It has been reported that partial substitution of Fe by Cr in Cu ferrite leads to tetragonal distortion with $c/a > 1$, owing to Jahn-Teller effect [16] and rhombohedral distortion in Co substituted Ni-Zn ferrite has been reported [17].

Rare earth ions are divided into two categories, one with radius closer to Fe ions and other with radius greater than Fe ions [18]. This difference in the ionic radius will lead to micro strains which may cause domain wall motion resulting in deformation of the spinel structure [19]. Substitution of Fe^{3+} by Tb^{3+} and Dy^{3+} in the cobalt ferrite has been reported to cause an increase in the coercive field to about 2kOe (~30% increase) [18], due to the contribution from the large single ion anisotropy from the rare earth sub lattice. Substitution of rare earth ion into the spinel structure has been reported to lead to the structural distortion [19-21] and to induce strains in the material and significantly modify the electrical and magnetic properties. Substitution of rare earth into the spinel lattice results in the changes in the magnetization and Curie temperature [22]. The occupations of rare earth ions on B sites of spinel were found to be responsible for the increase in the resistivity [23]. Small increase in the hyperfine field parameter was reported for rare earth substitution

Scanned by CamScanner

in the spinel [24]. Gd substitution in Ni-Mn ferrite causes decrease in the crystalline size [25] and Nd substitution was reported to cause negative effect on magnetic and structural properties [26]. Curie point shift to lower temperature and decrease in the conductivity was reported due to substitution of Yb, Er, Dy, Tb, Gd and Sm [27]. Increase in the rare earth substitution in the ferrite affects the relative density of sintered bodies negatively and lattice parameters positively [28]. Decrease in the molar magnetic susceptibility for rare earth substituted ferrites was reported [22]. In some circumstances increase in the conductivity due to rare earth substitution (Gd) while in some case decrease in the conductivity due to rare earth substitution (Yb) was reported [29]. Sm substitution in the ferrite was reported to cause the decrease in the average grain size and increase in the coercive field [30]. Doping of Cu-Zn ferrite with Sm, La, Nd, Gd and Dy shows high relative density and low porosity [31]. Mossbauer spectroscopic study for Sm and Nd doped ferrite was reported [32].

Properties of Spinel Ferrite:

I) Electrical Properties:

The electrical properties of magnitisable substances play vital role in many electro-technical applications. It depends on the method of preparation, sintering temperature and sintering span, chemical composition and type of substitution [33]. The ferrites such as cobalt ferrite, nickel ferrite, magnesium ferrite behave as semiconductors with low mobility of charge carriers. The conventional band theory fails to predict the semiconducting properties of these materials. In such cases, the conduction has to be explained on the basis of the hopping mechanism. Alloys have higher resistance and are therefore superior than metals where it is desired to reduce the eddy current [34]. Cu, Co, Ni when added to iron, it causes slight change in the resistivity of iron but when Si is added to iron, electrical resistance increases by six fold [12,35]. The temperature dependence of conductivity of magnesium ferrite has been investigated by Gillaud and Bertrand et al [36] and Bradbarn and Rigby [10]. Narshinhan [11] concluded that, in Mg Al Ferrite the most probable mechanism is electron hopping between Fe^{2+} and Fe^{3+} ions as,

$$Fe^{2+} \rightleftharpoons Fe^{3+} + e^{-}$$

Scanned by CamScanner

This process is expected to take place between two adjacent octahedral sites in a spinel lattice.

II) Magnetic Properties:

For the metal ion of first row of transition series, the magnetic properties originate from the very exposed 3d-orbitals. The intrinsic magnetic moments of atoms and molecules are composed of the victorial sum of orbital and spin moments of the unpaired electrons. Here three kinds of interactions are possible. They are spin-spin, orbital-orbital and spin-orbital interactions. The resultant magnetic moment can be calculated by means of Russell-Saunders coupling equation

$$\mu_{eff} = g\,\beta\,[J(J+1)]^{1/2} \qquad (1)$$

Where, β is Bohr magneton, J is the total angular momentum, which is the vertical sum of the total orbital angular momentum (L) and the total spin angular momentum (S). Ferrimagnetic materials with the moment of ions oriented in the same direction give rise to high values of magnetic moment while antiferromagnetic substances, with spins aligned in antiparallel fashion, show a resultant magnetic moment of zero value.

The magnetic properties of ferrites like saturation magnetization, susceptibility, hysteresis and permeability are intrinsic as well as structure sensitive. The intrinsic properties like susceptibility, saturation magnetization depend upon the nature of divalent metal ions where as structure sensitive properties like hysteresis behavior, resistivity, a. c. conductivity depend upon grain size and porosity. The details of magnetic behavior of ferrites were studied by Neel et al. [37]. Magnetic materials exhibit different kinds of magnetic ordering depending upon spin orientation. Hysteresis studies of ferrites give valuable data on saturation magnetization, coercive field force and remanance ratio. Ferrites are mainly classified in different categories based on their coercivity. Hysteresis properties are mainly dependent on crystal structure, cation distribution, chemical composition, sintering atmosphere, heat treatment and final fabrication. In ferrites, the metallic ions occupy two different sites i.e. tetrahedral and octahedral and there are three kinds of magnetic interactions between metallic ions. The magnetic interaction is explained by considering the

Scanned by CamScanner

intermediate O^{2-} ions and is known as super exchange interaction. Hence the exchange interaction between the neighboring atoms is indirect and takes place through non magnetic oxygen ions. It has been established that the interaction energies are negative and hence induce the antiparallel orientation, which gives lowest energy. An angle of 180° gives rise to the greatest exchange energy and the energy decreases very rapidly with increasing distance between the ions.

III) Mechanical Properties:

a) Porosity:

Porosity depends on the grade of ferrite [38]. The porosity has the effect on magnetic properties and low porosities are usually preferred. Some ferrites with porosity less than 1 are developed for specific application. The less porosity ferrites are used in the recording head which requires highly polished surfaces with greatest wear resistance. Ferrites with high permeability are used for transformer cores.

Porosity (P) of the sample can be determined by using the density of sample (d_s) and the x ray density (d_x) [30].

$$P = (1 - d_s / d_x) \qquad (2)$$

The porosity of the material is influenced by melting point of oxide, quality of oxide and sintering temperature. At higher sintering temperature the number of pores is reduced and due to this grains come in vicinity to each other and contact area between grains is enhanced which in turn decreases the porosity [39].

b) Density:

Porosity of the ferrites contributes effectively to the density [40-41]. The mechanical properties of ferrites are similar to the pottery, as it is prepared by the ceramics material formed by sintering. During sintering the oxides react to form crystallites or grains of the requisite composition and in this process the density of mass increases. This leads to imperfections and the sintered mass with voids within the grains and also at the grain boundries [38].

Advanced Oxidation Processes

Scanned by CamScanner

Advanced oxidation processes (AOP's), uniting together ozone and high output ultraviolet technologies, in conjunction with hydrogen peroxide and catalyst are successfully used to decompose many toxic and bio-resistant organic pollutants in aqueous solution to acceptable levels, without producing additional hazardous by-products or sludge which require further handling. Advanced oxidation processes involve the generation of hydroxyl (•OH) radicals which oxidize the pollutants. Advanced oxidation processes can be broadly classified into the following groups:

i) Homogeneous photocatalysis,

ii) Heterogeneous photocatalysis

i) Homogeneous photocatalysis

The applications of homogeneous photodegradation (single-phase system) to treat contaminated water, involves the use of an oxidant to generate radicals, which attack the organic pollutants to initiate oxidation. The major oxidants used are: Hydrogen peroxide (UV /H_2O_2), Ozone (UV /O_3), Hydrogen peroxide and Ozone (UV /O_3/ H_2O_2), Photo-Fenton system (Fe^{+3} / H_2O_2).

ii) Heterogeneous photocatalysis

Heterogeneous photocatalytic process consists of utilizing the near UV radiation to photo-excite a semiconductor catalyst in the presence of oxygen. Under these circumstances oxidizing species, either bound hydroxyl radicals or free holes, are generated as shown in Fig.1.6. Using photocatalysis, organic pollutants can be completely mineralized reacting with the oxidizers to form CO_2, water and dilute concentration of simple mineral acids. The process is heterogeneous because there are two active phases, solid and liquid. This process can also be carried out utilizing the near part of solar spectrum ($\lambda < 380$nm) which transforms into a good option to be used [140].

Scanned by CamScanner

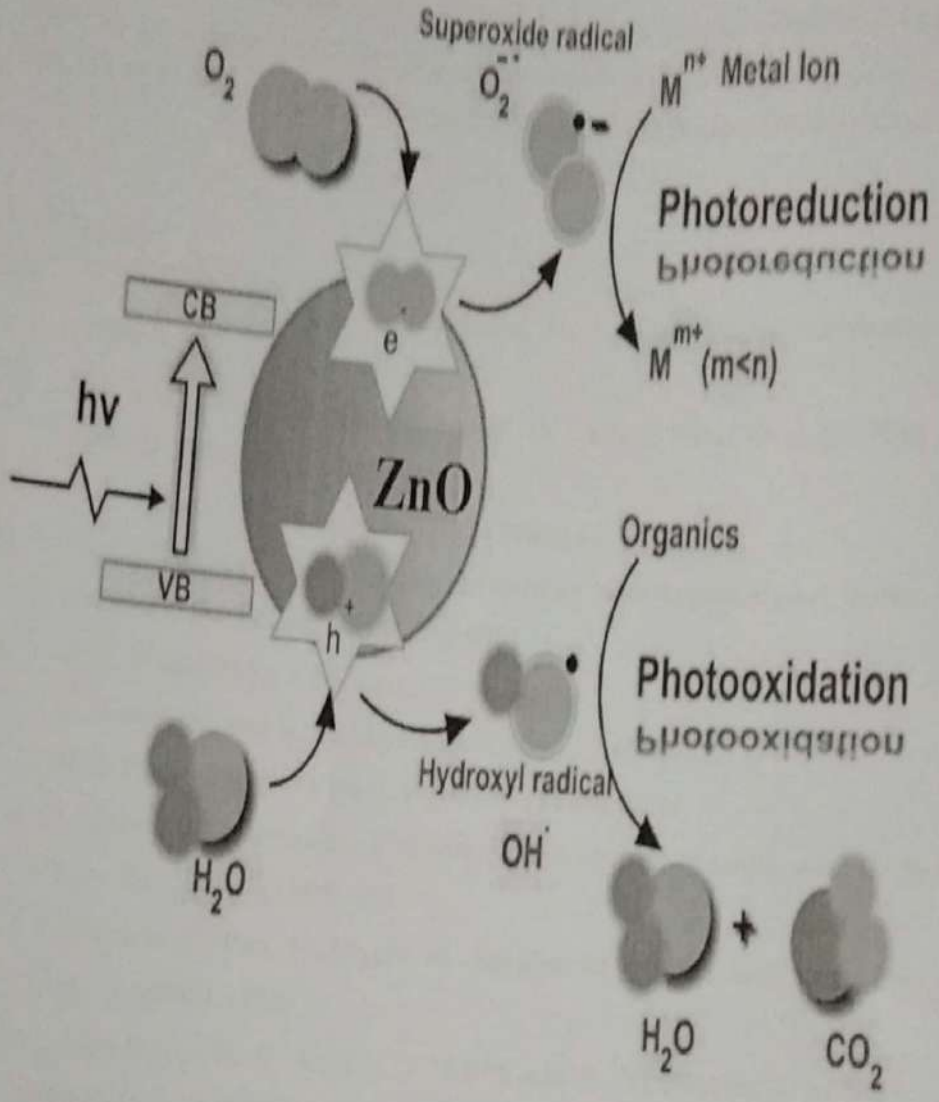

Fig.2 Scheme showing some of the events that might be taking place on an irradiated semiconductor particle

Scanned by CamScanner

The semiconductor may be in the form of a powder suspended in the water or fixed on a support. The most active photocatalyst for this application is the anatase form of TiO_2 /ZnO because of its high stability, good performance and low cost [42].

References:

[1] J. Ryu, S. Priya, K. Uchino and H. J. Kim, Phys. J. Electroceramics, 8 **(2002)** 112.

[2] M. Vopsaroiu, J. Blackburn and M. G. Cain, J. Phys. D: Appl. Phys., 40 **(2007)** 5027.

[3] J. P. Rivera, Ferroelectrics, 161 **(1994)** 165.

[4] E. C. Snelling, "Soft Ferrites, Properties and Applications", Butterworth and Co (Publishers) Ltd. London, **(1988)**.

[5] G. T. Rado, Phys. Rev. Lett., 13 **(1964)** 335.

[6] T. Watanabe and K. Kohn, Phase Trans., 15 **(1989)** 57.

[7] M. J. Fiebig, Phys. D: App. Phys., 38 **(2005)** R123.

[8] P. Calvani, M. Capizzi, F. Donato, S. Lupi, P. Maselli, and D. Peschiaroli, Phys. Rev. B, 47 **(1993)** 8917.

[9] S. Donthu, Z. Pan, B. Myers, G. Shekhawat, N. Wu and V. P. Dravid, Nano Lett., 5 **(2005)** 1710.

[10] C. Upadhyay, H. C. Verma, V. Sathe and A. V. Pimple, J. of Mag. and Mag. Materials, 132 **(2007)** 271.

[11] D. S. Mathew and R. Juang, J. Chemical Engg., 129 **(2007)** 51.

[12] V. L. Mathe and R. B. Kambale, Mat. Res. Bull., 43 **(2008)** 2116.

[13] C. N. R. Rao and B. Raveau, second edition.,Wiley-VCH, New York, **(1998)** 373.

[14] W. H. Von Aulock, Handbook of microwave ferrite materials, Academic press, New york London, **(1965)**.

[15] S. Chickazumi and S. H. Charap, Physics of Magnetism, Krieger Malabar, **(1978)**.

Scanned by CamScanner

[16] L. G. Antoshina, A. N. Goryaga and E. N. Evstafieva, J. Magn. Magn. Mater.,185 **(1998)** 101.

[17] J. Kulikowski and A. Bienkowski, J. Magn. Magn. Mater., 26 **(1982)** 297.

[18] N. Rezlescu, E. Rezlescu, C. Pasnicu and M. L. Craus, J. Phys.: Condens. Matter, 6 **(1994)** 5707.

[19] S. Solyman, Cera. Intern.,32 **(2006)** 755.

[20] F. Cheng, C. Liao, J. Kuang, Z. Xu, C. Yan, L. Chen, H. Zhao and Z. Liu, J. Appl. Phys., 85 **(1999)** 2782.

[21] N. Rezlescu and E. Rezlescu, Solid State Communications, 88 **(1993)** 139.

[22] M. A. Ahmed, N. Okasha and M. M. E. Sayed, Cera. Intern., 33 **(2007)** 49.

[23] G. L. Sun, J. B. Li, J. J. Sun and X. Z. Yang, J. Magn. Magn. Mater., 281 **(2004)** 173.

[24] S. E. Jacobo, S. Duhalde and H. R. Bertorello, J. Magn. Magn. Mater., 2253 **(2004)** 272.

[25] L. Zhao, Y. Cui, H. Yang, L. Yu, W. Jin and S. Feng, Mat. Lett., 60 **(2006)** 104.

[26] L. Zhao, H. Yang, X. Zhao, L. Yu, Y. Cui and S. Feng, Mat. Lett., 60 **(2006)** 1.

[27] N. Rezlescu, E. Rezlescu, P. D. Popa and L. Rezlescu, J. Alloys and Compounds, 275 **(1998)** 657.

[28] M. A. Ahmed, E. Ateia and F. M. Salem, Physica. B: Cond. Matter, 381 (1-2) **(2006)** 144.

[29] E. Rezlescu, N. Rezlescu, P. D. Popa and L. Rezlescu, J. Magn. Magn. Mater., 290 **(2005)** 1001.

[30] A. C. Costa, M. R. Morelli and R. H. Kiminami, J. Mat. Sci., 39 **(2004)** 1773.

[31] A. A. Sattar, A. H. Wafik, K. Shokrofy and M. Tabby, Phys. Stat. Sol., 171 **(1999)** 563.

[32] M. H. Mahmoud and A. A. Sttar, J. Magn. Magn. Mater., 277 **(2004)** 101.

[33] E. J. W. Verwey, Semicond. Mat. Eds. R. W. Ditchbum and N. F. mott (Butterworth scientific Pub. London, **(1951)**.

[34] Dr. Ing. Carl Heck, "Magnetic materials and their applications," Butterworth

Scanned by CamScanner

Co. (Publishers) Ltd. London, **(1974)**.

[35] J. P. Jakubovics, Magnetism and Magnetic materials, 2nd Edition, Institute of Material, London., **(1994)**.

[36] J. M. Yang and F. S. Yen, J. Alloys and Compounds, 450 **(2008)** 387.

[37] Z. L. Wang and Z. C. Kang, Functional and Smart Materials: Structural Evolution and Structure Analysis, Springer, **(1998)**.

[38] E. C. Snelling, "Soft ferrites, Properties and Applications", Butterworth and Co. (Publishers) Ltd., London, **(1988)**.

[39] M. K. Moinuddin and S. Ramana Murthy, J. Alloys and Compounds, 194 **(1993)** 105.

[40] A. Goldman, "Modern Ferrite Technology," Van Nostrand Reinhold, New York, **(1990)**.

[41] A. H. Morrish, "The Physical Properties of Magnetism", John Wiley and Sons, New York, **(1966)**.

[42] S. Malato, J. Blanco, A. Vidal, C. Richter, Appl. Catal. B: Environ., 37(2002) 1.

Scanned by CamScanner

Experimentals & characterization

Scanned by CamScanner

Synthesis of Mixed-Metal Oxides

The method of preparation of mixed-metal oxides can greatly influence the performance of the materials. Since mixed metal oxide material will consist of two or more metals, mixing will play a major role in the preparation. These applications mainly depend upon microstructure and surface properties of the fine powders which depend upon the method of preparation [1]. Mixed metal oxides are prepared by various methods such as sol-gel [2], hydrothermal [3], citrate precursor [4], co-precipitation [5] etc. A variety of oxides have been prepared in the last several years by the traditional ceramic method, which involves mixing and grinding of the powders of the constituent oxides, carbonates and other compounds and heating them at high temperatures with grinding when necessary. In order to achieve better control of structure, stoichiometry and phase purity with low energy consumption microwave assisted method is employed in the present investigation for the synthesis of mixed metal oxides.

Microwave Assisted Method

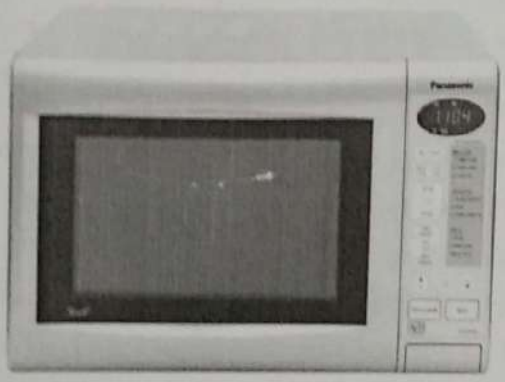

Fig.1 Photograph of Microwaveoven.

In the last decades, microwave heating has been applied in several areas as a very effective and non-polluting method of activation. Examples of this technology are materials processing, industrial and commercial applications, chemistry and biochemistry, among others. In the electromagnetic spectrum, the microwave radiation is located between infrared

Scanned by CamScanner

radiation and radio waves. The wavelengths are between 1mm and 1m with corresponding frequencies in the range of 300MHz to 300GHz. Besides telecommunication and microwave radar equipments occupy many of the band frequencies in this region, most routinely used, for industrial and scientific purposes are imposed by international convention be the 2.45GHz [6].

Microwave is a relatively new technology alternative for materials processing that provides new approaches for enhancing the material properties as well as economic advantages through energy saving and acceleration of product development. Clearly, advantages in utilizing this technology includes penetration of radiation, controlled electric field distributions, rapid heating, self-limiting reactions and selective and volumetric heating [7]. Depending on the response to microwave heating, materials can be classified into three principal groups with respect to their interaction with a microwave field: transparent or low loss materials where microwaves pass through them without any losses; conductors which reflect microwaves without any penetration; absorbing or high loss materials, which absorb microwaves and dissipate the electromagnetic energy as heat, depending on the value of the dielectric loss factor. Microwave heating of dielectric materials lies in the ability of the electric field to polarize the charge of the material where polarization cannot follow the rapid change of the electric field [8].

Microwave heating offers several potential advantages over conventional heating for inducing or enhancing chemical reactions. These include direct microwave interaction with certain classes of molecules, volumetric heating rather than heat flow through the vessel wall, less waste heat, increased control over heating rates and the possibility of selective enhancement of desired reactions. This is particularly attractive in the case of catalytic reactions, where it may be possible selectively to promote desirable reactions while suppressing undesirable ones. Also, as a fast, simple and energy efficient method, microwave synthesis has been developed and is widely used for the synthesis of zeolites and ceramic materials. During the synthesis there is a transfer of energy from microwaves to the material either through resonance or through relaxation there is an interaction of molecular dipole moment with high frequency electromagnetic radiation which results in rapid heating. In general material fall into three categories, with respect to their interaction with microwave radiations

Scanned by CamScanner

i) Microwave reflectors such as bulk metals and alloys.

ii) Microwave transmitters which are transparent to microwave like quartz, zircon, ceramics etc.

iii) Microwave absorbers, which constitute the most important class of materials for microwave synthesis, they take up the energy from microwave field and heat up very rapidly.

Compared with conventional methods, microwave synthesis has the advantages of very short reaction times, production of small particles with a narrow particle size distribution and high purity. These conveniences could be attributed to fast homogeneous nucleation and ready dissolution of the gel. Unfortunately the exact nature of the interaction of the microwaves with the reactants during the synthesis of materials is somewhat uncertain and speculative. However, it is well known that the interaction between dielectric materials, liquids or solids and the microwaves lead to what is generally known as dielectric heating in which electric dipoles in such materials respond to the applied electric field. In liquids, this constant reorientation leads to a friction between the molecules, which subsequently generate heat. Many microwave phenomena are poorly understood such as non-thermal effects and the superheating effect [6-8].

Characterization Techniques

I) X-ray Analysis

The most powerful tool available for the study of inorganic compounds is X-ray Diffraction technique. X-ray was discovered by Roentgen in 1985 and was invented in the year 1912 by Bragg. X- ray diffraction technique has emerged for the determining of the crystal structure, lattice parameters, stress measurements, phase equilibria and particle size [9-13].

The X-ray is electromagnetic radiations and wavelength of X-rays used in diffractions lies approximately in the range 0.5 to 2.5Å. X- ray diffraction is one of the most interesting

Scanned by CamScanner

and informative property of X-rays. The phenomenon explained as the scattering of X-ray by atoms accompanying variations in intensity in different directions due to the interference effect. They are produced when any electrically charged particle of sufficient kinetic energy is rapidly accelerated or suddenly stopped. In X-ray tube rapidly moving electrons strikes anode and at the point of impact X-rays are produced radiating in the all directions.

X-rays primarily interact with electrons in atoms. When X-ray photons collide with electrons, some photons from the incident beam will be deflected away from the direction where they originally travel. If the wavelength of these scattered X-rays did not change, the process is called elastic scattering in that only momentum has been conserved in the scattering process. The X-rays that are measured in diffraction experiments, as the scattered X-rays carry information about the electron distribution is strongly modulated by this interaction. When the X-ray beam strikes a stack of layers (array of atoms in the crystal), each layer produces a reflected beam. If all of these are in phase, then the diffracted beam will arise from the stack and for this to occur, the distance traveled by waves reflected from successive layers must differ by a whole number of wavelength. The angle between diffracted and transmitted beam is always 2θ. The relation between interplaner spacing "d" and angle θ is given by Bragg's law [14].

Generation of X –ray

X-rays are short-wavelength, high energy electromagnetic radiation, having the properties of both waves and particles. They can be described in terms of both photon energy (E) or wavelength (λ) and frequency (ν). The relation between energy, frequency or wavelength in the case of photon is:

$$E = h\upsilon = hc/\lambda \qquad \text{---------- (2.1)}$$

X-rays are produced whenever high energy electrons strike with metal target, any X-ray tube must contain (a) a source of electron (b) a high accelerating voltage (c) a metal target. All X-ray tubes contain two electrodes, an anode (the metal target) usually maintained, at ground potential, and a cathode maintained, at negative potential, normally of the order 30

Scanned by CamScanner

to 50 KV for the diffraction work. Interaction that occur between the beam (i.e. electron) and target will result in a loss of energy. A continuous spectrum is formed when the high energy electrons are slowed down rapidly by multiple collisions with the anode material, which give rise to white radiation, or so called Bremsstrahlung.

Bragg's Law

Since atoms are arranged periodically in a lattice, X-rays scattered from a crystalline solid can constructively interfere, producing a diffracted beam through these atoms. In 1912, W. L. Bragg recognized a predictable relationship among several factors. These factors are combined in Bragg's law:

$$n\lambda = 2d \sin\theta \qquad \text{---------- (2.2)}$$

n= order of diffraction.

d = interplaner distance in Å

θ = scattering angle in degree

λ = wavelength of the X-ray (Cu Kα 1-5406Å)

Block diagram of X ray Diffractometer and schematic diagrams of X ray Diffractometer are given in Figs. 2 and 3 respectively.

Scanned by CamScanner

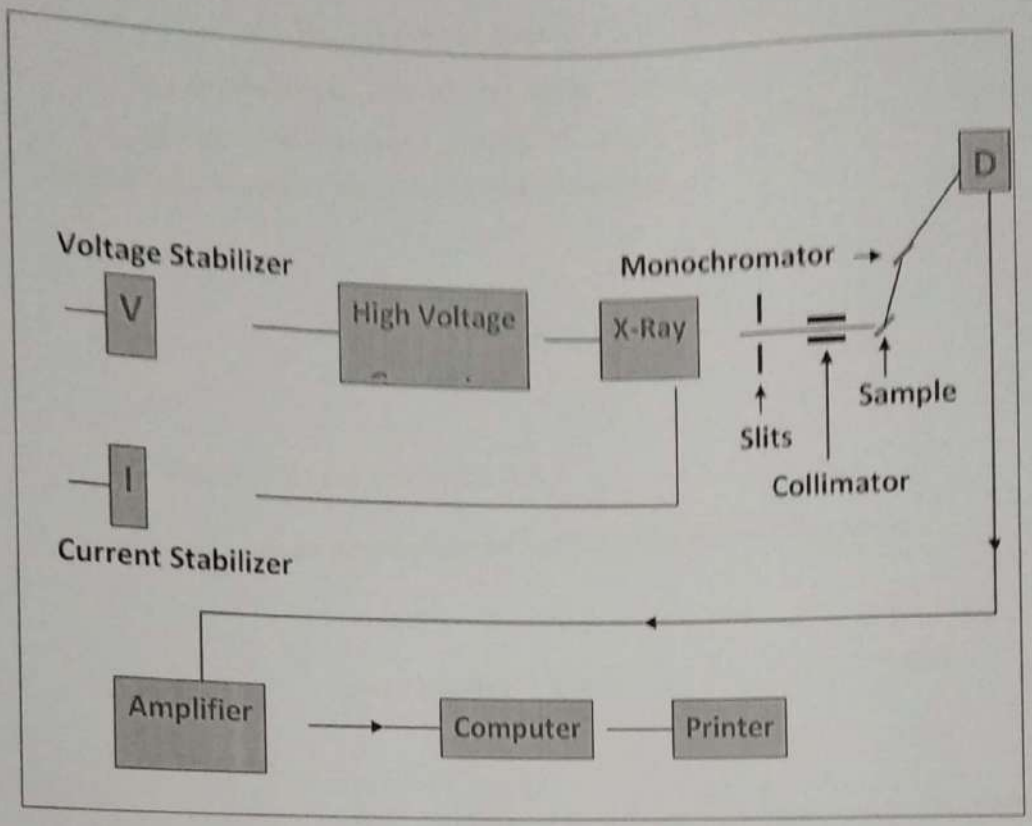

Fig 2 Block diagram of X-ray Diffractometer

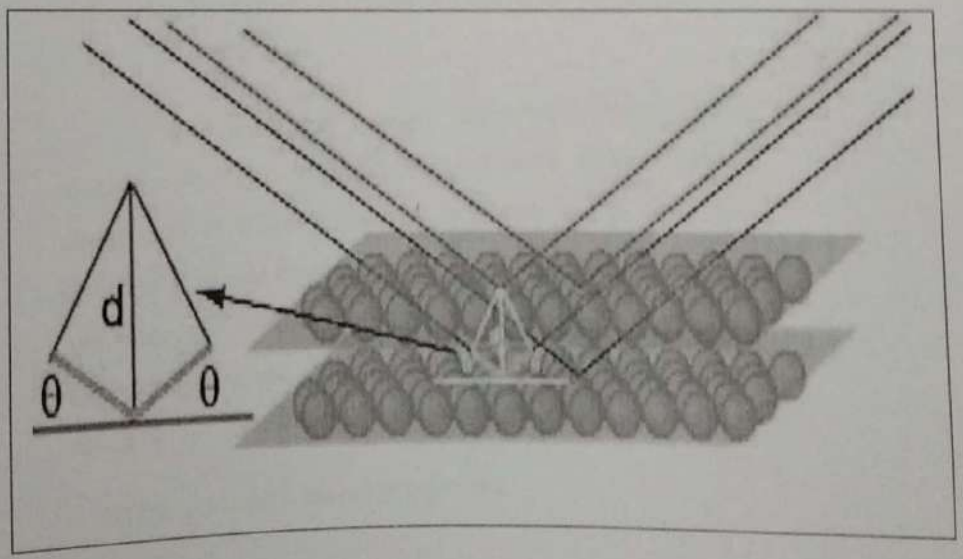

44

Scanned by CamScanner

Fig. 3 Schematic diagram of X-ray diffraction

The diffractograms were recorded within the range of 2θ between 20° to 80°. For cubic structure, the interplaner distance 'd', lattice constant 'a' and the Miller indices [hkl] of reflecting planes are related [15] by the equation

$$1/d^2 = h^2 + k^2 + l^2 / a^2 \qquad \text{---------- (2.3)}$$

Where, a = Lattice parameter in Å

In cubic system lattice parameter can be obtained by using following equation,

$$a = \lambda / 2 \sin\theta \, (h^2 + k^2 + l^2)^{1/2} \qquad \text{---------- (2.4)}$$

Knowing the value of lattice parameter 'a' and 'd' values for other planes were calculated by usual procedure.

II) Fourier Transform Infrared (FTIR) Spectroscopy

FTIR stands for Fourier Transform Infrared, the preferred method of infrared spectroscopy. The prepared samples were characterized by FTIR spectroscopy. The photograph of FTIR instrument is shown in Fig. 4. In infrared spectroscopy, when IR radiation is passed through a sample, some of the infrared radiation is absorbed by the sample and some of it is transmitted. The resulting spectrum represents the molecular absorption and transmission, gives information of type of bonding in the sample. This makes infrared spectroscopy useful for several types of analysis.

- FTIR can identify unknown materials

Scanned by CamScanner

• FTIR can determine the quality of a sample

• FTIR can determine the amount of components in a mixture.

The original infrared instruments were of the dispersive type. These instruments separated the individual frequencies of energy emitted from the infrared source. This was accomplished by the use of a prism or grating. A grating is a more modern dispersive element which better separates the frequencies of infrared energy. The detector measures the amount of energy at each frequency which has passed through the sample and results in a spectrum (Transmittance Vs frequency).

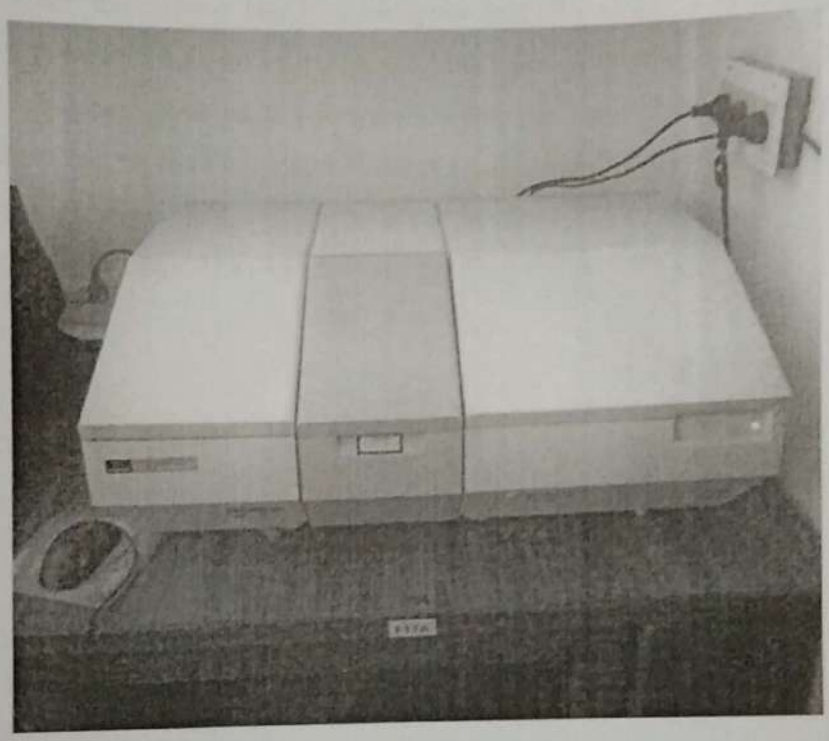

Fig.4 Fourier transform infrared (FTIR) spectroscopy

Fourier Transform Infrared (FTIR) spectrometry was developed in order to overcome the limitations encountered with dispersive instruments. The main difficulty was the slow scanning process. A method for measuring all of the infrared frequencies simultaneously, rather than individually, was needed. A solution was developed which employed a very

Scanned by CamScanner

simple optical device called an interferometer. The interferometer produces a unique type of signal which has all of the infrared frequencies "encoded" into it. The signal can be measured very quickly, usually on the order of second. Thus the time element per sample is reduced to a matter of a few seconds rather than several minutes.

Infrared spectroscopy deals with the energy changes corresponding to vibrational transitions in a molecule. If we take an example of a molecule consisting of two atoms, then when they come together to form a bond, they experience an attractive force between the nucleus and the electron cloud; at the same time they impart a repulsion due to the like charges present in both the nuclei as well as the electron cloud. Thus there is a compromise where the system stabilizes at distance when both the atoms are at equilibrium distance (r_{eq}). Any distortion to the bond length implies a change in the internuclear distance, thus this compression and extension of the bond can be thought to be analogous to that of a spring obeying Hooke's law. Thus we may write as,

$$F = -k\,(r - r_{eq}) \qquad \text{------- 2.6}$$

where,

F is the restoring force

k is the force constant

r is the internuclear distance

Classically this is an example of a simple harmonic model whose oscillation frequency is related as,

$$\upsilon = (1/2\pi)(k/\mu)^{1/2} \qquad \text{------- 2.7}$$

where,

μ = reduced mass

Scanned by CamScanner

k the force constant.

At temperatures above absolute zero, all the atoms in molecules are in continuous vibration with respect to each other. When the frequency of a specific vibration is equal to the frequency of the IR radiation directed on the molecule, the molecule absorbs the radiation. Each atom has three degrees of freedom, corresponding to motions along any of the three Cartesian coordinate axes(x, y, z). A polyatomic molecule of n atoms has 3n total degrees of freedom. Additionally, three degrees of freedom correspond to rotation of the entire molecule. Therefore, the remaining (3n – 6) degrees of freedom are true, fundamental vibrations for nonlinear molecules. Linear molecules possess (3n – 5) fundamental vibrational modes because only two degrees of freedom are sufficient to describe rotation. Among the (3n – 6) or (3n – 5) fundamental vibrations (also known as normal modes of vibration), those that produce a net change in the dipole moment may result in an IR activity. Thus any linear molecule having 3 atoms should theoretically possess four normal modes of vibration (symmetric stretching, bending, asymmetric stretching and binding). Hence it is possible to identify the presence of functional groups in a molecule.

III) Absorption Spectroscopy

Absorption spectroscopy measures the ranges of wavelengths of light a material can absorb, which is called the absorption spectrum. A typical absorption set up is as shown in Fig. 5.

Scanned by CamScanner

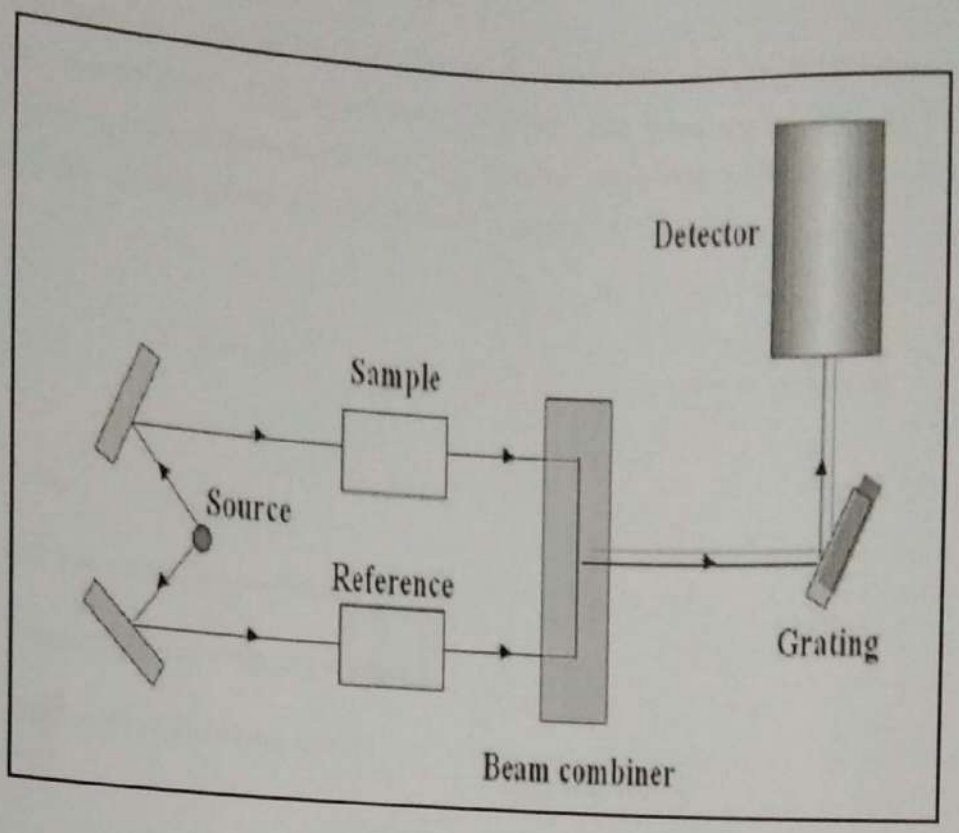

Fig.5 Schematic representation of the UV-Visible spectrophotometer

In today's spectrophotometer both deuterium and tungsten lamps are used as a source for characterization in the UV and visible regions respectively [16]. However xenon arc lamp can also be used which can serve the purpose for both UV and visible region. In such a dual beam spectrophotometer, light from either the visible or the ultraviolet source enters the grating monochromator before it reaches the filter. Broadband filters contained in a filter wheel are automatically indexed into position at the required wavelengths to reduce the amount of stray light and unwanted orders from the diffraction grating. The light from the source is alternatively split into one of two beams by a rotating mirror called a chopper which is shown in the Fig.5. The one beam is passed through the sample and the other through the reference. Double beam spectrophotometer has two detectors, and the sample and reference beam are measured at the same time. In other instruments, the two beams pass through a beam chopper which blocks one beam at a time. The detector, which is often a photodiode, alternates between measuring the sample beam and the reference beam. UV-Visible

Scanned by CamScanner

spectroscopy has been widely used during the characterization of the formation of metal oxide nanoparticles. The absorbance recording has been performed on UV-Visible spectrophotometer (Shimadzu 3600). The software associated with detector calculates the absorbance coefficient using Beer-Lamberts formula [17]:

$$A = \square bc \qquad \text{---------- (2.8)}$$

where,

□□□□ constant of proportionality

c = concentration of absorbing species

b = path length of absorbing species

Beer-Lamberts law states that absorbance is directly proportional to the path length 'b' and the concentration, c, of the absorbing species. Absorbance can also be calculated by using the formula [17].

$$A = \log_{10} (I_0 / I) \qquad \text{---------- (2.9)}$$

Where,

I_0 is the intensity of incident light and

I is the intensity of transmitted light.

IV) Scanning Electron Microscopy

Scanned by CamScanner

The scanning electron microscopy (SEM) is a most widely used tool for surface characterization of materials, especially for nanomaterials. SEM uses electron beam rather than light to examine a material and form image. The advantage of SEM over traditional optical microscope is that it has a large depth of field and high resolution, which allows to focus on fine particles and study closely spaced features [18]. For this study, a field emission scanning electron microscope (FESEM) was used. SEM consists of an electron gun, electronically controlled lens and apertures, X-ray detector and a sample chamber. Figure 6 shows the schematic diagram of a scanning electron microscope. The sample is placed on the sample stage inside the sample chamber, which is vacuumed before applying the electron beam. The electron gun located at the top of the column generates a beam of electrons, which is guided down the column using the gun alignment control. The beam is condensed by a pair of condensing lens and focused on the sample using an objective lens. A magnetic field is created by energizing the scan coils to deflect the electron beam back and forth in a controlled pattern. When the beam touches the surface of the sample, it produces secondary electrons. These induced secondary electrons are collected by an appropriate detector and is converted into a voltage signal. The varying voltage produced by the scan coils that creates the patterns on the surface of the sample, and the detected voltage signal from the sample are applied to the cathode ray tube (CRT), which creates the image on the screen. The quality of the image depends on the number of secondary electrons generated, which in turn depends on the energy of the electron beam generated by the gun. The voltage and current parameters of the gun are adjusted to get a good resolution image.

Scanned by CamScanner

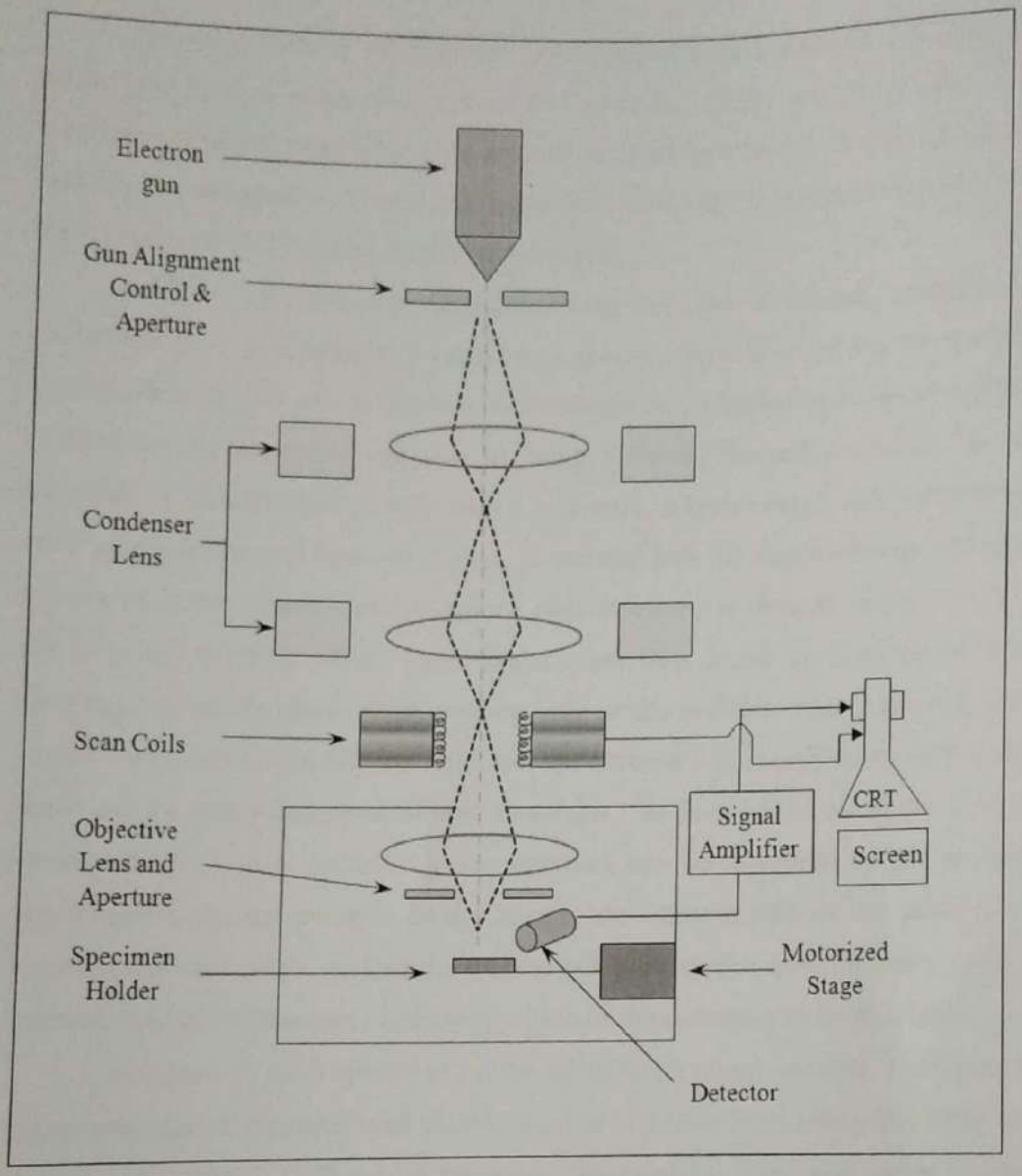

Fig.6 Schematic diagram of a scanning electron microscope

V) Energy Dispersive X-ray Spectroscopy

There are four primary components of the EDS set up:

1) Beam source
2) X-ray detector
3) Pulse processor
4) Analyzer

Scanned by CamScanner

Scanning electron microscopes are equipped with a cathode and magnetic lenses to create and focus a beam of electrons, and since the 1960s they have been equipped with elemental analysis capabilities. A detector is used to convert X-ray energy into voltage signals; this information is sent to a pulse processor, which measures the signals and passes them to an analyzer for data display and analysis.

EDS is an analytical technique used for the elemental analysis or chemical characterization of a sample. As a type of spectroscopy, it relies on the investigation of a sample through interactions between electromagnetic radiation and matter, analyzing X-rays emitted by the matter in response to being hit with charged particles. To stimulate the emission of characteristic X-rays from a specimen, a high energy beam of charged particles such as electrons, or a beam of X-rays, is focused into the sample being studied. At rest, an atom within the sample contains ground state electrons in discrete energy levels or electron shells bound to the nucleus. The incident beam may excite an electron in an inner shell, ejecting it from the shell while creating hole at the position of an electron from an outer, higher energy shell then fills the hole, and the difference in energy between the higher energy shell and the lower energy shell may be released in the form of an X-ray. The number and energy of the X-rays emitted from a specimen can be measured by an energy dispersive spectrometer. As the energies of the X-rays are characteristic of the difference in energy between the two shells, and of the atomic structure of the element from which they were emitted, this allows the elemental composition of the specimen to be measured.

Accuracy of EDS spectrum can be affected by many variants. EDS detectors cannot detect presence of elements with atomic number less than 5, meaning that EDS cannot detect H, He, Li, or Be[9]. Differing in the over-voltage of the EDS will result in different peak sizes and raising over-voltage on the SEM will shift the spectrum to the larger energies making higher energy peaks larger while making lower energy peaks smaller. Also many elements will have overlapping peaks (ex. Ti K_β and V K_α, Mn K_β and Fe K_α). The accuracy of the spectrum can also be affected by the nature of the sample.

Scanned by CamScanner

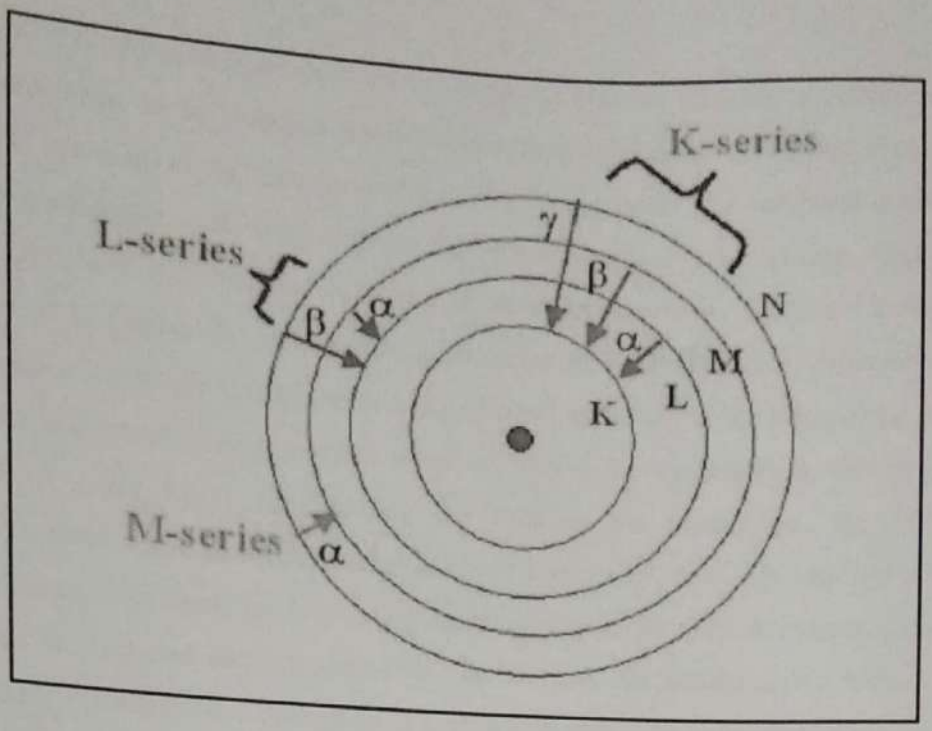

Fig.7 Schematic diagram showing the possible transition lines as obtained from an EDAX spectrum

An EDAX spectrum also shows the nature of X-rays emitted which means that a transition from the L-level to the K-level is known as the K_α line, transition from M-level to K-level is known as the K_β line and so on. This is shown in the Fig. 7. In this research work we have extensively used SEM for observing the morphology of hybrid-composites and the oxides. SEM measurements were performed on a JEOL, JSM-6360 Japan. Samples for SEM and EDAX analysis from the solutions at different stages of experiments discussed in this thesis.

VI) Transmission Electron Microscopy (TEM)

Principle and Instrumentation

The transmission electron microscope (TEM) operates on the same basic principles as the light microscope but uses electrons instead of light [19]. In TEM analysis, a thin

Scanned by CamScanner

specimen is illuminated with electrons in which the electron intensity is uniform over the illuminated area. As the electrons travel through the specimen, they are either scattered by a variety of processes or may remain unaffected by the specimen. The end result is that a non-uniform distribution of electrons emerges from the exit surface of the specimen that contains all the structural and chemical information about the specimen. Electron microscope is constructed to display this non-uniform distribution of electrons in two different ways. A "light source", typically a tungsten or LaB_6 filament at the top of the microscope emits the electrons that travel through vacuum in the column of the microscope as shown in Fig.8. Instead of glass lenses for focusing the light in the microscope, the TEM uses electromagnetic lenses to focus the electrons into a very thin beam. The electron beam then travels through the specimen. Depending on the density of the material present, some of the electrons are scattered and disappear from the beam. At the bottom of the microscope the unscattered electrons hit a fluorescent screen, which gives rise to a "shadow image" of the specimen with its different parts displayed in varied darkness according to their density. The image can be studied directly by the operator or photographed with a camera.

In the case of bright-field imaging an aperture is inserted into the back focal plane of the objective lens, thus blocking out most of the diffraction pattern except that which is visible through the aperture where as in dark-field imaging one or more of the diffracted beams is allowed to pass through and the direct beam are blocked by the aperture.

Scanned by CamScanner

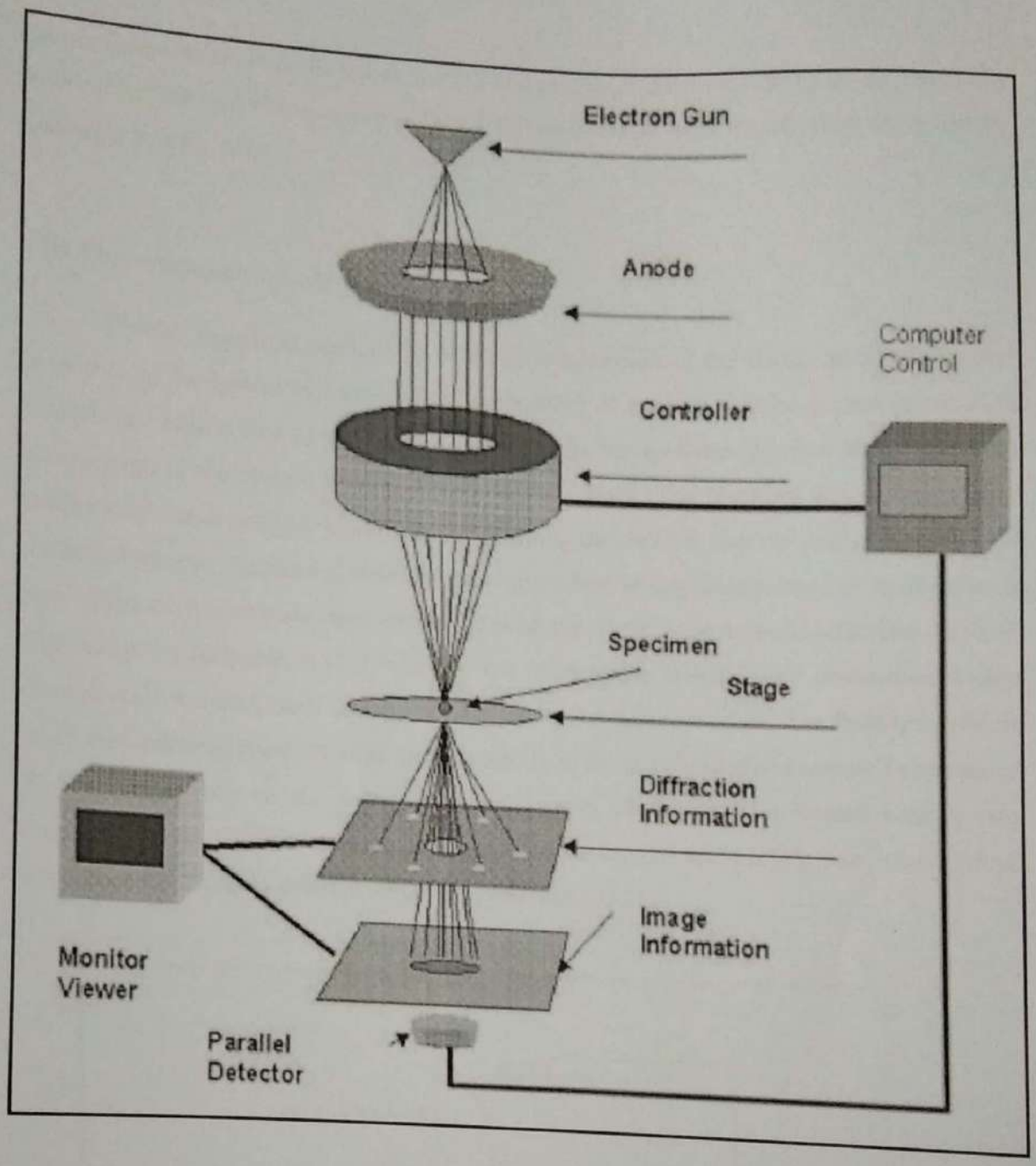

Fig.8 Schematic representation of the Transmission Electron Microscope

Some useful information like planar defects, stacking faults can be obtained through dark-field imaging. Bright field imaging depends on the mass-thickness of the sample. Areas of the sample that are thicker will have fewer transmitted (unscattered) electrons, hence will appear darker. In selected area electron diffraction (SAED), an aperture is used to define the area from which a diffraction pattern is formed in a TEM specimen. The resulting patterns

Scanned by CamScanner

contain information about the lattice spacing and sample orientation. The TEM measurements were carried out by TEM on a Tecnai 20 G2 FEI make (UGC-DAE Consortium for Scientific Research, Indore, India).

VII) Thermogravimetric Analysis

Thermo analytical methods involve the measurement of the change in some physical properties of the system as a function of temperature or time. Results of thermo gravimetric analysis are represented by a plot of weight changes versus temperature or time. The main components of the thermo balance are shown in a Fig.9. The resulting weight loss versus temperature curve provides information concerning the thermal stability and composition of the initial sample, the thermal stability and composition of any intermediate of the residue, if any. There are two characteristic temperatures of any single stage for non isothermal reaction. The inception temperature (Ti) which is the temperature at which the cumulative weight change reaches a maximum that can be detected by the thermo balance. The final temperature is Tf that indicates completion of the reaction. In a TG signal the characteristic temperature, Ti and Tf depends on the instrumental and sample parameters like furnace heating rate, recording speed, ambient atmosphere, amount of the sample and particle size. These effects have been discussed in detail at length in references [20-21].

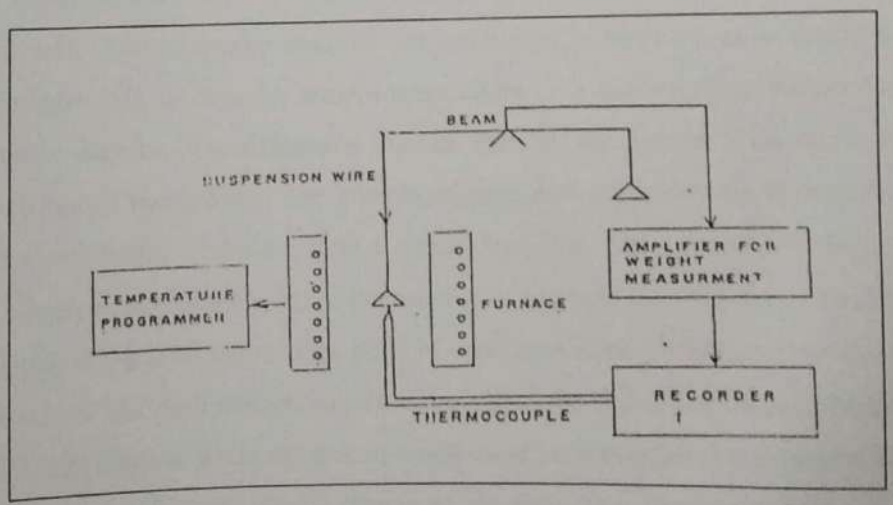

Scanned by CamScanner

Fig.9 Main Components of the Thermobalance

The TG instrument requires to be calibrated for weight as well as temperature. Weight calibration at room temperature is done with standard weight. Weight calibration at high temperature is done by registering the weight changes occurring in the thermal decomposition steps of some of the recommended materials such as calcium oxalate monohydrate. The calibration of the instrument with the standard compounds is necessary to correct for the apparent weight change arising due to connective flow of medium during heating of the furnace from room to high temperature [22], due to changing density of the gaseous environment around the sample or due to change in composition of the gas mixture. Temperature measurement in thermogravimetry is done using thermocouples made of chromel-alumel or platinum-rhodium. The thermocouples are calibrated by making use of Curie temperatures of some metals and their alloys [23] where apparent weight change is detected at the point of ferromagnetic to paramagnetic transition.

VIII) Differential Thermal Analysis (DTA)

DTA is a technique in which the temperature difference (ΔT) between the sample and a thermally inert reference material are continuously recorded as a function of furnace temperature (Tf), or time (t), sample temperature (Ts) and reference temperature (Tr). The schematic diagram of a differential thermal analyzer and typical DTA curve are shown in Figs.10 and 11 respectively. The initiation temperature represents the temperature where the DTA signal begins to deviate from a steady base line. The extrapolated onset temperature (Te) corresponding to the point of intersection of the base line with the tangent drawn to the rising part of the DTA curve at the point of maximum slope is often preferred to the initiation temperature. The peak temperature indicates either the end of the reaction or transformation or the temperature at which the rate of transformation is maximum and finally Tf denotes the temperature at which the signal returns to the base line. The temperature changes in the sample can be due to enthalpy changes caused by phase transitions, fusion decomposition reaction, oxidation or reduction reactions etc. The nature of the DTA curve and the

Scanned by CamScanner

magnitude of the peak depend on a large number of instrumental factors and also on sample characteristics.

The instrumental factor that influences the DTA signal are the geometry and material of the sample holder, nature of the thermocouple and its location, the heating rate and the atmosphere around the sample. The sample characteristics like the particle size, amount of sample used, its heat capacity, thermal conductivity and packing density also play vital role in affecting the DTA curve. Delineation of phase boundary using DTA is done by measuring evolution or absorption of heat accompanying phase changes, when the sample is heated or cooled at constant rate. The phase changes correspond to the melting and freezing of pure compounds or eutectics.

The DTA instrument requires calibration for both temperature and enthalpy. Several standard materials like pure materials and well characterized compounds have been recommended for these purposes. The melting point of metals like In, Zn, Sn, Sb, Ag and Au and phase transitions in Li_2SO_4, $BaCO_3$ etc. can be used for temperature calibration. Enthalpy calibration can be done using the heats of solid–solid transitions or fusion of the above materials or organic compounds of high purity.

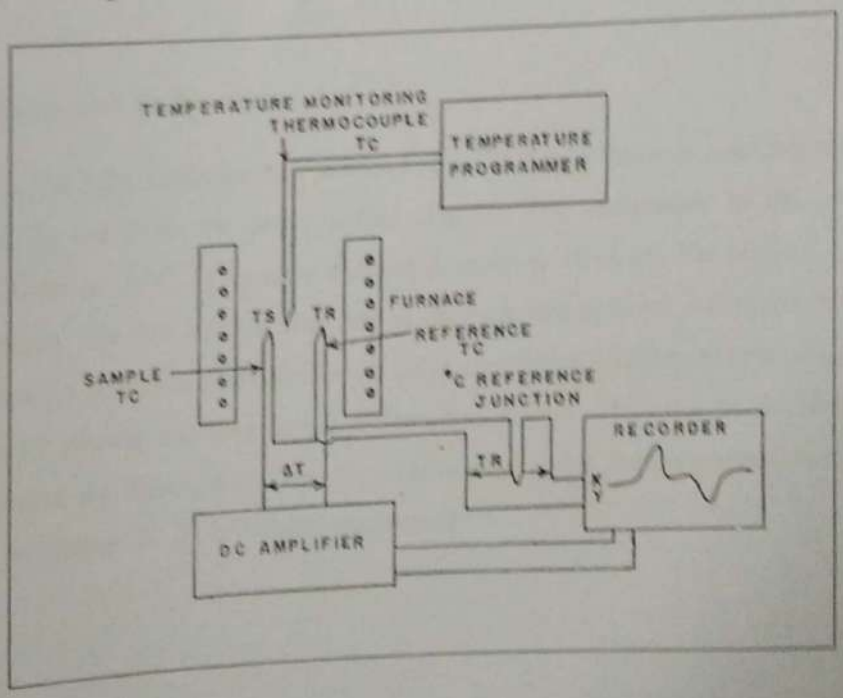

Fig.10 Block diagram for DTA

Scanned by CamScanner

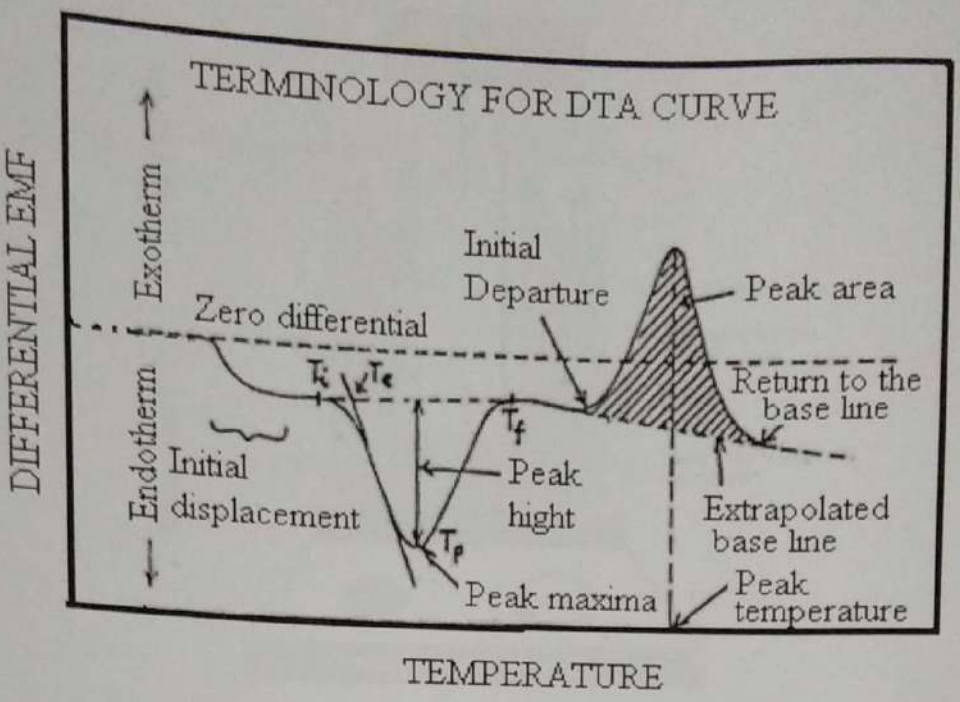

Fig.11 Schematic diagram of DTA curve.

IX) Photocatalytic Reactor

The light irradiation was provided by a 125 W high-pressure mercury lamp which was placed 10 cm above the slurry surface (Fig.12). The temperature of the suspension was maintained at 20°C by using a circulated water to eliminate the heating effect of light irradiation. The dye solution after adding photocatalyst powders was magnetically stirred in the dark for 30 min to establish the adsorption-desorption equilibrium prior the photoreaction. Magnetic stirring was kept during the reaction process. The color of the suspension faded along with the illumination. The degradation of dye and the decolorization of the solution were determined by a UV-Visible spectrometry

Scanned by CamScanner

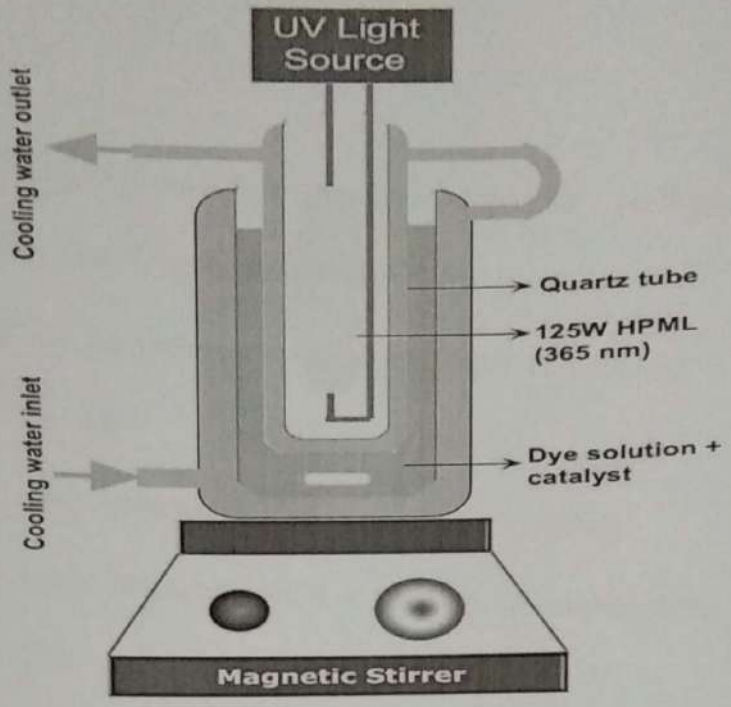

Fig. 12 Schematic representation of UV-Visible photocatalytic reactor

Scanned by CamScanner

References

[1] B. K. Das, Preparation and Characterization of Mater. (Ed), J. M. Honing, C. N. R. Rao, New York, Academic Press, (1981).

[2] S. Sunder, B. K. Srivastava, D. Krishnamurthy, Ind. J. Pure and Appl. Phys., 2 (2004) 366.

[3] T. Pannaparagil, Komarneni's, IEEE Trans. Mag., 15(1989)423.

[4] N. S. Gajbhiye, U. Bhattacharya and V. S. Darshane, Thermochim. Acta, 264 (1995) 219.

[5] B. A. Mulla and V. S. Darshane, Ind. J. Chem., 22 (1983) 143.

[6] M. Iwamoto, T. Abe, Y. Tachibana, J. Mol. Catal. A, 55 (2000) 143.

[7] L. Combemale, G. Caboche, D. Stuerga, D. Chaumont, Microwave Research Bulletin, 40 (2005) 529.

[8] K. Borgohain, N. Morase, S. Mahumani, J. Appl. Phys., 92 (2002) 1292.

[9] L. S. Dent, Glasser "Crystallography and its application" Van Nostrand Reinhold Company Ltd., London, (1977).

[10] L. V. Azaroff,"Elements of X-ray Crystallography" Mc. Graw Hill Company, New York, (1968).

[11] B. D. Cullity, Elements of X-ray diffraction, Addison-Wesely publishing Company, (1978).

[12] A. R. West, Solid State Chemistry and its applications, John Willy and Sons Pvt. Ltd., (1989).

Scanned by CamScanner

[13] B. E. Douglas and H. Darl, Mc Daniel, Concepts and Models of Inorganic Chemistry Oxford and IBH Publishing Co. PVT. Ltd., (1970).

[14] W. H. Bragg and W. L. Bragg, Proc. Roy. Sco. London, (A), 88 (1923) 428.

[15] A. E. Clark and E. P. Wolfhart "Ferromagnetic Materials" I Ed. Amsterdam: North-Holland, (1982), 531.

[16] R. D. Waldron, Phys. Rev., 99 (1955) 1727.

[17] S. O. Kasap, "Principles of Electronic Materials and Devices", II Ed.., Tata McGraw-Hill Publishing Ltd., P 376.

[18] D. Scharf, "Magnifications: Photography with the Scanning Electron Microscope", Schocken Books, (1977).

[19] R., B. Bangar, F. M. Winnik, Y. Morishima, Langmuir, 17 (2001) 4416.

[20] G. H. Jonker, J. Phys. Chem. Solids, 9 (1959) 165.

[21] T. Holestein, Ann.Phys., (Paris), 8 (1959)325.

[22] J. Livage, M. Henry and C. Sanchez, Prog. Solid State Chem., 77 (1992)153.

[23] J. M. Honig and C. N. R. Rao (Eds.) Preparation and Characterization of Materials, Academic Press, New York, (1981).

Scanned by CamScanner

Synthesis, characterizations and Photocatalytic activity of ZnO nanoparticles for dye degradation

Scanned by CamScanner

Introduction:

The unique and fascinating properties of nanostructure materials have triggered tremendous motivation among the scientist to explore the possibilities of using them in a wide range of possible applications such as photovoltaic energy conversion materials [1, 2] and water purification as a friendly environmental photocatalysts [3]. One material that has been in great interest from wide range of technological field associated with nanotechnology is zinc oxide (ZnO) [4]. ZnO has been used in various applications such as photo-electric devices [5], electronic devices [6], surface acoustic wave devices [7], field emitters [8], sensors [9], ultraviolet lasers [10] and solar cells [11]. Also zinc oxide, a II-VI semiconductor material with a large direct band gap (3.37 eV) and a relatively high exciton binding energy (60 MeV) at room temperature, has attracted considerable attention with respect to the degradation of various pollutants such as acid red 18 [12], 4-nitrophenol [13], acridine orange [14], azo dye [15] and so on, due to its being relatively cheap, good chemical stability [16].

In the past decades, photocatalytic techniques have been shown to constitute one of the most promising process for the wastewater treatment because of its advantages over the traditional techniques, such as quick oxidation, no formation of polycyclic products and oxidation of pollutants up to the parts per billion (ppb) levels. Methyl orange (MO) is an azo dye and has been widely used in textiles, foodstuffs, paper and leather industries. However, the release of MO and its products in the environment cause serious pollution problems. In almost all applications of nanomaterial device, fabrication represents one of the crucial aspects for the realization of the potential and commercialization. In this direction, chemists, in particular, have been developing a variety of synthetic methods. Among them microwave synthesis is important with respect to time, temperature, energy. However, the production of cheap, clean, reliable and durable materials with controlled properties for realistic and practical applications of nanotechnology.

Recent advances in nanoscale science and technology are fuelling a new wave of revitalization in the field of catalysis. Nanomaterials whose characteristic length scale lies in nanometric range i.e 1-100 nm. These materials display properties intermediate between molecular and bulk materials because of their size and large surface area to volume ratios. Nanomaterials are of ideal size for the unique catalytic properties. The researchers efforts gone so far indicate that the catalysis in nanosize range exhibit high catalytic activity.

Scanned by CamScanner

The environmental concerns and regulations have been increased in the public, political and economical world over the last two decades because the quality of life is strongly connected to a clean environment. Development of efficient catalytic process with nanostructured catalyst is the need of the time from economy as well as environmental view points. Nanomaterials as photocatalyst is an emerging area today. The discovery of nanoparticles has turned the whole field in a new direction. This has opened up another avenue and established a relationship between photosynthesis and photocatalysis, some oxides ZnO, TiO_2 and WO_3 have enough band gap energies to get excited by UV or visible light and the redox potential can promote a series of oxidation and reduction reactions.

The photocatalytic treatment of waste containing dyes has also been widely reported [17-18]. ZnO has attracted much attention with respect to the degradation of various pollutants because of its high photosensitivity, stability and wide band gap. Previous studies have proved that ZnO can degrade some organic pollutants under UV irradiation [19-20]. However, the fast recombination rate of the photo-generated electron and hole pairs may decrease the photocatalytic activity. The combination of transition metals (such as silver, platinum and iron) and semiconductor has been reported to improve the charge-transfer and photocatalytic activity [21-22].

Many researchers have highlighted on the performance of ZnO for photodegradation of some organic compounds [23-24]. In addition, ZnO has more efficiency than TiO_2 [25] and recent researches have pointed out that ZnO can also be used in the acidic or alkaline conditions by the proper treatment [26-27]. Therefore, continued study of ZnO is necessary and quite needed. It is well known that highly reactive OH• radicals and holes are generated on the surface of photocatalyst under the radiation of UV. Therefore, the surface characteristic of ZnO determined by the different methods will influence this property as well as the final degradation efficiency. The particle size of photocatalyst is one of the most important factors. There were many comparative studies about the photocatalytic efficiency of between TiO_2 and ZnO for degradation of pollutants, which emphasized the effectiveness of TiO_2 and ZnO [3, 28]. In these studies, Degauss (P-25) TiO_2 (mean diameter, 25 nm) and commercial ZnO (mean diameter, 200 nm) are the most commonly used effective photocatalysts. Besides that, the photocatalytic properties of colloidal ZnO nanoparticle with diameter in the range from 5 to 15 nm prepared by chemical deposition method are also

Scanned by CamScanner

discussed widely [29-30]. Nevertheless, the researches about the photocatalytic property of ZnO photocatalyst with diameter size 30–60 nm and micron size are still remained limitedly, especially the ZnO nanoparticles prepared by thermal evaporation that have a higher photocatalytic activity. In order to compare the photocatalytic property of ZnO with that of TiO_2 roundly, the research about the photocatalytic property of ZnO with different sizes is significant. Except for size, the morphology and fabrication methods of the photocatalyst are the other crucial factors that influence the degradation efficiency severely [31]. Demonstrating the relationship between the surface characteristics of photocatalyst and the photocatalytic activities of ZnO is beneficial to the development of catalyst and can be used as a photocatalyst with high photocatalytic activity.

Amongst various methods, researchers have reported the microwave assisted method [32-34]. By using PVA as a capping agent, it is possible to control shape and narrow size distribution of ZnO nanoparticles. The aim of study is to optimize the preparation of ZnO nanorods as a photocatalyst. The photocatalytic activities were evaluated using methyl orange as a model compound.

Scanned by CamScanner

Experimental

I) Reagents

Zinc nitrate, sodium hydroxide, high molecular weight Polyvinyl alcohol (PVA) (2000) and A.R. Grade methyl orange were purchased from Aldrich chemicals. All solutions were prepared in mili Q water.

II) Preparation of Photocatalyst

The nanosized ZnO rods were prepared by microwave-assisted sol-gel method. Aqueous solution of zinc nitrate (0.01M) and polyvinyl alcohol (1 % w/v) were mixed and the solution thus prepared was set to stir constantly with addition of (0.01M) solution of sodium hydroxide simultaneously for half an hour. After completion of the reaction, white precipitate of zinc hydroxide was obtained. The precipitated zinc hydroxide solution was kept for 10 minutes under microwave irradiation with a power output of 695 W by following on-off cycle. The solution was allowed to cool up to room temperature. The cooled solution was then centrifuged in presence of water and acetone to remove all the impurities. The process of centrifugation was repeated three times to remove most of the impurities from the solution and allowed to dry naturally. Annealing of the product was carried out at various temperatures for three hour in temperature controlled furnace. The pure annealed powder of ZnO is used for the characterization. The physiochemical properties solely depend upon preparation of materials. In our study it is planned that by using minimal energy to form complete growth of ZnO nanorods with desired size and shape. The schematic flow chart for the preparation of nanocrystalline ZnO is shown in Fig. 1.

Scanned by CamScanner

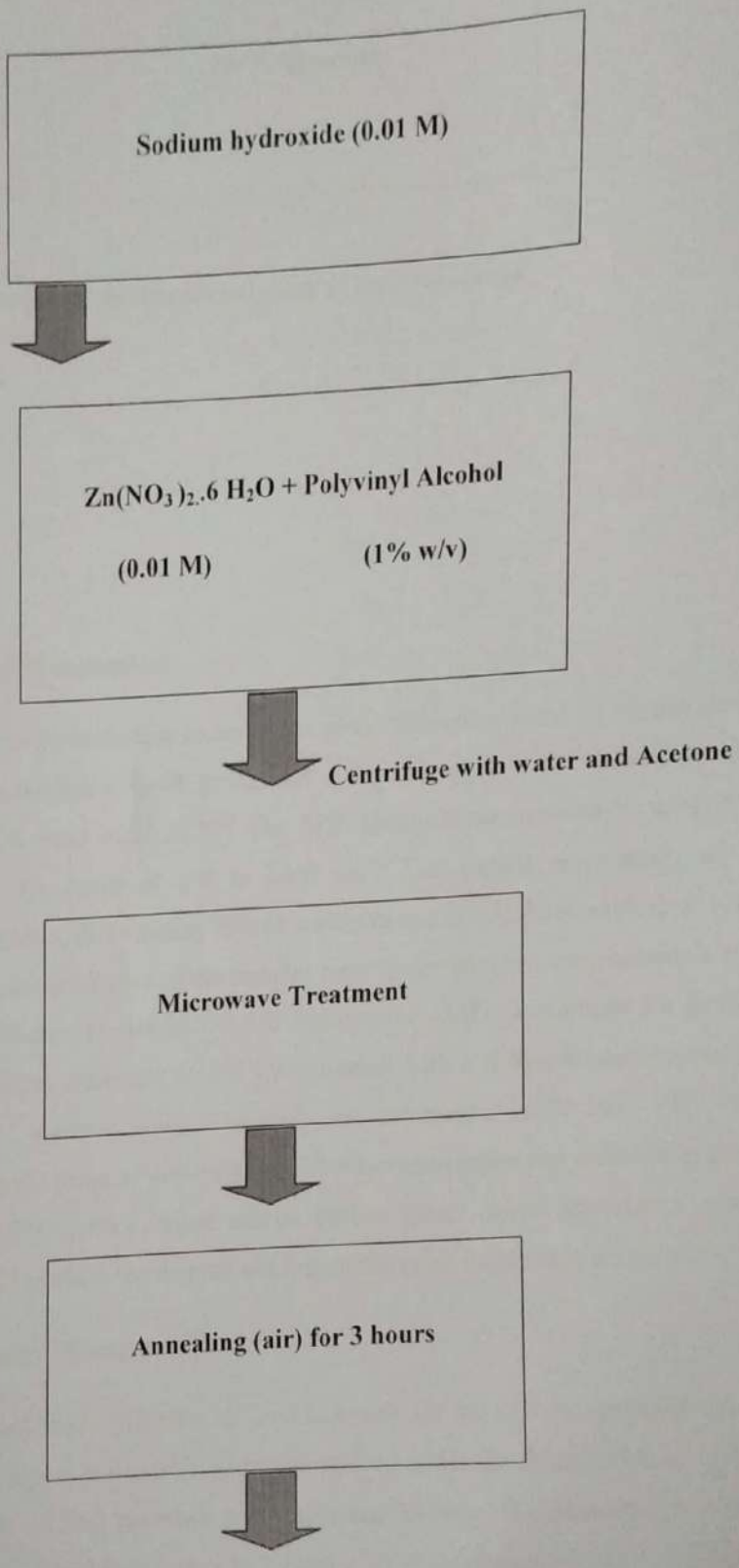

Scanned by CamScanner

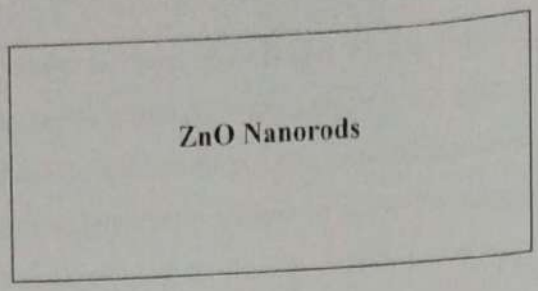

Fig.1 Schematic flow chart for the preparation of ZnO Nanorods

Characterization of Photocatalyst

X - ray diffraction technique recorded the phase formation of the all the materials by using X- ray diffractometer (Model Bruker D8 Advance) using CuKα radiation with λ= 1.5406 Å over the 2θ range of 20 to 80°. The FTIR spectra were recorded by using FTIR-8400, Shimadzu in the range of 400 to 4000 cm^{-1}. The surface morphology of ZnO nanocrystals were studied by Scanning Electron Microscope (JEOL JSM-6360A) at various magnifications. The morphologies of the samples were observed using transmission electron microscopy (TEM Model: Tecnai 20 G2 FEI make) UGC-DAE Consortium for Scientific Research, Indore (India), operating at 100 kV equipped with a field emission source. UV-Visible absorption spectra were recorded on Shimadzu (UV-160 PC Japan) spectrophotometer in the range of 400 - 800 nm. Thermo-gravimetric and differential thermal analysis (TGA and DTA) was carried out on Perkin Elmer themo-gravimetric analyser (Model: Pyris 1 TGA) to study the thermal stability of the synthesized ZnO nanorods.

Photocatalytic Activity Measurements

The photodegradation efficiency of ZnO nanorods for the definite concentration (1X 10^{-5}M) of methyl orange in aqueous solution was studied under the illumination of UV. The photocatalytic activity of ZnO nanorods were evaluated reliably. The photocatalytic reactor consist of two parts: a 100 ml Pyrex glass bottle and a 15 W low-pressure lamp with 254 nm,

Scanned by CamScanner

which was positioned parallel to Pyrex glass bottle. All the experiments were carried out at temperature 27°C. Reaction suspensions were prepared by adding photocatalyst (20 mg) powder into 100 ml methyl orange solutions. The suspensions were ultrasonically sonicated for 30 minutes and then magnetically stirred in dark for about 30 minutes to ensure adsorption equilibrium prior to the UV-irradiation. The suspensions containing methyl orange and photocatalyst were irradiated by the UV light with continuous stirring. The degradation of the methyl orange was monitored as a function of the time by using UV-Visible spectrophotometer, in the range of 400-800 nm. ZnO nanorods annealed at 200°C temperature were used for all the photocatalytic experiments.

For investigating the effect of pH on the photodegradation efficiency of ZnO nanorods, the pH values of the pure dye solutions were varied by adding NaOH (1M) and HCl (1M) to the dye solutions before the addition of catalyst. Analytical samples were withdrawn from the reaction suspensions after various reaction times and centrifuged at 8000 rpm for 15 min to remove the nanoparticles. The photodegradation efficiency was monitored by recording the absorbance of the solution samples at its maximum absorption wavelength of 465 nm with UV-Visible spectrophotometer. The decolorization efficiency as a function of time was calculated by the absorbance values of the original and analytical samples.

Results and Discussion

I) XRD Analysis

Fig.2 shows the XRD patterns of ZnO nanorods annealed at different temperatures for 3 hours. All peaks are identical to those of hexagonal phase with wurtzite structure (JCPDS No. 36-1451) [35]. Diffraction peaks at the different scattering angles (2θ) 31.52, 34.59, 36.03, 47.94, 56.75, 62.93, 66.407, 67.64, 69.07 and 77.91° are attributed to the reflections from the planes [100], [002], [101], [102], [110], [103], [200], [112], [201] and [004] respectively. The lattice parameters were found to be a = 3.25 Å and c = 5.23 Å. Crystallite size of the samples were calculated by Scherrer's relation.

$$t = 0.9\lambda / \beta\cos\theta$$

where,

t = crystallite size in Å,

Scanned by CamScanner

λ = wavelength in Å,

β = FWHM in radian

θ = scattering angle in degree.

At room temperature very small growing few peaks of ZnO were appeared (Fig. 2 (d)). The amorphous nature of the ZnO formed at room temperature is due to the non-availability of sufficient thermal energy for the diffusion of atom on the surface for nucleation. It is observed that crystallinity of the ZnO increases with increasing the annealing temperature. At 100°C temperature the crystallinity of nanorods begin to increase slowly. At annealing temperature of 200°C and 300°C the crystallite size were found to be 50 and 70 nm respectively. Therefore 200°C temperatures was selected as the optimum annealing temperature for the synthesis of ZnO nanorods.

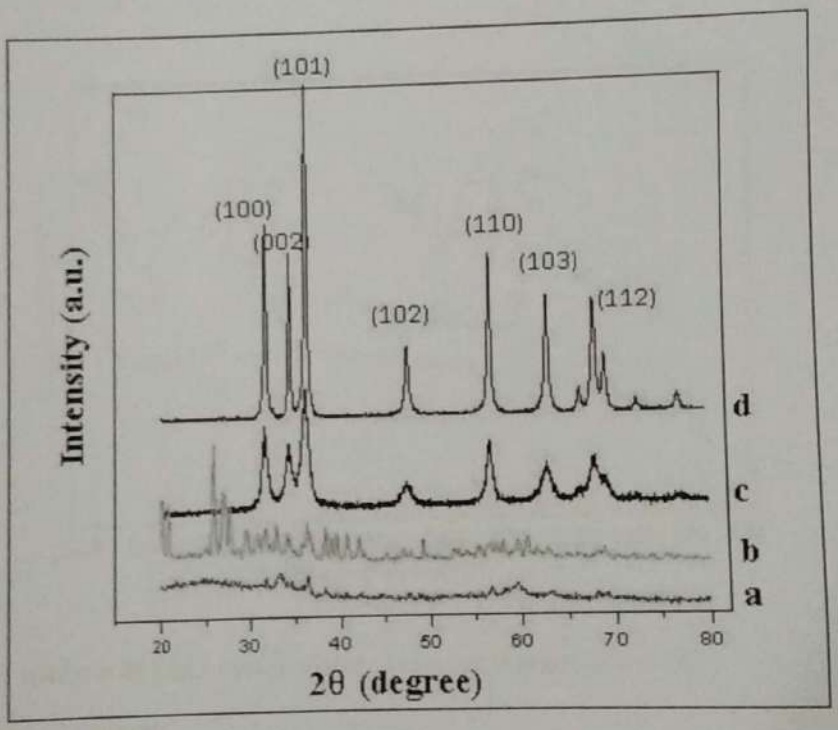

Fig. 2 XRD patterns of ZnO nanorods at (a) room temperature,

(b) 100°C, (c) 200°C and (d) 300°C

II) FTIR Analysis

FTIR spectra of ZnO nanorods annealed at different temperatures are shown in Fig.3.

Scanned by CamScanner

The FTIR spectra of bulk ZnO (a) showed a high intensity broad band around 480 cm^{-1}, which is the characteristic frequency of Zn-O. A similar band was observed in nano ZnO (b). The broad absorption at about 3400 and 1640 cm^{-1} are assigned to the -OH groups of PVA and water molecules. The bands at 1061, 1468, 2489, 2920 and 2952 cm^{-1} are attributed to the C-H stretching and bending modes respectively. Based on the FTIR observations it can be concluded that there is adsorption of OH groups of PVA and water molecules on the surface of ZnO nanorods [36].

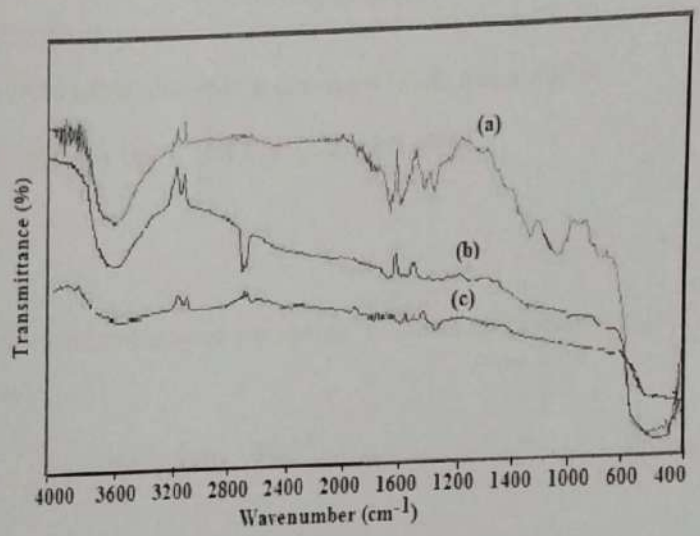

Fig.3 FTIR spectra of ZnO nanorods at (a) room temperature, (b) 100°C, (c) 200°C

III) Optical Properties

Scanned by CamScanner

UV-Visible absorption spectra of ZnO nanorods at R.T., 100°C, 200°C and 300°C are shown in Fig. 4(a-d). These spectra show maximum absorbance band edges at 375, 389, 393 and 399 nm respectively.

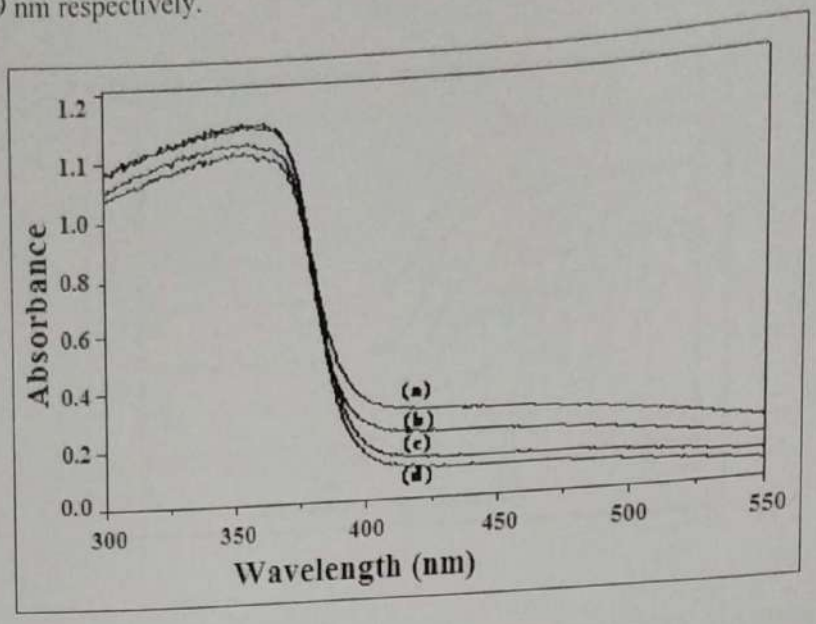

Fig.4.The UV-Visible absorption spectra of ZnO nanorods at

a) RT, (b) 100°C, (c) 200°C and (d) 300°C

From these spectra the band gap energy for the samples were obtained by using following relation.

$$(\alpha h\upsilon) = A\,(h\nu - E_g)^{1/2}$$

where,

α = optical absorption coefficient

$h\upsilon$ = photon energy

E_g = band gap

A = constant

The plots of $(\alpha h\upsilon)^2$ against $h\upsilon$ shown inFig.5 (a) to (d).The band gap energy values were found to be 3.11, 3.15, 3.18 and 3.24 eV for ZnO nanorods at RT, annealed at 100°C,

Scanned by CamScanner

200°C and 300°C respectively. The optical band gap values were obtained by extrapolating the linear portion of the plots of $(\alpha h\upsilon)^2$ versus $h\upsilon$ to $\alpha = 0$.

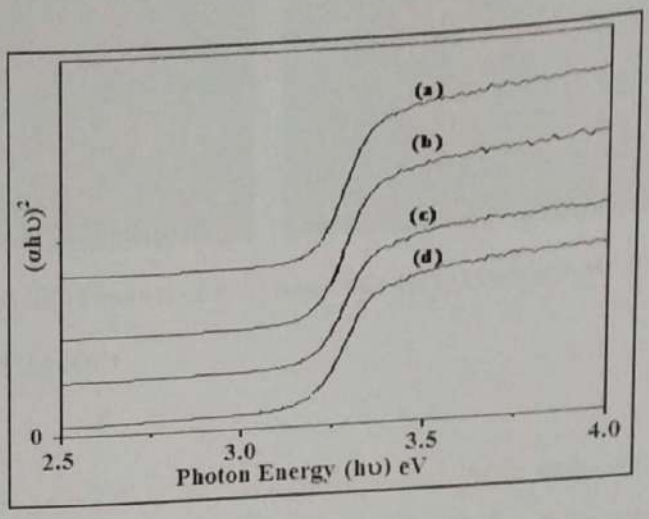

Fig.5 Plot of $(\alpha h\upsilon)^2$ against $h\upsilon$ for ZnO nanorods at (a) RT, (b) 100°C, (c) 200°C and (d) 300°C

IV) SEM and EDAX Analysis of ZnO nanorods

Figs. 6 (a) and (b) depicts the SEM images of ZnO nanorods at room temperature and 200°C respectively. Fig. 6(a) consists of randomly distributed grains with larger size and irregular shape of nanorods. Fig. 6(b) shows ZnO nanorods of few micrometers in length and having diameter of about 50 nm indicating the controlled size and regular shape of the nanocrystals. Thus by using the microwave irradiation and PVA as capping agent it is possible to control over size and shape of the material.

Scanned by CamScanner

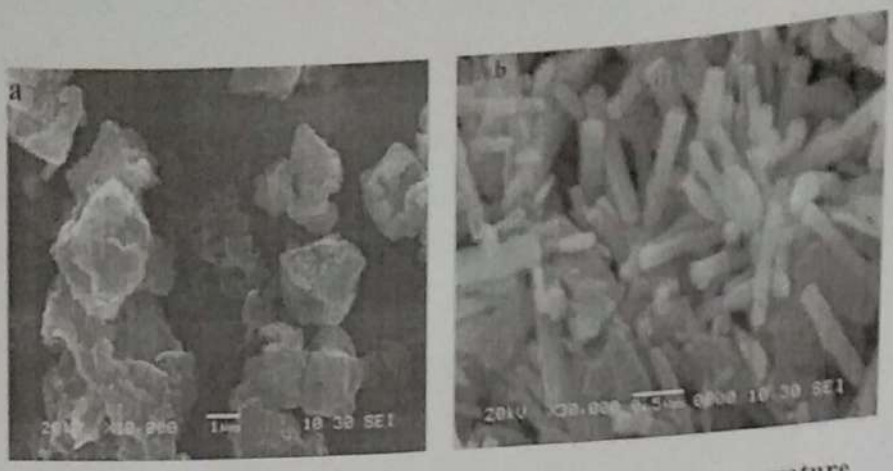

Fig.6 SEM images of ZnO nanorods at (a) room temperature and (b) 200°C

The elemental analysis of the samples were carried out by using energy dispersive X-ray spectrometer (EDS), these are shown in Fig. 7. The EDAX spectra indicate the presence of Zn and O elements without any impurity. The % composition of Zn and O obtained from EDS analysis of ZnO nanorods annealed at 200^0 C.

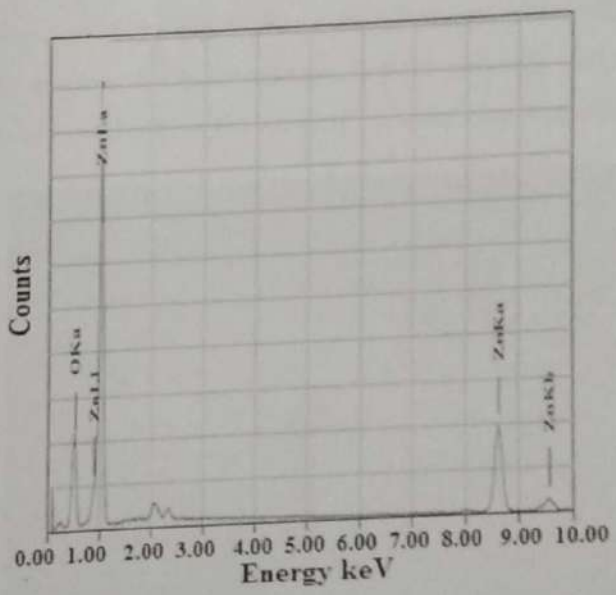

Fig.7 EDAX spectra of ZnO nanorods annealed at 200°C

V) Transmission Electron Microscopy Study

Scanned by CamScanner

TEM image of ZnO nanorods annealed at 200°C is given in Fig. 8 and its selected area electron diffraction (SAED) pattern is given in Fig.9. The TEM image suggests that the size of ZnO nanorods is about 50 nm and this value is in the close vicinity to value obtained from XRD and SEM.

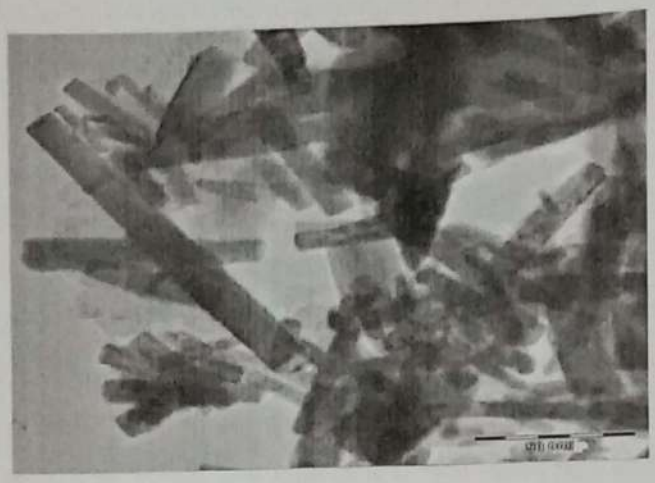

Fig.8 TEM image of ZnO nanorods annealed at 200°C

The SAED pattern in the Fig. 9 shows the reflections of the different planes of the hexagonal wurtzite structure. It clearly indicates that the nanorods with aligned orientation and the high degree of crystallinity in the sample [37], which also support the XRD results.

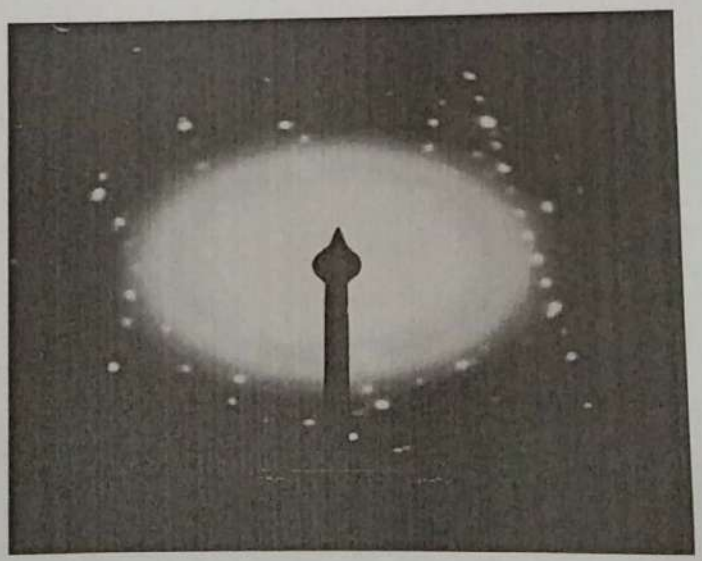

Fig.9 SAED pattern of ZnO nanoparods annealed at 200°C

Scanned by CamScanner

VI) TGA-DTA Analysis

The TGA-DTA measurements are used primarily to determine the thermal and oxidative stabilities of materials as well as its compositional properties. The technique can analyze materials that exhibit weight due to decomposition, oxidation. TGA-DTA analysis of ZnO nanorods heated at the rate 10°C / minute from 30 to 700°C, are given in Figs. 10 (a) and (b). The DTA curve in Fig.10(a) shows thermal decomposition of ZnO at room temerature with an endothermic peak at 50°C is due to the dehydration of water and DTA curve 10(b) shows decomposition of zinc oxide nanorods annealed at 200°C with an endothermic peak at 280°C. The TGA curves 10(a) and (b) shows the 5% weight loss near 50 to 100°C and 50 to 200°C for ZnO and ZnO annealed at 200°C respectively. The total weight loss about 15% upto 450°C for ZnO and about 25% weight loss upto 350°C for ZnO nanorods annealed at 200°C is attributed to thermal decomposition of ZnO and the formation of nanosized ZnO rods. The weight loss over 500°C was extremely small and attributed to removal of bounded −OH groups.

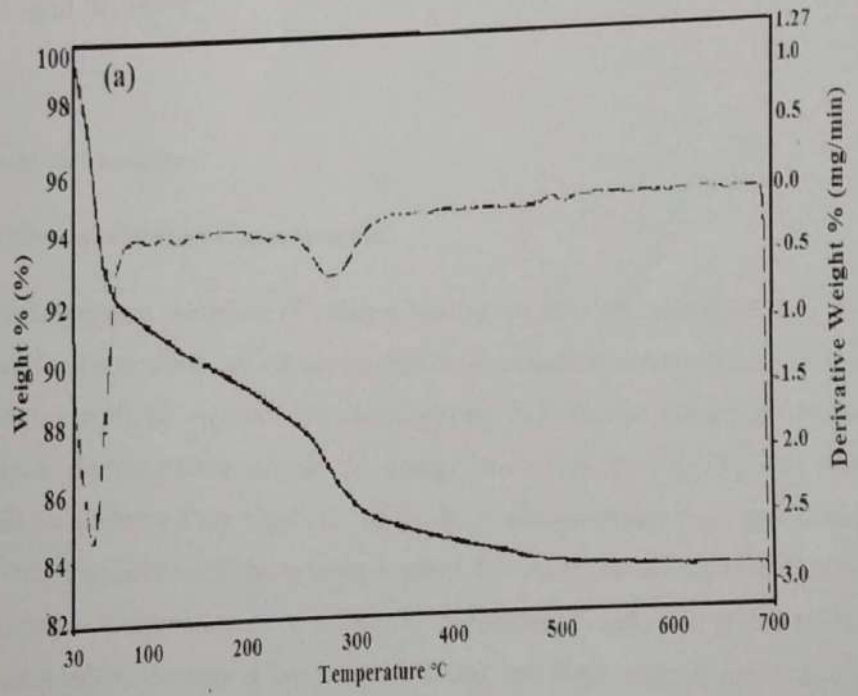

Scanned by CamScanner

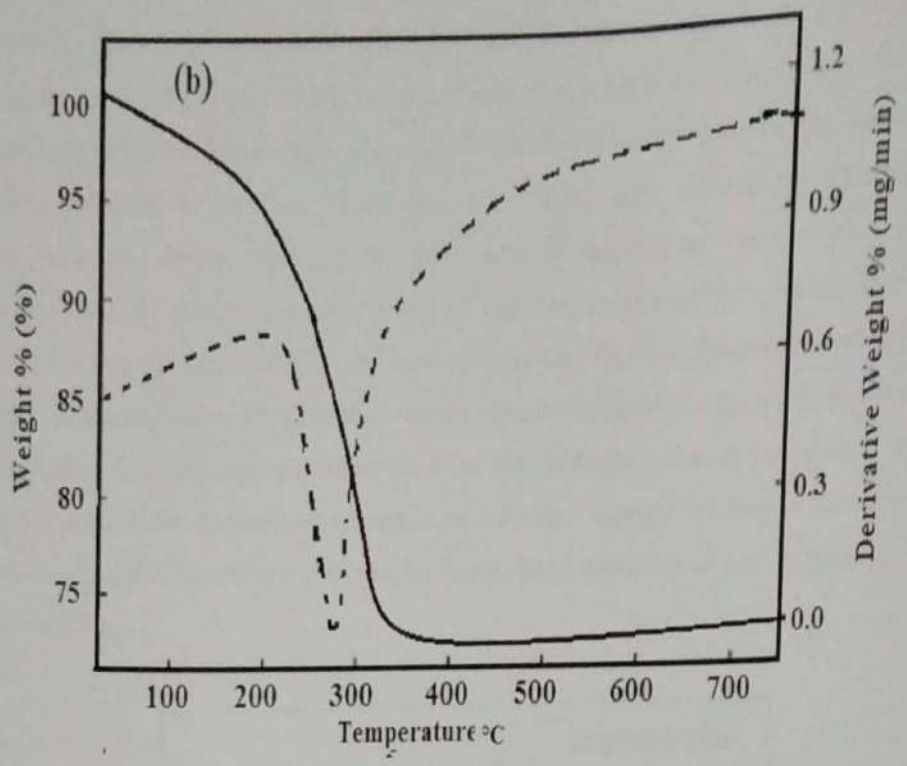

Fig.10 TGA-DTA curve of ZnO nanorods at (a) room temperature and (b) 200°C

Photocatalytic Activity

(a) Effect of Catalyst Concentration

To investigate the effect of catalyst loading on the final decolorization efficiency, a series of experiments were carried out by varying the catalyst amount from 0.1 to 0.3 g/dm^3 in the solution with 20 mg/dm^3 dye concentration. UV-Visible absorption spectra of the photocatalytic decolorization of methyl orange are given in Fig. 11 and the rate of degradation is illustrated in Figs. 12 (a-c). It is demonstrated that the decolorization efficiency was increased with the catalyst loading. However, the increase of final efficiency after 80 minutes illumination is not directly proportional with the multiple increase of catalyst. Many other researchers have been verified that there was an optimum amount of catalyst loading under different experimental conditions [38]. When the catalyst concentration is below this optimal value, it is assumed that the photocatalytic degradation is

Scanned by CamScanner

determined by the effective surface of catalyst and the absorption of UV light. At lower catalyst loading, the absorption of light controls the photocatalytic process due to the limited catalyst surface, whereas the possible aggregation of catalyst is also the limiting factor. In this study, with the multiple increase of catalyst, the surface that absorbs the photon is not increasing in a geometrical ratio for the inclination to aggregation. Moreover, there is a decrease in UV light penetration as a result of light scattering effect with an increase of turbidity of the suspension, leading to the reduction of the effective photoactivated volume of suspension. The integration of these two reasons results in small increase of decolorization efficiency rather than the linearity increase with the multiple increase in catalyst loading. From the photocatalytic degradation experiments 0.2g/dm^3 catalyst loading is found suitable, which shows almost 95% efficiency it may be due to large surface area and proper adsorption of MO on catalyst.

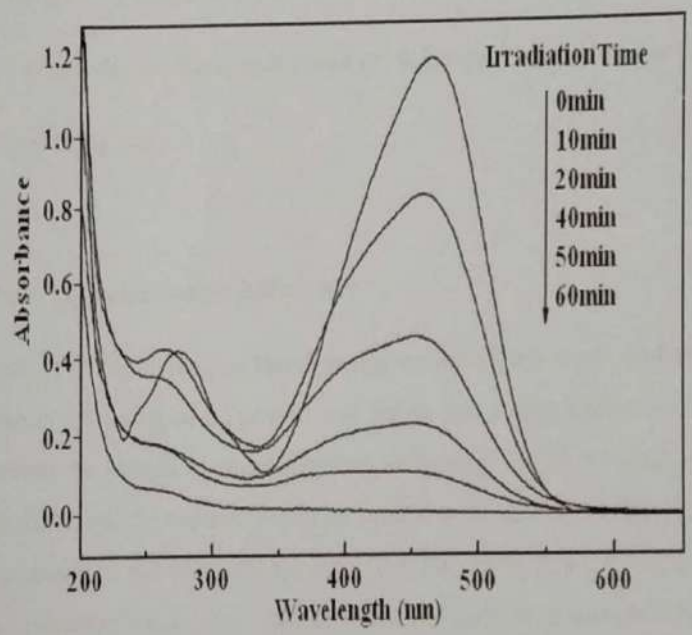

Fig.11 UV-Visible absorption spectra of the photocatalytic decolorization of methyl orange by ZnO nanorods

Scanned by CamScanner

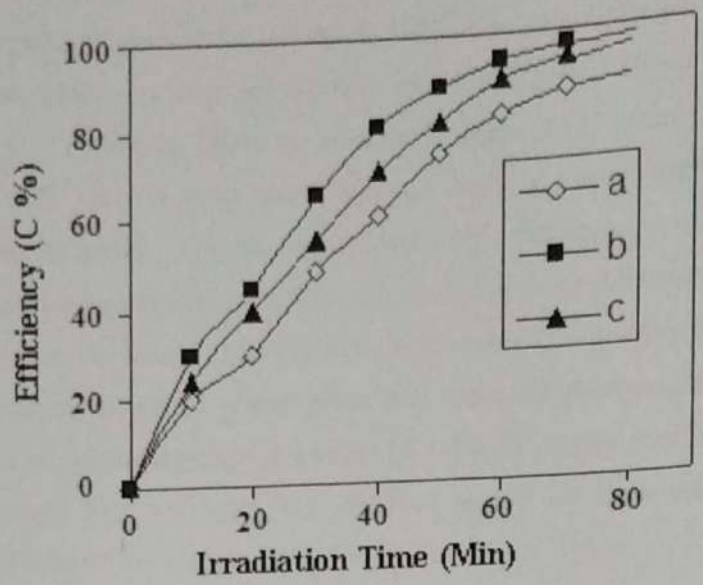

Fig.12 Effect of catalyst concentration on the photodegradation efficiency of ZnO nanorods (a) 0.1g/ dm^3, (b) 0.2g/ dm^3 and (c) 0.3g/ dm^3

(b) Effect of pH on Degradation Efficiency

The effect of pH values on the degradation efficiency were studied in the pH range 3 to 12 at the catalyst loading of 0.2g/ dm^3 and initial dye concentration is 20 mg/dm^3. Figs.13. (a-e) demonstrate the results of decolorization efficiency for 80 minutes light illumination in the solution at different pH values. It can be seen a fast increase in the degradation of methyl orange with increase in pH values from 3 to 10 followed by the slight decrease at pH 12. As an amphoteric nature of oxide, ZnO can be dissolved both at acidic and alkaline environment. Evgenidou et al. has measured the zinc ion to verify that the low initial reaction rates at acidic pH and are attributed to dissolution and photodissolution of ZnO. In this work, at the lower pH value (pH = 3), due to the dissolution of ZnO, the effective catalyst is reduced greatly, which induces the depressing of photodegradation process [3].

In the pH range of 5 to 10, the surface characteristic of ZnO nanorods were the limiting factor and this pH range can change its surface charge property. It has been reported that the pH of zero point charge for ZnO is 9 [39]. When pH value is higher than 10, the ZnO

Scanned by CamScanner

surfaces are negatively charged by adsorbing OH^- ions, which favors the formation of hydroxyl radicals. However, when pH is lower than 5, the ZnO surfaces are preferentially covered by the dye molecules. Therefore, with the increase of pH value, the higher pH can provide higher OH^- ions to form more hydroxyl radicals, consequently enhancing the photodegradation efficiency. On the other hand, with the increase of pH value, the electrostatic repulsion between the methyl orange anion and oxide surface gradually increases [40] and in that case, the slow diffusion of surface-generated OH^- towards the double layer at the low concentration of methyl orange anion will make the photodegradation process of methyl orange slower than direct charge transfer [41]. For the competition of the two factors, the highest decolorization efficiency was obtained at pH 10. However, at pH 12, the decolorization efficiency was comparatively slow.

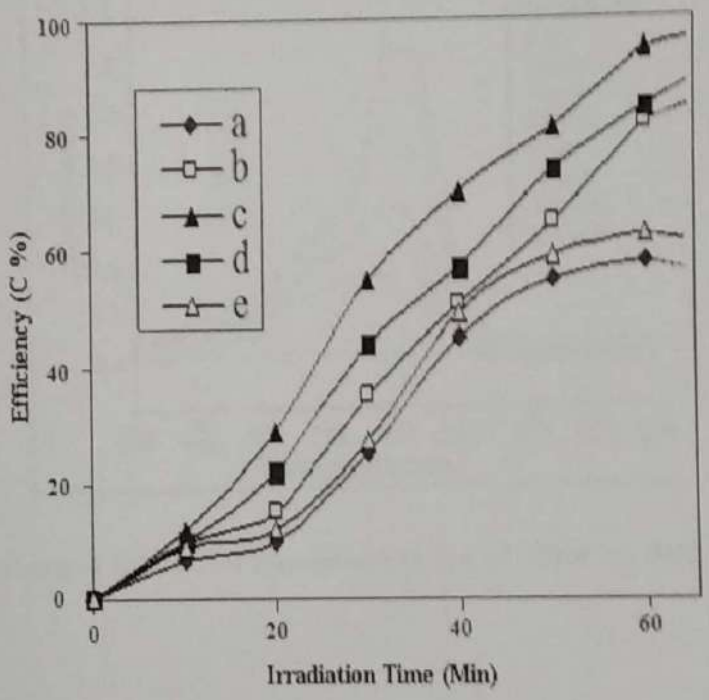

Fig.13. Effect of pH values on the photodegradation efficiency of ZnO nanorodsfor MO (a) pH = 3, (b) pH = 5, (c) pH = 7, (d) pH = 10 and (e) pH = 12

Scanned by CamScanner

The photodegradation efficiency of ZnO nanorods for the definite concentration of RhB in aqueous solution was studied under the illumination of UV. The photocatalytic activity of ZnO nanorods were evaluated reliably. The photocatalytic reactor consist of two parts: a 100 ml Pyrex glass bottle and a 15 W low-pressure lamp with 254 nm, which was positioned parallel to Pyrex glass bottle. All the experiments were carried out at temperature 27 ± 1°C. Reaction suspensions were prepared by adding photocatalyst powder into 50 ml RhB solution. The suspensions were ultrasonically sonicated for 30 minutes and then magnetically stirred in dark for about 30 minutes to ensure adsorption equilibrium prior to the UV-irradiation. The suspensions containing RhB and photocatalyst were irradiated by the UV light with continuous stirring. The degradation of the RhB was monitored as a function of the time by using UV-Visible spectrophotometer, in the range of 400-800 nm. The maximum absorption peak of RhB was obtained at 557 nm (Fig 14).

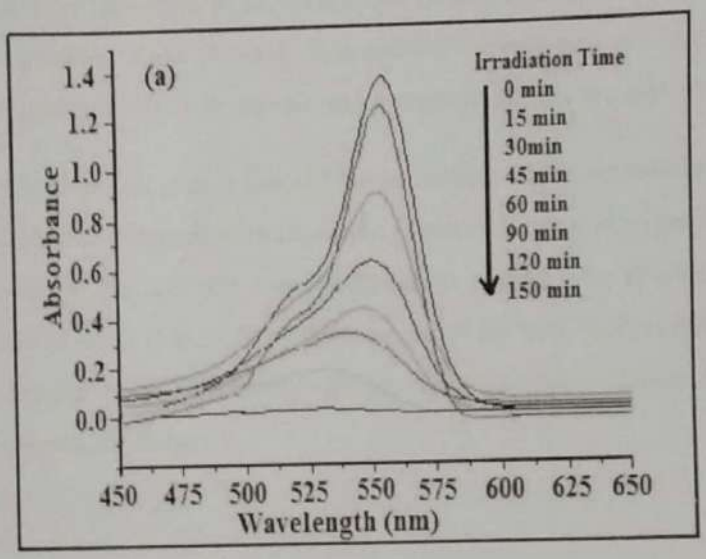

Fig.14 The absorption spectra for photodegradation of RhB by ZnO nanorods

(c) Mechanism for photodegradation of MO and RhB by ZnO nanorods

In solids, the electrons occupy energy bands as a consequence of the extended bonding network. In a semiconductor, the highest occupied and lowest unoccupied energy bands are separated by a band gap, a region devoid of energy levels. Activation of

Scanned by CamScanner

semiconductor photocatalyst is achieved through the absorption of a photon of ultraviolet band gap energy which results in promotion of an electron (e-) from the valence band (VB) into the conduction band (CB) with the generation of hole in the valence band. The resulting hole is an oxidizing agent and the electron is a reducing agent. In the generally accepted mechanism for the photocatalytic process, the hole can react with water to generate the hydroxyl radical and the electron can reduce molecular oxygen, hydrogen peroxide or some other oxidizing agent in the solution. This creates the reactive radicals responsible for the removal of hazardous components from the water.

Mechanism

Light absorption ($\lambda \leq 360$ nm) resulting in the formation of an electron-hole pair in the ZnO grain engenders multiple processes. Radiative processes take place upon recombination, and are the origin of an exciton emission and a broad visible (green) emission band for nanocrystalline ZnO [42-43]. Non-radiative processes are e.g. redox reactions occurring on the surface of ZnO, if organic and inorganic species are adsorbed on it [44-45].

First an electron-hole pair is formed on the surface of the semiconductor (Eq. 1). The hole has high oxidative potential permitting the direct oxidation of organic species (dye) to reactive intermediates (Eq. 2). Very reactive hydroxyl radicals can also be formed either by the decomposition of water (Eq. 3) or by the reaction of the hole with hydroxyl group (Eq. 4). The hydroxyl radical is an extremely strong, non-selective oxidant that leads to the degradation of organic chemicals:

$$ZnO + h\nu \rightarrow ZnO\ (e_{CB}^- + h_{VB}^+) \quad (1)$$

$$h_{VB}^+ + \text{dye} \rightarrow \text{reactive intermediate} \quad (2)$$

$$h_{VB}^+ + H_2O \rightarrow H^+ + {}^\bullet OH \quad (3)$$

Scanned by CamScanner

$$h_{VB}^{+} + OH^{-} \rightarrow \bullet OH \quad (4)$$

The electrons in the conduction band (e_{CB}^{-}) after diffusion to the catalyst surface reduce molecular oxygen to superoxide anion (Eq. 5). In the presence of organic scavengers, this radical leads to organic peroxides (Eq. 6) or hydrogen peroxide (Eq. 7).

$$e_{CB}^{-} + O_2 \rightarrow \bullet O_2^{-} \quad (5)$$

$$\bullet O_2^{-} + \text{dye} \rightarrow \text{dye} - OO\bullet \quad (6)$$

$$\bullet O_2^{-} + HO_2\bullet + H^{+} \rightarrow H_2O_2 + O_2 \quad (7)$$

Electrons in the conduction band are also responsible for the production of hydroxyl radicals, which have been reported as the primary cause of organic matter mineralization (Eq. 8) [46-47].

$$\bullet OH + \text{dye} \rightarrow \text{degradation of the dye} \quad (8)$$

An interesting consequence of these non-radiative processes is the photoinduced change in the oxide surface wettability [48-49]. The surface becomes hydrophilic upon illumination. The process is reversible and after keeping in dark, the surface recovers its original wetting property. The proposed mechanism is the trapping of two holes by a surface lattice $\bullet O_2$-, which leaves the surface. The oxygen defect induces dissociative adsorption of water molecules at the neighbouring zinc ions [50].

ZnO/ UV process is known to have many advantages:

Scanned by CamScanner

1) A large number of organic compounds dissolved or dispersed in water can be completely mineralized.

2) The rate of reaction is relatively high if large surface area of the catalyst can be used.

3) ZnO is available at a relatively modest price and can be recycled on a technical scale.

4) UV lamps emitting in the spectral region required to initiate the photocatalytic oxidation are well known and are produced in various sizes.

5) Absorption cross-section of ZnO can be improved by its surface modifications, e.g. by transition metal ion doping.

Conclusions

We have developed a new, rapid, environment friendly and energy saving microwave assisted method for the synthesis of photocatalylic ZnO nanorods and its photocatalytic activity for the degradation of methyl orange and rhodamine-B. The microwave assisted method is very simple to implement, which can be easily extended to the preparation of other oxide nanoparticles also. It was found that the ZnO nanorods prepared by microwave assisted method played the key role in the photocatalytic performance through studying the degradation efficiency of ZnO photocatalyst. The shape of ZnO is nanorods with wurtzite structure. As the annealing temperature increases the particle size and crystallinity increases. Annealing temperature for the ZnO was reduced as low as 200°C. Also the SEM images of the samples with and without microwave irradiation show the possible role of microwave irradiation in controlling shape and size of nanorods. The photocatalytic results indicated that the catalyst loading and pH values affected the degradation efficiency of ZnO nanorods. Obviously, we learned that the photodegradation efficiency might be increased with the increase of catalyst loading.

References

[1] K. Ishibashi, A. Fujishima, J. Photochem. Photobiol. A, 134 (2000) 139.

[2] M. I. Litter, Appl. Catal. B, 23 (1999) 89.

Scanned by CamScanner

[3] E. Evgenidou, K. Fytianos, I. Poulios, Appl. Catal. B: Environ., 59 (2005) 81.

[4] Y. L. Guo, Y. L. Ji, H. Xu, J. Am. Chem. Soc. Commun., 124 (2002)14864.

[5] M. Purica, E. Budianu, E. Rusu, Thin solid Films, 383 (2001) 284.

[6] T. Aoki, Y. Hatannaka, D. C. Look, Appl. Phys. Lett., 76 (2000) 3257.

[7] C. R. Gorla, N. W. Emanetoglu, S. Liang, J. Appl. Phys., 85 (1999) 2595.

[8] H. S. JO, J. Y. Lao, Z. F. Ren, Appl. Phys. Lett., 83 (2003) 4821.

[9] B. Baruwati, D. K. Kumar, S. V. Manorama, Sens. Actuators B: Chem., 119 (2006) 676.

[10] H. Q. Yan, R. R. He, J. Johnson, J. Am. Chem. Soc., 125 (2003) 4728.

[11] N. Senoussaoui, M. Krause, J. Muller, Thin Solid Films, 451 (2004) 397.

[12] N. Sobana, M. Swaminathan, Separation and Purification Technology, 56 (2007) 97.

[13] K. M. Parida, S. S. Dash, D. P. Das, J. Colloid Interface Sci., 298 (2006) 787.

[14] B. Pare, B. Jonnalagadda, H. Tomar, P. Singh, V. W. Bhagwat, Desalination, 232 (2008) 80.

[15] Z. Yuanhui, C. Chongqi, Z. Yingying, L. Xingyi, Z. Qi. W. Kemei, Z. Jiefang, Z. Yingjie, Inorganic Chemistry, 46 (2007) 6675.

[16] R. Y. Hong, T. T. Pan, J. Z. Qian, H. Z. Li, J. Chem. Eng., 19 (2006) 71.

[17] S. A Qaradawi, S. R. Salman, J. Photochem. Photobiol. A: Chem., 148 (2002)161.

Scanned by CamScanner

[18] Y. Liu, X. Chen, J. Li, C. Burda, Chemosphere, 61 (2005) 11.

[19] H. Mansilla, J. Villaseñor, G. Maturana, J. Baeza, J. Freer, N. Durán, J. Photochem. Photobiol. A: Chem., 78 (1994) 267.

[20] C. Richard, F. Bosquet, J. F. Pilichowski, J. Photochem. Photobiol. A: Chem., 108 (1997) 45.

[21] A. Wood, M. Giersig, P. Mulvaney, J. Phys. Chem. B, 105 (2001) 8810.

Scanned by CamScanner

[22] A. L. Stroyuk, V. V. Shvalagin, S. Y.Kuchmii, J. Photochem. Photobiol. A: Chem., 173 (2005) 185.

[23] C. A. K. Gouvea, F. Wypych, S. G. Moraes, N. Duran, Nagata, Peralta, N. P. Zamora, Chemosphere, 40 (2000) 433.

[24] C. Lizama, J. Freer, J. Baeza, H. D. Mansilla, Catal. Today, 76 (2002) 235.

[25] P.V. Kamat, R. Huehn, R. A. Nicolaescu, J. Phys. Chem. B, 106 (2002) 788.

[26] R. Comparelli, E. Fanizza, M. L. Curri, P. D. Cozzoli, G. Mascolo, A. Agostiano, Appl. Catal. B: Environ., 62 (2005) 144.

[27] O. A. Fouad, A. A. Ismail, Z. I. Zaki, R. M, Mohamed, Appl. Catal. B: Environ., 62 (2006) 144.

[28] S. Sakthivel, B. Neppolian, M. V. Shankar, B. Arabindoo, M. Palanichamy, V.Murugesan, Sol. Energy Mater. Sol. C, 77 (2003) 65.

[29] S. B. Park, Y. C.Kang, J. Aerosol. Sci., 28 (1997) 3473.

[30] M. L. Curri, R. Comparelli, P. D. Cozzoli, G. Mascolo, A. Agostiano, Mater. Sci. Eng. C, 23 (2003) 285.

[31] D. Li, H. Haneda, Chemosphere, 51 (2003) 129.

[32] K. Ivanov, Vladimir, Shaporev, S. Alexey, Sharikov. Yu. Felix, Baran, Ye. Alexander, Superlattices and Microstructures, 42 (2007) 421.

[33] L. Jin-song, C. Jie-ming, L. Zi-quan. J. Guang-bin, Z. Ming-bo, Materials Letters, 61 (2007) 4409.

[34] A. M. Peiro,C. Domingo, J. Peral, X. Domenech, E. Vigil, M. A.Hernandez- Fenollosa, M. Mollar, B. Mari, J. A. Ayllon, Thin Solid Films, 483 (2005) 79.

Scanned by CamScanner

[35] T. Andlmar, Y. Gorg, M. Polking, M. Yin, I. Kuskovsky, G. Neumark, S.O. Brien, J. Phy. Chem.B, 109 (2005) 14314.

[36] G. Feng, W. S. Fen, K. L. Meng, J. Z. Guang, X. Dong, Y. D. Rong , Langmuir, 20 (2004) 3528.

[37] M. Yin, Y. Gu, L.Igor, Kuskovsky, T. Andelman, Y. Zhu, G. F. Neumark, S. O'Brien, J. Am. Chem. Soc., 126 (2004) 6206.

[38] A. A. Kyol, H. C. Yatmaz, M. Bayramoglu, Appl. Catal. B: Environ., 54 (2004) 19.

[39] G. A. Parks, Chem. Rev., 65 (1965) 177.

[40] C. Wang., J. Zhao, X. Wang., B. Mai, G. G. Sheng, P. Peng, P. Fu, J. Appl. Catal. B. Environ., 39 (2002) 269.

[41] I. Poulios, M. Kositzi, A. Kouras, J. Photochem. Photobiol. A: Chem., 115 (1998) 175.

[42] L. El Mir, A. Amlouk, C. Barthou, S. Alaya, Physica B: Physics of Condensed Matter., 388 (2007) 412.

[43] Z. Y. Xiao, Y. C. Liu, L. Dong, C. L. Shao, J. Y. Zhang, Y. M. Lu, D. Z. Zhen, X. W. Fan, J. Coll. Interface Sci., 282 (2005) 403.

[44] M. A. Behnajady, N. Modirshahla, R. Hamzavi, J. Hazard. Mater. B, 133 (2006) 226.

[45] N. Daneshvar, M. H. Rasoulifard, A. R. Khataee, F. Hosseinzadeh, J. Hazard. Mater., 143(2007) 95.

[46] N. Daneshvar, D. Salari, A. R. Khataee, J. Photochem. Photobiol. A: Chem., 162 (2004) 317.

Scanned by CamScanner

[47] I. K. Konstantinou, T. A. Albanis, Appl. Catal. B: Environ., 49 (2004) 1.

[48] S. Kataoka, M. A. Anderson, Thin Solid Films, 446 (2004) 232.

[49] Y. Li, W. Cai, G. Duan, B. Cao, F. Sun, F. Lu, J. Coll. Interface Sci., 287 (2005) 634.

[50] N. Sakai, A. Fujishima, T. Watanabe, K Hashimoto, J. Phys. Chem. B, 105 (2001) 3023.

Scanned by CamScanner

Synthesis, characterizations and Photocatalytic activity of MnCopper ferrite nanoparticles for dye degradation

92

Scanned by CamScanner

Introduction

The ferrites with spinel structure are technological important class of magnetic oxides due to their magnetic properties, high electrical resistivity and low eddy current and dielectric loss [1]. The structural, electrical and magnetic properties of ferrites are strongly dependent on their chemical composition, the cation distribution and their method of preparation [2, 3]. Spinel ferrites of the general chemical formula AB_2O_4 belong to the group of magnetic oxides whose crystal structure has space group $Fd3m\text{-}O_h^7$. The anions (oxygen atoms) form a face-centered cubic close packing with tetrahedral and octahedral voids partly occupied by cations A and B.

The non-destructive methods are useful in determining the precise configuration of atoms and ions in ferromagnetic semiconductors. Among the various classes of ferrites are the common, most diverse and possess richest class in terms of physical, chemical and structural properties. As a result, numerous applications of ferrites, such as fabrication of microelectronic circuits, sensors, piezoelectric devices, fuel cells, dielectrics, lasers, magnets and catalysts have been discussed [4-7].

Ferrite prepared by a ceramic route involves high-temperature to complete the solid-state reaction between the constituent oxides or carbonates. The particles obtained by this method are rather large and non-uniform in size. These non-uniform particles, on compacting, result in the formation of voids or low density. In order to overcome these difficulties by using wet chemical methods like coprecipitation, hydrothermal processing, combustion etc., have been considered for production of homogeneous, fine and reproducible ferrites [8-14]. Among these synthesis techniques, sol-gel autocombution method has several advantages over others for preparation of nanosized metal oxides as the process begins with a relatively homogeneous mixture and involves low temperature conditions resulting in a uniform ultrafine porous powders.

In this topic, we report preparation of nanosized titanium substituted Mn substituted Cu-ferrites by sol-gel autocombution method. The substitution of trivalent metal ions like manganese influences the electrical and magnetic properties of Cu- ferrites. The structural, and magnetic properties investigated by X-ray diffraction (XRD), TEM, SAED, Energy dispersive x-ray spectroscopy, and FTIR spectroscopy have also been discussed in details.

Scanned by CamScanner

There is a pressing need to curb the environmental pollution currently due to large scale production of organic pollutants by various industries. A number of organic pollutants present in water have to be treated suitably to limit the concentration of pollutants to the prescribed limit set by the governmental authorities. Their toxicity, stability towards natural decomposition and persistence in the environment has been the cause of much concern to societies and regulation authorities around the world. Photocatalytic degradation of organic pollutants using light radiation is a potential method. Therefore, design and development of photocatalysts that can work efficiently with visible light is of utmost importance at present. Therefore, photocatalytic activity of the Cu-Mn ferrites was studied by using hazardous dyes.

Materials and Methods:

I) Synthesis Technique:

The nanocrystalline mixed metal oxide system $CuFe_{2-x}Mn_x O_4$ where x = 0.0, 0.5, 1.0, 1.5and 2.0 were prepared by sol-gel autocombution method. Analytical grade ferric nitrate [Fe $(NO_3)_2.6H_2O$],copper nitrate [$Cu(NO_3)_3.3H_2O$], manganese nitrate [$Mn(NO_3)_2.4H_2O$], and citric acid [$C_6H_8O_7.H_2O$] were used to prepare system compositions.Metal nitrates and citric acid were dissolved in minimum quantity of deionized water with 1:1 molar ratio for all compositions. The pH of the solution was adjusted to about 9.0 to 9.5 using ammonia solution. This solution transforms to dry gel on heating to 353K. On further heating the dried gel undergo a self propagating combustion process and transform to floppy loose powder. The obtained powder was then calcined at 1173 K for 8 h in air atmosphere. The calcined powders were mixed with 2 % polyvinyl alcohol and pressed to pellets by applying uniaxial pressure of 8 ton /cm^2. These pellets were gradually heated to about 773K to remove out the volatile organic binder material.

II) Characterization Techniques:

Thermal analysis of the different compositions of the unsintered Copper and manganese substituted Copper ferrite system was carried out from the curves of TG-DTA.

Scanned by CamScanner

Stability of the dry citrate complexes was checked by scanning the thermograms in the temperature range of 10-1000°C in static air at the flow rate of 10^0C/min.

The FT-IR spectra were recorded in the range of 400 to 1000 cm^{-1} on instrument Perkin Elmer – IR spectrophotometer (model E-2829) in KBr pellets.

The SEM micrograph of the samples was obtained using scanning electron microscope (JEOL JSM 6360). The grain size of all the samples was calculated by cottrolls method.

Transmission electron microscope (Philips CM 20) was used to evaluate the nanostructure of the typical samples. To study the phase structure of the spinel an SAED pattern of the samples was also taken. Photocatalytic performance was studied by using hazardous dyes like Methyl Red. Methyl Red is a well-known common azo-dye, used in the industry. The photocatalytic activity was studied for Methyl Red dye in presence of Ultra-violet light for different times.

Results and Discussion:

I) Thermogravimetric analysis

TG and DTA curves for the dried sample of $CuFeMnO_4$ sample are presented in **Figure 1.** As shown in the figure, in the TG curve, the percent weight loss with the temperature is observed. A continuous weight loss was observed from TG curve upto 550° C of the sample in the formation of stable oxide compound. However DTA curves show one exothermic peak around 280°C. At this temperature, a decomposition of mixed-metal citrate complexes by fragmentation and thermal degradation of organic content occur and this results the formation of stable mixed-metal oxides.

Scanned by CamScanner

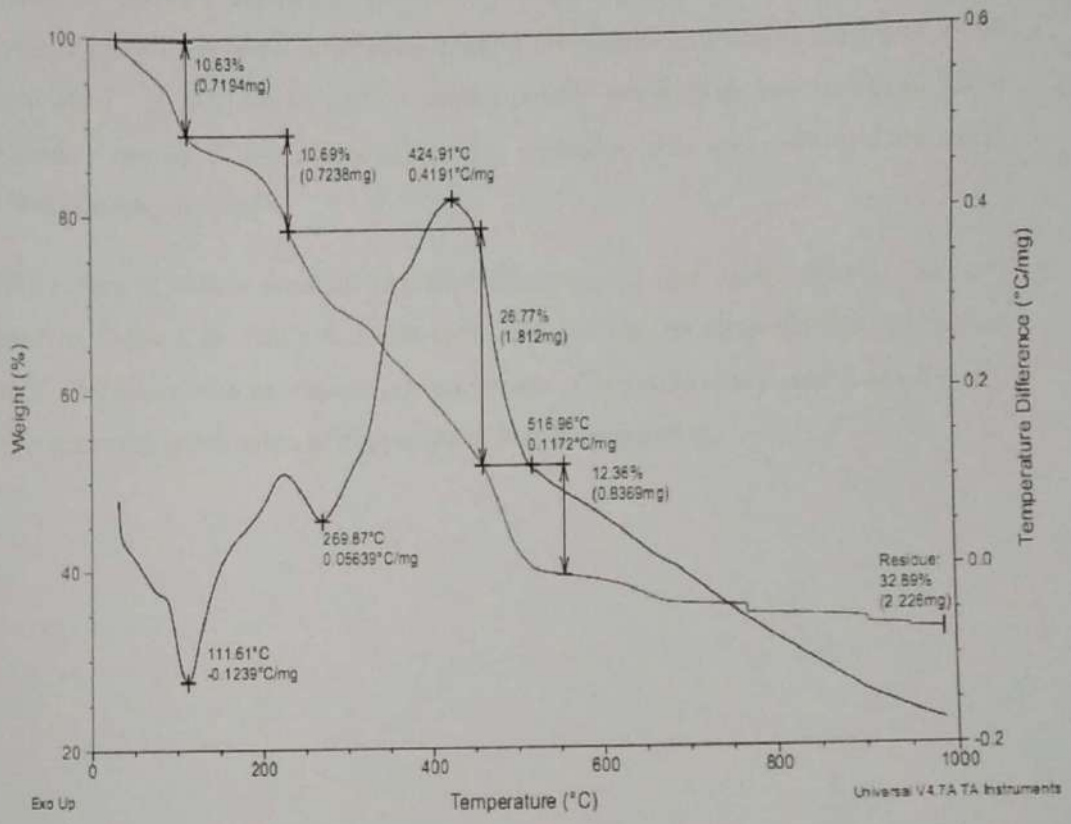

Fig.1 TGA-DTA Spectrum for $CuFeMnO_4$

Scanned by CamScanner

II) X-ray diffraction study:

Typical X-Ray diffraction patterns of samples $CuFe_{2-x}Mn_x$ O_4obtained by gel combustion followed by annealing at 1173 K are shown in **Fig. 2**. The diffraction pattern for all the samples shows the crystalline nature. The diffraction data indicate that the samples have cubic spinel structure and well matched with JCPDS card no.01-1110 for $NiMn_2O_4$ and JCPDS card on.34-1400 for $CuMn_2O_4$.The lattice parameters were calculated for the cubic phase. Where a, is lattice parameter, (hkl) is the Miller indices and d is the interplanar distance. **Fig. 2** reveals the linear decreasing trend in the lattice parameter is attributed to the replacement of Ni^{2+} (0.78Å) ion by Cu^{2+}, a slightly smaller ion with an ionic radius (0.70Å), in the system. From the X-ray diffraction peaks, crystallite size was estimated by using Debye Scherrer's formula [15]

The values of lattice constant (a), crystallite size (t) and X-ray density (dx) are summarized in **Table 1 to Table 6.** From these tables it can be observed that the lattice parameter 'a' decreases with increase in copper content. Crystallite size't' and X-ray density 'dx' value varies with substitution of copper metal ions concentration.

Scanned by CamScanner

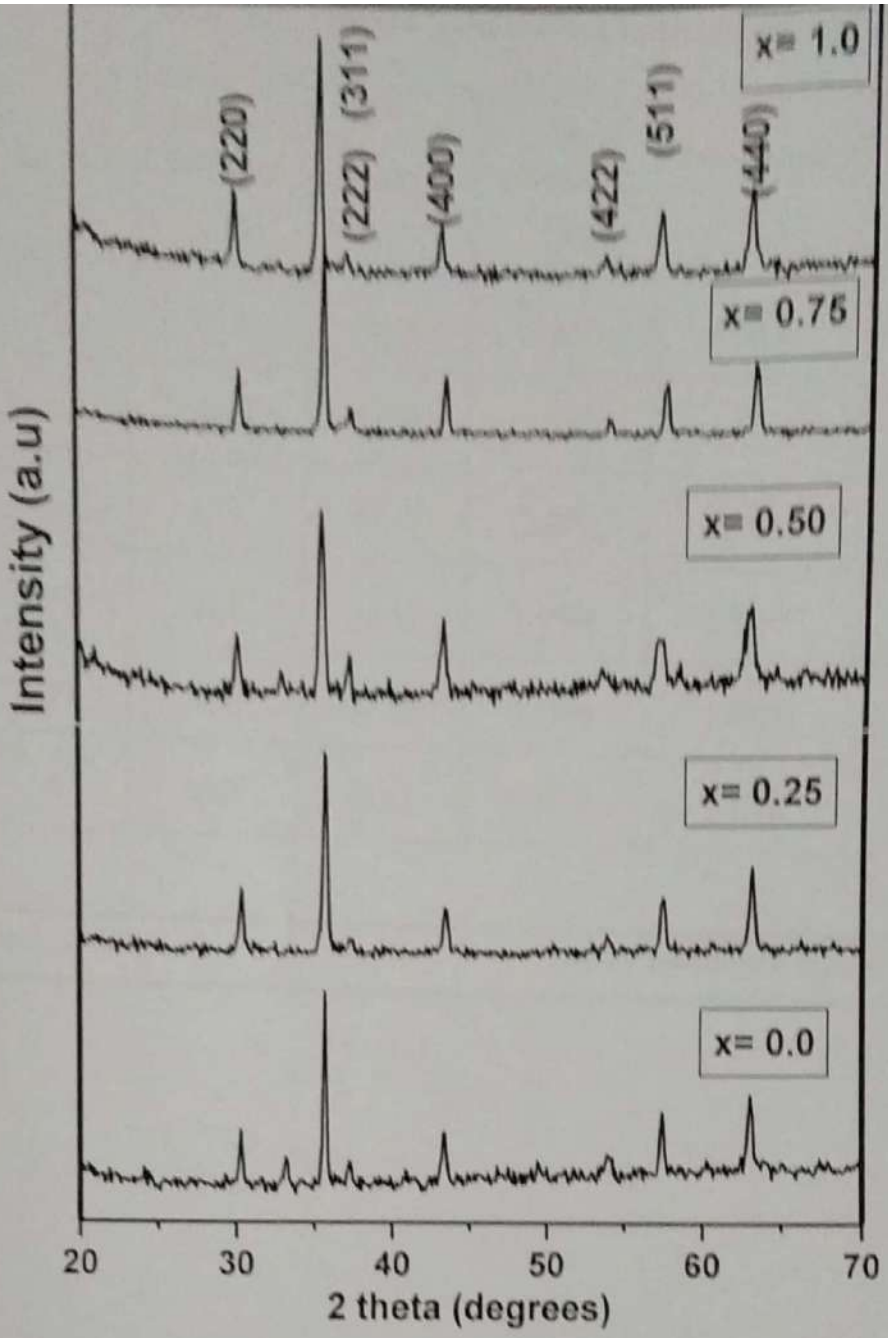

Fig.2 X-ray diffraction patterns of $CuFe_{2-x}Mn_x O_4$system

Scanned by CamScanner

Table No. 1 Indexed X-ray diffract meter pattern of $CuFe_2O_4$

Sr. No.	Relative Intensity I (%)	2θ	d (observed) (Å)	d (calculated) (Å)	hkl
1	43.2	30.38	2.9393	2.9466	220
2	100.0	35.79	2.5068	2.5131	311
3	15.4	43.49	2.074	2.079	400
4	21.6	45.43	1.9948	1.9997	410
5	31.0	57.56	1.5999	1.6039	511
6	48.0	63.15	1.4710	1.4746	440

Structure: Cubic	Lattice constant: a = 8.389 Å

Scanned by CamScanner

Table No. 2 Indexed X-ray diffraction pattern of $CuFe_{1.5}Mn_{.5}O_4$

Sr. No.	Relative Intensity I (%)	2θ	d (observed) (Å)	D (calculated) (Å)	hkl
1	36.3	30.34	2.9431	2.9504	220
2	100	35.72	2.5116	2.5178	311
3	18.4	43.42	2.0824	2.0875	400
4	12.9	45.37	1.9971	2.0020	410
5	7.2	54.08	1.6944	1.6986	422
6	15.3	57.45	1.6026	1.6066	511
7	20.1	62.38	1.4874	1.4911	440

Structure: Cubic **Lattice constant: a= 8.382Å**

100

Scanned by CamScanner

Table No. 3 Indexed X-ray diffraction pattern of $CuFeMnO_4$

Sr. No.	Relative Intensity I (%)	2θ	d (observed) (Å)	D (calculated) (Å)	hkl
1	41.9	18.545	4.7805	4.7924	111
2	33.9	30.35	2.9421	2.9494	220
3	100.0	35.79	2.5068	2.5131	311
4	30.2	43.58	2.0749	2.0800	400
5	17.8	53.09	1.6933	1.6886	422
6	24.2	57.58	1.5994	1.6034	511
7	30.2	63.11	1.4718	1.4718	440

Structure: Cubic	Lattice constant: a = 8.364Å

Scanned by CamScanner

Table No. 4 Indexed X-ray diffraction pattern of $CuFe_{0.5}Mn_{1.5}O_4$

Sr. No.	Relative Intensity I (%)	2θ	d (observed) (Å)	D (calculated) (Å)	hkl
1.	51.4	18.44	4.8075	4.8194	111
2	22.8	23.325	3.8105	3.8200	220
3	100.0	33.10	2.7037	2.7105	300
4	76.8	35.560	2.5225	2.5288	311
5	35.2	55.36	1.6580	1.6622	331
6	22.8	57.01	1.6140	1.6181	333
7	22.0	62.50	1.4847	1.4884	440

Structure: Cubic **Lattice constant: a = 8.361 Å**

Scanned by CamScanner

Table No. 5 Indexed X-ray diffraction pattern of $CuMn_2O_4$

Sr. No.	Relative Intensity I (%)	2θ	d (observed) (Å)	d (calculated) (Å)	hkl
1	29.6	18.63	4.7589	4.7707	111
2	15.4	23.165	3.8365	3.8460	220
3.	28.7	36.12	2.4843	2.4905	311
4	18.7	38.28	2.3490	2.3548	222
5	17.3	43.915	2.060	2.0651	400
6	23.8	65.80	1.4181	1.4216	440

Structure: Tetragonal **Lattice constants: a= 8.354 Å**

Table.6 Data on lattice parameter, crystallite size, x-ray density, of $CuFe_{2-x}Mn_x O_4$samples.

Composition	Lattice constant 'a', (A^0)	X-ray density, (gm/cm^3)	Crystallite size, (nm)
X=0.0	8.389	5.22	21
X=0.25	8.382	5.27	

Scanned by CamScanner

			28
X=0.50	8.364	5.33	28
X=0.75	8.361	5.36	21
X=1.00	8.354	5.39	21

III) Fourier Transform Infra-red study:

The FTIR absorption spectra were recorded in the range 350-1000cm^{-1} .The IR spectra for Mn substituted lithium ferrospinels show two strong bands. The high frequency band υ_1 is in the range 586-610 cm^{-1}and the lower frequency band υ_2 is in the range 440-466cm^{-1}. The high frequency band is due to the vibration of the tetrahedral M---O bond and the low frequency band is due to the vibration of the octahedral M---O bond. The variation of the IR frequency with Cu content is represented in Table 7.

Table.7 IR frequency and force constants for $CuFe_{2-x}Mn_x O_4$

Composition x	υ_1 cm^{-1}	υ_2 cm^{-1}
0.0	546	436
	554	445

Scanned by CamScanner

0.25		
0.50	567	459
0.75	587	467
1.0	601	475

IV) Scanning Electron Microscopy:

The SEM images of Copper substituted Nickel Magnetites are shown in the Fig.**3**. It is observed that, the average grain size goes on decreasing on substitution of Cu content. The average grain size was smaller than 0.1μm for all compositions.

Scanned by CamScanner

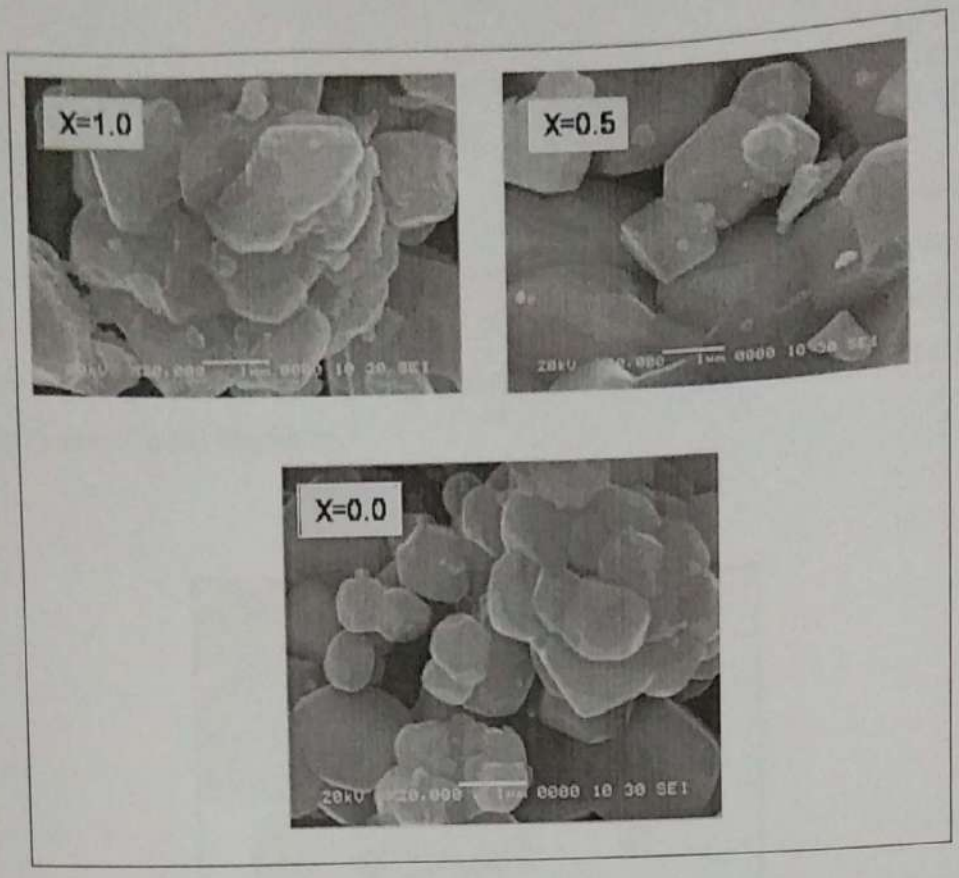

Fig.3 Typical SEM images for $CuFe_{2-x}Mn_x O_4$

x =0.0, 0.5 and 1.0

Scanned by CamScanner

V) Transmission electron microscopy:

The morphology and grain size of Copper substituted Nickel Magnetites powders were characterized by TEM (Fig.**4**).It is noted that all particles are uniform and the average grain size is ~50 nm. Selected area electron diffraction pattern (SAED) of the particles is shown in the Fig.**4**. It suggests the polycrystallinity of individual crystallite and also confirms the formation of spinel Magnetites.

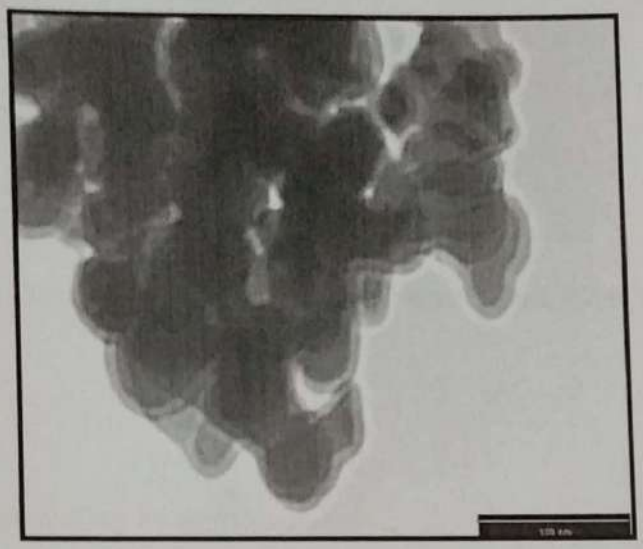

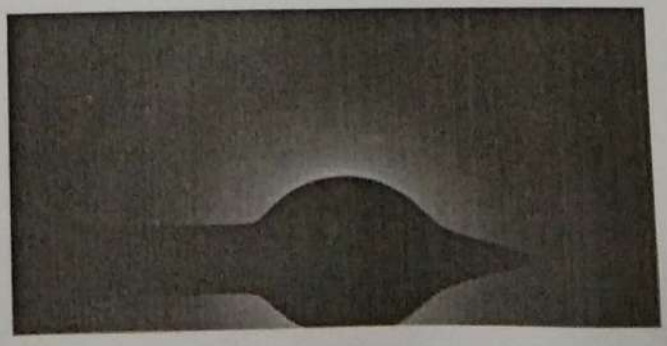

Scanned by CamScanner

Fig.4 Typical TEM images and SAED pattern for $CuMn_2O_4$

VI) Energy dispersion x-ray analysis:

The composition of the nanocrystalline metal oxides has been determined using the energy dispersion x-ray analysis (EDAX). The X-ray spectra for x = 2.0, compositions are shown in **Fig.5** . From the EDAX spectra, the presence of Ni, Mn, Cu and O is confirmed in the sample. The quantitative analysis of EDAX spectrum revealed the relative atomic ratio of Ni: Mn: Cu which is close to the expected values for $CuFe_{2-x}Mn_x O_4$system

Scanned by CamScanner

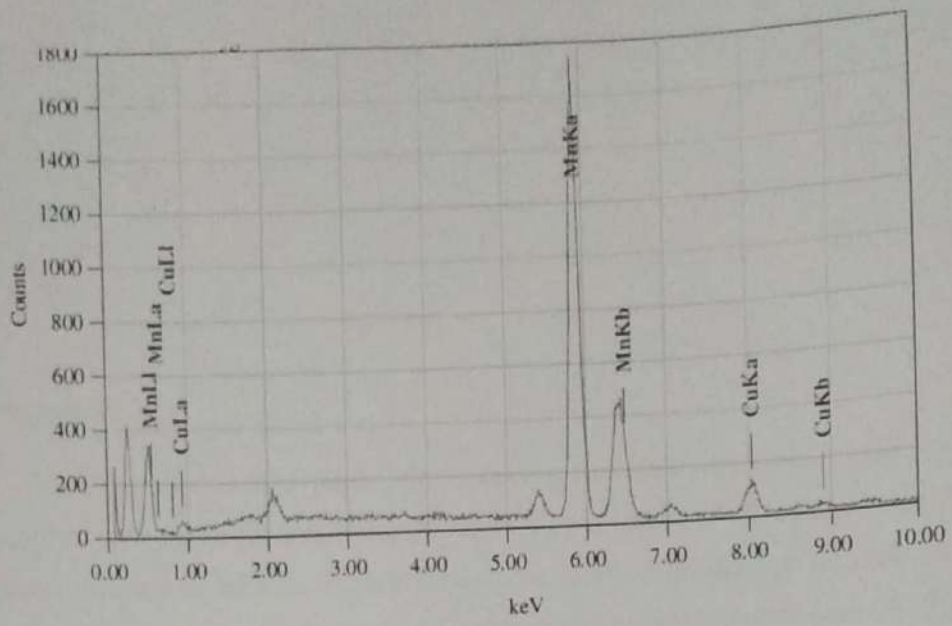

Fig.5. EDS patterns for the system Cu Mn_2O_4sample **(x =2)**

Scanned by CamScanner

Photocatalysis:

There are number of different semiconducting materials which are readily available, but only few are suitable for sensitizing the photo-mineralization of wide range of pollutants. The semiconductor to be used as photocatalyst for photo-mineralization of wide range of organic pollutants must be (i) photoactive (ii) able to utilize visible and or near UV light (iii) biologically & chemically inert and (iv) photo-stable. It is generally found that only n-type semiconductor oxides are stable towards photo-anodic corrosion, although such oxides usually have bandgaps, which are sufficiently larger than the semiconductors which absorb only UV light.

The textile dyes and dye intermediates with high aromaticity and low biodegradability have emerged as major environmental pollutants and nearly 10-15% of the dye is lost in the dyeing process and is released in the wastewater which is an important source of environmental contamination. Considerable amount of water is used for dyeing and finishing of fabrics in the textile industries. The wastewater from textile mills causes serious impact on natural water bodies and land in the surrounding area. As dyes are designed to be chemically and photolytically stable, they are highly persistent in natural environments. The improper handling of hazardous chemicals in textile water also has some serious impact on the health and safety of workers putting them into the high-risk bracket for contracting skin diseases like chemical burns, irritation, ulcers, etc. and respiratory problems.

Methyl Red is common azo-dyes, used in the industry. The performance of Mn substituted Nickel Copper Ferritenanoparticles for the photocatalytic degradation of Methyl Red for different hours is presented in **Fig. 6.**

The catalytic activity of the photocatalyst was studied by following the rate of photodegradation of Methyl Red. The experiment of photocatalytic reaction was conducted in

Scanned by CamScanner

a 100-ml Pyrex glass vessel with magnetic stirring and a UV lamp (8W, with the main wavelength of 253.7nm) positioned over the glass beaker. The as-prepared substituted MnCopper Ferrite nanoparticles were used as photocatalyst during the activity. It can be, concluded that enhanced photodegradation is directly related to the reduced particle size of the ferrite, which implies that photosensitization is the process primarily involved. The photocatalytic activity goes on decreasing with substitution of Mn content. Therefore, this study reveals that Copper Ferrite shows better photocatalytic activity towards Methyl red as compared to other Copper Magnite.

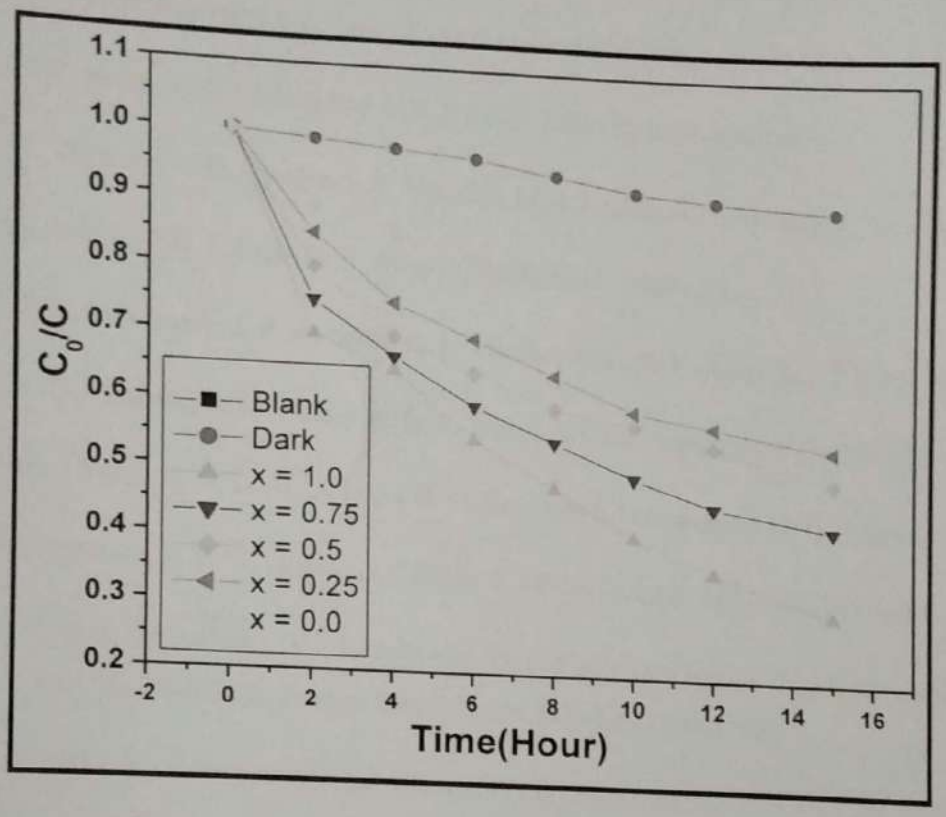

Fig.6 Photocatalytic study for $CuFe_{2-x}Mn_x O_4$system

Scanned by CamScanner

References:

[1] J.G. Bednorz, K.A. Müller, Z. Phys. B 64 (1986) 189.

[2] H.H. Kung, Transition Metal Oxides: Surface Chemistry and Catalysis, Elsevier, Amsterdam, 1989.

[3] G.Blasse, Philips Res.Rept. (Netherlands), 20(1965)528.

[4] J. B. Goodenough, Mag. and Chem. Bond, John Wiley, New York, 1966.

[5] J. B. Goodenough and A.L. Loeb, Phys.Rev.98 (1955) 391.

[6] A.P.B. Sinha, N.R. Sanjana and A.B. Biswas, Acta Cryst.10 (1957)439.

[7] P. P. Hankare, P. D. Kamble, S.P. Maradur, M.R. Kadam, U. B. Sankpal, R.P. Patil, R.K. Nimat, P.D. Lokhande, J. Alloys Compd. 487 (2009) 730.

[8] R. J. H. Voorhoeve, J. P. Remeika, L. E. Trimbe, Ann. N. Y. Acad. Sci. 272 (1976) 3.

[9] S. S. Deshpanade, S. U. Sonavane, R. V. Jayaram, Catal. Commun. 9 (5) (2008) 639.

[10] D.H. Zhang, H. B. Li, G. D. Li , J. S. Chem, Dalton Transactions (47), (2009) 10527.

[11] P. Srivastava, I. P. S. Kapoor, G. Singh, J. Alloys Compd. 485 (1-2) (2009) 88.

[12] M. Florea, M.Alifanti, V.I. Parvulescu, D. Mihaila-Tarabasanu, L. Diamandescu, M. Feder, C. Negrila, L. Frunza, Catal. Today 141 (3-4) (2009) 361.

[13] K. George and S. Sugunan, Catal. Comm. 9 (13) (2008), 2419.

[14] T. Nitadori, S. kurihani, M. Misono, J. Catal. 96 (1986) 221.

[15] R. C. Kambale, P. A. Shaikh, C. H. Bhosale, K. Y. Rajpure, Y. D. Kolekar, Smart Mater. Struct.18(2009) 85014.

Scanned by CamScanner

ACKNOWLEDGEMENT

The author is thankful to the **University Grants Commission, Western Regional Office Pune,** for sanctioning and funding this minor research project .

I express my sincere thanks to Trustees of Shri Shivaji Shikshan Prasarak Mandal, Barshi and Late Principal Dr. Madhukar Fartade, Principal Dr. P. R. Thorat for all their support, kind co-operation and continuous encouragement.

I am thankful to Dr. L. A. Ghule, Dr. R. S. Pandav and Dr S R Kulal for their valuable guidance and co-operation. The authors are thankful to Dr. T. N. Lokhande Head of Chemistry Department and colleagues Dr. Gurame V. M., Dr. Gaikwad S. H., Mr. Patil S.H, Dr. Shaikh A. B., Dr. Jamale D. K., Mr.Vidhute J. P., Dr. Kate P. R., administrative staff of the college and friends for their full co-operation and help in completing this research work.

Mr. S. G. Jadhav

Scanned by CamScanner

विश्वविद्यालय अनुदान आयोग
University Grants Commission
मानव संसाधन विकास मंत्रालय भारत सरकार
Ministry of Human Resource Development, Govt. of India
पश्चिम विभागीय कार्यालय गणेशखिंड,पुणे- ४११००७
Western Regional Office, Ganeshkhind, Pune – 411007

No. F. 47-630/13 (WRO)

Ph: 020 – 25696896, 25696897,
Fax: 020 – 25691477
Website- www.ugc.ac.in
Email: wrougc@gmail.com

28 JAN 2015

The DDO,
University Grants Commission,
Pune – 411007.

Subject: Financial assistance to college teachers for undertaking Minor Research Projects – Release of first installment during XIIth Plan.

Sir/Madam,

I am directed to convey the sanction of the Commission. The UGC on the recommendations of the Expert Committee has approved the Minor Research Project in the subject of **Chemistry** entitled "Photo-Catalytic Degradation of some dyes by nanoparticles: Kinetice & Mechanistic study" to be undertaken by **Mr. S. G. Jadhav,** of **SHRI SHIVAJI MAHAVIDYALAYA, SHIVAJI NAGAR, BARSHI, SOLAPUR-413 411.** The financial assistance of the UGC would be limited to Rs. 305000 for a period of two years and convey an "on account grant" of 1st Installment of Rs **245000**/- (Rupees Two lakh forty five thousand only) is presently being sanctioned as the first installment.

Non-Recurring Grant for Two years	**Amount (Rs)**	**Recurring grant**	**1st Year Amount**	**2nd Year Amount**	**Grant to be approved as Ist Inst.**
Books & Journals	25000	Contingency	20000	20000	NR 100% Rec. 1st Year
Equipment	160000	Special Need	0	0	
		Travel/Field work	10000	10000	
		Chemicals & Glassware	30000	30000	
		Others	0	0	
Total (Rs.)	185000		60000	60000	**245000**
Total Allocation :(NR+Rec)	305000				

NOTE:

- **The grants should be utilized within the time period as specified under the GFR, 2005**

The grant is subject to the terms and conditions as mentioned below.

1. The project should be implemented as per the UGC guidelines of scheme for Minor Research Project which are available on UGC website i.e. www.ugc.ac.in.
2. The sanctioned amount is debitable to the Plan Head 3 (31) and is valid for payment during the financial year 2014-15.

Sr. No	Component	Head of A/c 3(31)	Amount
1.	General Component 76%	3(A)	**245000**
2.	SC 16%	3(B)	
3.	ST 8%	3(C)	

114

Scanned by CamScanner

Scanned by CamScanner

3. The amount of the grants shall be drawn by the DDO, UGC (WRO), Pune on the Grants-in-aid bill and shall be disbursed to and credited to the Principal of the college through Electronic mode as per the following details:

a.	Details (Name & Address) of Accounts Holder:	PRINCIPAL, SHRI SHIVAJI MAHAVIDYALAYA SHIVAJI NAGAR, BARSHI, SOLAPUR, 413 411
b.	Account No.:	20159309235
c.	MICR Code:	
d.	IFSC Code:	MAHB0001174
e.	Type of Account:	Saving Account

4. The grant is subject to adjustment on the basis of Utilization Certificate in the prescribed Performa submitted by the University/ College/ Institution.
5. The University/ College shall maintain proper accounts of the expenditure out of the grants, which shall be utilized, only on approved items of expenditure.
6. The University/ Institution may follow the General Financial Rules, 2005 and take urgent necessary action to amend their manuals of financial procedures to bring them in conformity with GFRs, 2005 and those don't have their own approved manuals on financial procedures may adopt the provision of GFRs, 2005 and instruction/ guideline there under from time to time.
7. The Utilization Certificate to the effect that the grant has been utilized for the purpose for which it has been sanctioned shall be furnished to UGC as early as possible after the close of current financial year
8. The assets acquired wholly or substantially out of UGC's grant, shall not be disposed of or encumbered or utilized for purposes other than those for which the grant was given, without proper sanction of the UGC, and should at any time the College cease to function, such assets shall revert to the University Grants Commission.
9. A Register of the assets acquired wholly or substantially out of the grant shall be maintained by the University/ College in the prescribed proforma.
10. The grantee institution shall ensure the utilization of grants-in-aid for which it is being sanctioned/ paid. In case non-utilization / part utilization, the simple interest @ 10% per annum as amended from time to time on utilization amount from the date of drawl to the date of refund as per provision contained in General Financial Rules of Govt. of India will be charged.
11. The Univ. /College shall follow strictly the Government of India/ UGC's guidelines regarding implementation of the reservation policy [both vertical (for SC, ST & OBC) and horizontal [for persons with disability etc.)] in teaching and non-teaching posts.
12. The University/ College shall fully implement to Official Language Policy of Union Govt. and comply with the Official Language Act, 1963 and Official Languages (use for official purposes of the Union) Rules, 1976 etc.
13. The sanction issues in exercise of the delegation of powers vide Commission office order No. 130/2013 [F. No. 10-11/12 (Admn. IA & B)] dated 28/5/2013.
14. The University/ Institution shall strictly follow the UGC Regulations on curbing the menace of Ragging in Higher Education Institutions, 2009.
15. The University/ Institution shall take immediate action for its accreditation by National Assessment & Accreditation Council (NAAC).

115

Scanned by CamScanner

Scanned by CamScanner

16. The accounts of the University/ Institution will be open for audit by the Comptroller & Auditor General of India in accordance with the provisions of General Financial Rules, 2005.
17. The annual accounts i.e. balance sheet, income and expenditure statement and statement of receipts and payments are to be prepared strictly in accordance with the Uniform Format of Accounting prescribed by Government.
18. An amount of Rs. /- out of Rs. /- has been utilized against this office sanction letter of even dated by the university/Institute/College vide Ref No. dated for the purpose for which it was sanctioned and noted in grant in aid/ BCR register at Pg. No. 1 & S. No.
19. Future grant will be released on receipt of Statement of Expenditure Utilization Certificate (Item-wise).
20. Funds to the extent are available under the Scheme.
21. This issues with the concurrence of IFD vide Diary No. (IFD) dated (N. A.)
22. This issues with the approval of Head of Office.
23. Entry has been made in BCR at Pg. No. 1 & S. No. 142

Yours faithfully

27/1/15

(Naresh Pal Meena)
Education Officer

Copies forwarded for information and necessary action to:

1. THE PRINCIPAL
   SHRI SHIVAJI MAHAVIDYALAYA, SHIVAJI NAGAR BARSHI,
   SOLAPUR -413 411.
2. MR. S. G. JADHAV, SHRI SHIVAJI MAHAVIDYALAYA,, SHIVAJI
   NAGAR, BARSHI, SOLAPUR -413 411.
3. DIRECTOR (BCUD), SOLAPUR UNIVERSITY, SOLAPUR PUNE
   RD, KEGAON, SOLAPUR- 413255
4. DIRECTOR, HIGHER EDUCATION, CENTRAL BLDG, PUNE
5. ACCOUNTANT GENERAL, MAHARASHTRA STATE, MUMBAI
6. GUARD FILE.

(L. N. Sahu)
Section Officer

S. S. Mahavidyalaya
BARSHI
Inward No.: 1057
Date : 02.02.15

Scanned by CamScanner

Scanned by CamScanner

Annexure – II

UNIVERSITY GRANTS COMMISSION
BAHADUR SHAH ZAFAR MARG
NEW DELHI – 110 002
ACCEPTANCE CERTIFICATE FOR RESEARCH PROJECT

Name: **Mr. S. G. Jadhav**
No.F. **47-630/13 dated 28-01-2015**

Title of the Project: "**Photo Catalytic Degradation of some dyes by nanoparticles :Kinetics and mechanistic study**"

1. The research Project is not being supported by any other funding agency.
2. The terms and conditions related to the grant are acceptable to the Principal Investigator and University /College /Institution.
3. At Present I have no research project approved by UGC and the accounts for the previous project, if any have been settled.
4. The College/University is fit to receive financial assistance from UGC and is included in the list of section 2(f) & 12(B) prepared by the UGC.
5. The Principal Investigator is a retired teacher and eligible to receive honorarium as he/ she is neither getting any honorarium from any agency nor is he/she gainfully employed anywhere.
6. (i)His/her date of birth is ...03...06...1960

   (ii) Age: **52 Years**
7. The date of Implementation of the Project is **28.01.2015**

(Mr. S. G. Jadhav)
Principal Investigator
Minor Research Project

(Dr. P. B. Thorat)
PRINCIPAL
Shri Shivaji Mahavidyalaya,
Barshi, Dist. Solapur-413411

117

Scanned by CamScanner